MAGNETIC CIRCULAR DICHROISM OF METAL OXIDES ISOLATED IN NOBLE GAS MATRICES

BY

DAVID HINTON POWELL

A DISSERTATION PRESENTED TO THE GRADUATE
COUNCIL OF THE UNIVERSITY OF FLORIDA
IN PARTIAL FULFILLMENT OF THE REQUIREMENTS
FOR THE DEGREE OF DOCTOR OF PHILOSOPHY

UNIVERSITY OF FLORIDA

1979

TO MY PARENTS

ACKNOWLEDGEMENTS

The author believes that the acknowledgement section of a dissertation should not be a stuffy, formal affair, but rather a short note between friends, stuck in a convenient place like the refrigerator door. After all, the only people who read acknowledgements are those who expect to be mentioned. And all of you, gentle readers, deserve a heartfelt thanks.

Dr. Martin Vala, you have been a source of encouragement and optimism during the course of this endeavor. For the completion of a project, it is necessary to believe that some day it will work, even when the whole house just fell in.

Bob Brittain, your drive and persistence really helped maintain our momentum. Synergy is a word which is descriptive of our partnership.

Ed Voigtman, you taught me to enjoy electronics, a task in which many others had failed. Your knowledge and willingness to help were vital to the completion of this research.

Joe Baiardo, you showed me that computers can be tamed for the service of mankind, simply by learning the rules and then bludgeoning them into submission.

Ed Whitehead, you taught me the joy of working with metal. Machining has the double rewards of precision sculpture and useful creations. Thank you for opening this door for me.

Bunnie and the rest of the family, when feelings are too deep for words only the eyes can reflect the heart.

To Drs. William Weltner, Willis Person, Samuel Colgate, John Eyler, and Ms. Laura Wagner, I wish to express my appreciation to each of you for your various contributions.

TABLE OF CONTENTS

Chapter		Page
	ACKNOWLEDGEMENTS	iii
	LIST OF TABLES	vi
	LIST OF FIGURES	vii
	ABSTRACT	x
I	INTRODUCTION	1
II	THEORY OF MAGNETIC CIRCULAR DICHROISM	9
	Introduction	9
	Basic Equations	10
	Selection Rules for MCD and Angular Momentum of Diatomic Molecules	23
III	MATRIX ISOLATION APPARATUS	37
	Spectroscopic Apparatus	46
IV	EXPERIMENTAL TECHNIQUES	62
V	RESULTS OF TiO EXPERIMENTS	67
VI	RESULTS OF ZrO AND HfO EXPERIMENTS	107
	Introduction	107
	Results for Zirconium Monoxide	107
	Results for Hafnium Monoxide	141
VII	CONCLUDING REMARKS	159
	APPENDIX	162
	BIBLIOGRAPHY	173
	BIOGRAPHY	179

LIST OF TABLES

Table Number		Page
1	Ground State Configurations of the Diatomic Oxides of Groups IVb and Vb....................	68
2	Absorption Bands of TiO in an Argon Matrix.....	75
3	MCD Peak Positions of the γ' System of TiO in an Argon Matrix................................	85
4	ZFA and MCD Peak Positions for Broad Bands Associated with the γ and γ' Systems of TiO Isolated in Argon Matrices.....................	93
5	MCD Peak Positions for the γ System of TiO Isolated in an Ar Matrix.......................	95
6	Ultraviolet Transitions Observed for TiO in Argon and Neon Matrices........................	104
7	Ti Atomic Transitions Observed in an Argon Matrix at 14°K.................................	105
8	ZFA and MCD Bands for ZrO......................	110
9	Zr Atomic Transitions Observed in Ar Matrices..	127
10	Ultraviolet Bands Observed for ZrO in Ar.......	133
11	Correlation between ZrO and HfO bands in Ne and Ar Matrices...................................	143
12	ZFA Peak Positions in the Ultraviolet Spectra of HfO in Ar Matrices.........................	155

LIST OF FIGURES

Figure		Page
1	Pseudo-A_1 terms	24
2	Magnetic field splittings and polarized transitions to an atomic P state	26
3	Magnetic field splittings in atoms and diatomics with L or Λ = 1	31
4	Spin-orbit coupling in diatomic molecules	33
5	Generation of A_1 and C_o terms	36
6	Matrix deposition apparatus	39
7	Inert gas manifold	45
8	Vacuum system	48
9	Optical train for absorption experiments	50
10	Electronics for absorption experiments	53
11	Optical train for MCD experiments	55
12	Electronics for MCD experiments	56
13	Feedback circuit for MCD	59
14	Molecular orbital diagram for TiO	71
15	Absorption spectrum of TiO	74
16	Magnetic field splittings and MCD allowed Transitions in the α bands of TiO	77
17	ZFA and MCD spectra for the α bands of TiO	79
18	MCD spectrum of the γ and γ' bands of TiO	83
19	Magnetic field splittings and MCD allowed transitions in the γ and γ' bands of TiO	84

20 Expanded scale MCD spectrum of the (0,0) band of the γ' system of TiO........................ 87

21 Temperature dependent MCD spectra of the broad 7600 Å band observed in Ar matrices of TiO..... 91

22 MCD spectrum of the ε band of TiO.............. 98

23 ZFA spectrum of the ultraviolet region of an Ar matrix of TiO and Ti............................ 101

24 MCD spectrum of the ultraviolet region of an Ar matrix of TiO and Ti............................ 103

25 Singlet electronic states and observed transitions of ZrO.................................... 109

26 Magnetic field splitting and MCD allowed transitions of ZrO and HfO.......................... 112

27 MCD and ZFA spectra of the C and D systems of ZrO in an Ar matrix............................ 114

28 ZFA spectrum of the A system of ZrO in an Ar matrix.. 118

29 MCD spectrum of the A system region of ZrO in an Ar matrix.................................. 121

30 Magnetic field splittings and A_1 term for the $^3\Pi \leftarrow {}^1\Sigma^+$ transition of ZrO....................... 123

31 MCD spectrum of the weak visible bands of ZrO in an Ar matrix.............................. 125

32 ZFA spectrum of the ultraviolet region of an Ar matrix containing Zr and ZrO................... 130

33 MCD spectrum of the ultraviolet region of an Ar matrix containing Zr and ZrO................... 131

34 ZFA and MCD spectra of the ultraviolet region of an Ar matrix containing Zr and ZrO.......... 135

35 Deslandre Table for the ultraviolet transitions of ZrO.. 137

36 MCD of ZrO and HfO matrices illustrating the presence of TaO in the matrices................ 140

37 ZFA and MCD Spectra of the $(^1\Sigma-{}^1\Sigma)$ F and G bands of HfO in an Ar matrix................... 145

38 ZFA spectrum of the ($^1\Pi$-$^1\Sigma$) D and E bands of HfO in an Ar matrix............................147

39 MCD spectrum of the ($^1\Pi$-$^1\Sigma$) D and E bands of HfO in an Ar matrix............................148

40 Predicted magnetic field splitting and A_1 terms for the forbidden ($^3\Pi_1$-$^1\Sigma$ and $^3\Pi_0$-$^1\Sigma$) of HfO...151

41 ZFA and MCD spectra of the A and B bands of HfO in an Ar matrix................................153

42 ZFA and MCD spectra of the ultraviolet region of an Ar matrix containing HfO.................157

Abstract of Dissertation Presented to the
Graduate Council of the University of Florida in
Partial Fulfillment of the Requirements for the
Degree of Doctor of Philosophy

MAGNETIC CIRCULAR DICHROISM OF METAL OXIDES ISOLATED IN RARE GAS MATRICES

By

David H. Powell

December 1979

Chairman: Martin Vala
Major Department: Chemistry

The diatomic oxides of Groups IVb and Vb have been isolated by co-condensation of a molecular beam of the monoxides with rare gases at 14°K. Zero field absorbance (ZFA) and magnetic circular dichroism (MCD) spectra were obtained for all six molecules. A detailed analysis of the results obtained for TiO, ZrO and HfO is presented.

An apparatus for the preparation of rare gas matrices containing high-temperature metal oxides has been constructed. ZFA and MCD spectra were obtained using a computer controlled system, and data were stored on magnetic tape cassettes. The ZFA spectra were obtained using a double beam technique employing a single detector, two light beams modulated at different frequencies, and two lock-in

amplifiers. The MCD spectra were obtained using a low field electromagnet (5500 gauss), a photoelastic modulator, and a feedback circuit which controlled the detector gain to correct for variations in the background light intensity.

The ground state of TiO is $^3\Delta_R$. At the low temperatures employed in this study, only transitions from the $^3\Delta_1$ multiplet are observed. Since the $^3\Delta_1$ multiplet is magnetically non-degenerate, no $\mathcal{C}_o$ terms are seen in the MCD spectra. The results of this study confirm the assignment of the γ, γ', α and ε systems of TiO to $A^3\Phi$, $B^3\Pi$, $C^3\Delta$ and $E^3\Pi$, respectively. Several ultraviolet transitions of perturbed high energy bands are attributed to $^3\Pi$ and $^3\Phi$ states. Transitions attributable to Ti atoms are observed, and several assignments are revised in concordance with the MCD data.

The ground state of ZrO is confirmed as $^1\Sigma^+$ by the lack of MCD $\mathcal{C}_o$ terms observed for ZrO bands. The assignment of the A system as $^1\Sigma \leftarrow {}^1\Sigma^+$ and the C system as $^1\Pi \leftarrow {}^1\Sigma^+$ is also confirmed. The D system assignment is revised from $^1\Pi \leftarrow X^1\Sigma^+$ to $^1\Sigma^+ \leftarrow X^1\Sigma^+$, and weak transitions observed at 4855 Å and 4632 Å are assigned to a $^1\Pi \leftarrow X^1\Sigma^+$ system. A forbidden intermultiplicity transition is confirmed as $B^3\Pi \leftarrow X^1\Sigma^+$. Seventeen Zr atomic transitions are observed in MCD and ZFA spectra along with new ultraviolet bands of ZrO assigned to high energy $^1\Pi \leftarrow X^1\Sigma^+$ transitions.

The ground state of HfO is confirmed as $^1\Sigma$ as well as the F and G systems which are attributed to $^1\Sigma \leftarrow {}^1\Sigma$ or $^3\Pi_0 \leftarrow {}^1\Sigma$ transitions in the past. The MCD spectra favor the former designation. Similarly, the B system is either $^1\Pi \leftarrow {}^1\Sigma$ or $^3\Pi_1 \leftarrow {}^1\Sigma$; however, the MCD data are inconclusive for this state. The D and E systems of HfO are confirmed as $^1\Pi \leftarrow {}^1\Sigma$ transitions, and an ultraviolet transition near 2600 Å is proposed as $^1\Pi \leftarrow {}^1\Sigma$. This band has been previously reported in gas emission spectra but has not been seen previously in matrix studies.

CHAPTER 1

INTRODUCTION

On September 13, 1845, Michael Faraday wrote in his journal, "Today worked with lines of magnetic force, passing them across different bodies (transparent in different directions) and at the same time passing a polarized ray of light through them."[1] The phenomenon he observed was to later bear his name. When plane-polarized light is passed through any transparent substance collinearly with an external magnetic field, the plane of polarization is rotated--the Faraday effect.

Linearly polarized light consists of equal amounts of right (RCP) and left (LCP) circularly polarized components (see Chapter 2 for a further discussion of circularly polarized light). If the refractive indices for RCP and LCP light are unequal, optical rotation occurs. This inequality can be generated in two ways. Natural optical activity is a result of low symmetry in a molecule or in the unit cell in the case of crystals, and its wavelength dependence is known as optical rotatory dispersion (ORD). If the absorption coefficients for an electronic transition are different for RCP and LCP, this is called circular dichroism (CD). In natural optical activity the molecular dissymmetry causes the electrons to move in a helical path on excitation,[2] and the difference in absorption coefficients depends upon the handedness of the helix. The second way to bring about the inequality is by an external magnetic field, $\vec{H}$, in the propagation direction of the light. In magnetic optical rotation (MOR) the right- and left-handed circular motions about $\vec{H}$ no longer interact equivalently with the medium, and in regions of absorption the absorption coefficients of RCP and LCP light differ in the presence of a magnetic field, giving rise to magnetic circular dichroism (MCD).

Natural optical activity had early triumphs in inorganic and organic chemistry, but this was not the case with MCD and MOR. The early work was restricted almost entirely to MOR measurements and predominantly to transparent spectral regions, since polarizabilities were most easily calculated outside regions of absorption. The quantum mechanical bases for these studies were developed around 1930 by Rosenfeld,[3] Kramers,[4] and Serber.[5] The familiar A-B-C terminology follows the work of Serber (see Chapter 2). But, it was not until nearly 120 years after Faraday's work, that the modern methods of analyzing MCD were developed in the thesis work of Phillip J. Stephens in 1964.[6] The basic effects causing magnetic optical activity were long understood, but the important features of his work included improvement in the methods of analysis in regions of absorption and an increased understanding of the useful information contained therein. MCD has now completely replaced MOR since MCD eliminates many problems due to background rotations from other electronic transitions of the system from windows, solvents, etc., which are often much larger than the effect of interest. MOR is contributed to by all transitions of the systems and therefore is generally less informative.

MCD can provide data on both the ground and excited states of a molecule. In the case of the ground state properties, there is some overlap with magnetic susceptibility and magnetic resonance experiments, although in some cases MCD possesses advantages over these techniques, *vide infra*. The prime utilization of MCD has been in obtaining excited state information which is unavailable otherwise. Excited state magnetic moments and g values have been obtained in addition to information on spin-orbit coupling and Jahn-Teller interactions.[7]

The field of MCD expanded very rapidly during the 1960's, and a review by Stephens[8] in 1974 lists nearly 400 references for the period 1960-1973, whereas a similar review[9] of the period from Faraday's time until 1965 had only 133 references.

The Faraday effect is closely related to the Zeeman effect; in fact, MCD is the difference between LCP and RCP Zeeman spectra and provides no new information when the Zeeman components of a transition are resolved. However, the resolution of Zeeman components is often difficult, requiring very high magnetic fields and, in the case of broad bands, is not feasible for the current state of magnet technology. The advantage of MCD is that it is a signed technique and does not require high fields; the present study used a very small electromagnet with a comparatively weak field of ~5500 gauss. Sometimes MCD can be observed when the absorption band of a sample is too weak to be observed. Typical values for the minimum detectable absorbance is 10^{-3} whereas the minimum detectable MCD is 10^{-5}. This situation has been observed for sharp lines on paramagnetic species at low temperatures. An example occurs in spin-forbidden transitions of octahedral and tetrahedral Co(II) species.[10,11]

Analytical applications of MCD have also been made for the detection and quantification of various species, especially biological molecules. In fact, since porphyrins exhibit large visible MCD effects, the technique was used in an attempt to detect their presence in lunar rock samples.[12]

Transitions can sometimes be resolved in MCD and not in absorption. A transition overlapping a stronger transition is resolvable if the MCD is much larger for one of the transitions due to the selections rules for MCD or if the transitions have different MCD signs. For example, tryptophan and tyrosine can be distinguished from each other even though their absorption bands overlap.[13,14] The requirement of making the Kramers-Kronig transformation of MOR data to MCD data in order to analyze the results is eliminated in MCD.[15-18]

The technique of MCD lends itself well to use in conjunction with the method of matrix isolation spectroscopy. Matrix isolation was first employed by George Pimentel[19] in 1954 for trapping unstable reactive intermediates and involves the codeposition of a large amount of solvent gas with a small amount of solute gas species at low temperature.

The solvent gas freezes and traps the solute, thus isolating the solute molecules from each other. Solvent to solute ratios are typically > 1000:1. This method then allows one to study the spectra of the solute at leisure and has a number of primary advantages:

1. The matrices are usually deposited and observed at temperatures < 25°K. This simplifies the electronic spectra in that "hot bands" are usually eliminated.
2. Except for a few molecules (H_2O, HCl, NH_3 and NH_2) the rotational structure of the spectra is eliminated since the species are no longer free to rotate in the crystal lattice.
3. The electronic absorption bands are often narrow enough to enable use of isotopic substitution to look for 0-0 transitions.
4. Reactive species can be prevented from reacting by the matrix, and higher concentrations of them are then available for study.

The basic assumption of this technique is that the matrix does not interact with the solute, and essentially gas-like information is obtained. Although this is a good first approximation, matrix interactions do occur which shift the energies of electronic transitions, and the solute can be trapped in multiple sites (different micro-environments) in the crystalline lattice which leads to changes in the spectra. Often these site effects can be detected by warming the matrix slightly to allow controlled diffusion to occur and allowing the solute molecules to settle in the more stable sites thus simplifying the spectra. Lattice modes and Jahn-Teller distortions due to interactions with the matrix have also been observed. Recently, Mowery et al.[20] have observed Jahn-Teller distortions in the MCD of matrix of Mg. An excellent, although somewhat dated, discussion of matrix isolation is contained in Beat Meyer's book on low temperature spectroscopy.[21]

Although there has been considerable work done on matrices using optical and magnetic spectroscopy, few experiments have been done using polarized light or Zeeman studies.[22] The first report of MCD being applied to a matrix isolated molecule was in 1973 by A. J. Thomson,[23] and only a handful of molecules have been studied since then: Hg,[24] O_2,[24,25] Cl_2,[26] Mg,[20] Xenon halides,[27] benzene,[28] OsO_4,[29] and acrolein.[30] MCD possesses a special advantage for study of the ground state magnetic properties of matrix isolated species. At present if the electron spin resonance spectrum is undetectable, the magnetic properties are unknown since measurement of magnetic susceptibilities of matrices is not possible due to the small qunatities of material involved.

The study reported here involves the matrix isolation and MCD of a group of molecules known as the high-temperature diatomic oxides. The designation "high-temperature" stems from the fact that these molecules are generated via heating the triatomic and higher oxides to temperatures above 1500°K. The molecules studied are the diatomic oxides of Groups IVb and Vb of the Periodic table and are among the most stable molecules known. Their open shell structure provides some interesting visible spectroscopy, and they often have magnetic moments in their ground and excited states which are amenable to MCD studies.

The presence of these oxides has been observed in the stellar spectra of class M and S stars whose surface temperatures are less than 3000°K.[31] There is also evidence for low concentrations of TiO, ZrO and VO in the comparatively cooler regions of sunspots and in χ-Cygni.[32] HfO and TaO have been tentatively identified in the spectrum of R-Cygni.[33] NbO has also been tentatively identified in an R-type star in the constellation Gemini.[32] The spectrum of TiO is also of technological interest since TiO is observed in jet engine exhaust and during re-entry of space capsules.[34] ZrO is also seen in red giants[35] and S-type stars.[36]

An excellent review of the matrix isolation of high-temperature molecules was published in 1978 by Weltner,[37] and his extensive work in this field provides the basis upon which this work rests.

The matrix materials were Ar and Kr. These noble elements are ideally suited as isolants and have often been the substances of choice. They are particularly suited for MCD studies since their crystal structures are cubic close packed and therefore isotropic--a requirement for MCD. Neon matrices were not available since our apparatus could not achieve the low temperatures required.

The remainder of this thesis shall discuss the theory of MCD, the details of the apparatus constructed for this experiment, and the procedure employed in obtaining the results. A detailed description of the results for

Group IVb (TiO, ZrO, and HfO) is presented. Group Vb results are treated in a more detailed discussion in the thesis of the author's compatriot and friend, Robert D. Brittain.[38] Finally, suggestions for further extensions of this work are presented in Chapter VII.

CHAPTER II

THEORY OF MAGNETIC CIRCULAR DICHROISM

Introduction

In this chapter the pertinent equations which describe magnetic circular dichroism (MCD) will be developed. The approach will follow the series of articles by Stephens,[6,39,40] emphasizing the approximations and limitations of the method. A convenient starting point is a basic description of circularly polarized light.

Light consists of electric and magnetic fields varying sinusoidally with the direction of propagation. In unpolarized light the directions of the electric field vector, $\vec{E}$, and the magnetic field vector, $\vec{H}$, are random. In plane polarized light the $\vec{E}$ and $\vec{H}$ vectors are constant in direction but vary in magnitude. If plane polarized light is passed through a transparent birefringent medium in which the speed of light depends upon the direction of polarization of the light, then part of the beam will be delayed with respect to the other, depending upon the difference in refractive indices and the thickness of the medium. If the plane polarized beam enters the birefringent medium at 45° to two perpendicular axes with differing indices of refraction, equal magnitude components of the projection of the electromagnetic vectors will be phase shifted relative to each other. When this phase shift is equal to the wavelength, λ, the emergent beam will be plane polarized again. If the phase shift is not equal to λ, the resultant $\vec{E}$ and $\vec{H}$ will trace helical paths on emergence. Whenever the tracing is clockwise while looking toward the source, the beam is considered right polarized and vice versa for left polarized. If the phase shift equals $\frac{\lambda}{4}$, the cross section of the helix will be a circle, and the light is referred to as circularly polarized. A phase shift different from an integral multiple of $\frac{\lambda}{4}$ causes an elliptical tracing and the light is elliptically polarized. In circularly polarized light the $\vec{E}$ and $\vec{H}$ vectors are constant in magnitude but vary in direction, but in elliptically polarized light they change both in magnitude and direction.

A medium exhibits circular dichroism when it propagates right and left circularly polarized light with unequal absorption. Natural circular dichroism is a relatively rare phenomenon, whereas magnetic circular dichroism (MCD) is a property of all matter. MCD occurs when a magnetic field is applied along the propagation direction of the circularly polarized light.

Basic Equations

The solutions of Maxwell's equations for circularly polarized light of angular frequency ω traveling in the positive z direction in a Cartesian coordinate system yield for the electric field vector

$$\vec{E}_{\pm}(z,t) = E_{o}^{o}\,exp[i\omega(t-\hat{n}_{\pm}z/c)](\vec{i}\pm i\vec{j}) \qquad (1)$$

and for the magnetic field vector

$$\vec{H}_{\pm}(z,t) = (\hat{n}_{\pm}/\hat{\mu})E_{o}^{o}\,exp[i\omega(t-\hat{n}_{\pm}z/c)](\mp i\vec{i}+\vec{j}) \qquad (2)$$

where + refers to right circularly polarized light (RCP) and - to left circularly polarized light (LCP). E_{o}^{o} is the electric field at z=0; t is the time; $i=\sqrt{-1}$; and c is the speed of light. The vectors $\vec{i}$ and $\vec{j}$ are the unit vectors in the x and y directions, respectively. The complex magnetic permeability in the xy plane which must be isotropic is represented by $\hat{\mu}$. The complex refractive index is $\hat{n}_{\pm}$ and equals $\eta_{\pm}-ik_{\pm}$ where $\eta_{\pm}$ is the real part of the refractive index and $k_{\pm}$ is the absorption coefficient. $\hat{n}_{\pm}$ is a function of the external magnetic field via the effect of the field upon $k_{\pm}$.

The intensity of the light, I(z), at a point z is the energy passing through a unit area normal to the z axis in unit time and is given by the time average of the Poynting vector $(c/4\pi)(\vec{E}\times\vec{H})$

$$I_{\pm}(z) = (c/4\pi)Re\{\hat{n}_{\pm}/\hat{\mu}\}(E_{o}^{o})^{2}exp(-2\omega k_{\pm}z/c) \qquad (3)$$

Making the approximation that the magnetic permeability is unity and substituting $\omega = 2\pi\nu = \mathcal{E}/\hbar$ where $\mathcal{E}$ is the energy of the light and $\hbar$ is Planck's constant divided by 2π, yields

$$I_{\pm}(z) = (c/4\pi)\eta_{\pm}(E_{o}^{o})^{2}exp(-2\mathcal{E}k_{\pm}z/\hbar c) \qquad (4)$$

Setting the magnetic permeability equal to unity excludes magnetic materials from consideration. Equation 4 can be further simplified to

$$I_{\pm}(z) = I_{\pm}(0)\,exp(-2\mathcal{E}k_{\pm}z/\hbar c) \tag{5}$$

whence

$$k_{\pm} = [\hbar/\eta_{\pm}\mathcal{E}|E_{\pm}(z)|^{2}][-\frac{\delta I_{\pm}}{\delta z}(z)] \tag{6}$$

where $|E_{\pm}(z)|^2$ is the magnitude of the electric field at z. The derivative portion of this equation is the energy absorbed per unit time per unit volume at z and is related to the probability of absorption per unit time ($P_{a\to j}$) at z at the energy of the transition from state a to state j,

$$-\frac{\delta I}{\delta z}(z) = \sum_{a,j} N_a\, P_{a\to j}(z)\mathcal{E} \tag{7}$$

where N_a is the number of absorption centers of state a per unit volume.

By limiting our discussion to electric dipole transitions and ignoring electric quadrupole and magnetic dipole interactions, we can relate the above probabilities of absorption to the electric dipole transition matrix elements via time-dependent perturbation theory, thereby assuming that the effective Hamiltonian, $\mathcal{H}_o$, is a sum of independent components, i.e.,

$$\mathcal{H}_o = \mathcal{H}_o^o + \mathcal{H}_o' \tag{8}$$

where

$\mathcal{H}_o^o$ = the Hamiltonian for the system in the absence of light. The superscript "o" indicates the absence of the radiation field, and

H_o' = the Hamiltonian for the perturbation due to the radiation field.

The subscript zero indicates the absence of an external magnetic field. This treatment leads to

$$P_{a\to j}(z) = \frac{\alpha^2\pi}{\hbar}|E_\pm(z)|^2|\langle a|m_\pm|j\rangle|^2\delta(E_{ja}-E) \tag{9}$$

where

$|a\rangle$ = eigenstate of H_o^o of energy E_a.
$|j\rangle$ = eigenstate of H_o^o of energy E_j.

E_{ja} = $E_j - E_a$.

α = Lorentz effective field correction factor and relates the electric field due to the light at the absorption center to the macroscopic E field.

δ = Kronecker delta operator. This term arises from the neglect of transition lifetimes and will be eliminated later.

$m_\pm$ = $m_x \pm im_y$ and is the transition dipole moment operator for RCP and LCP transitions.

The equation for $k_\pm$ then becomes

$$k_\pm = \frac{2\pi^2\alpha^2}{\eta_\pm}\sum_{a,j} N_a|\langle a|m_\pm|j\rangle|^2\delta(E_{ja}-E) \ . \tag{10}$$

This expression can be transformed into more familiar spectroscopic notation in terms of absorbance

$$exp\{-2Ekz/\hbar c\} = 10^{-A} = \frac{I(z)}{I(o)} = 10^{-\varepsilon cz} \tag{11}$$

where

A = absorbance.
I(z) = the intensity at point z.

$I(o)$ = the intensity at $z = 0$
ε = the molar extinction coefficient.
c = concentration of absorbers.

This leads to an equation for the absorbance:

$$\frac{A_\pm}{E} = \left(\frac{\varepsilon_\pm}{E}\right)cz = \gamma_\pm\{\textstyle\sum_{a,j}\left(\frac{N_a}{N}\right)|\langle a|m_\pm|j\rangle|^2\delta(E_{ja}-E)\}cz \quad (12)$$

where

$$\gamma_\pm = \frac{N\pi^2\alpha^2 \log_{10} e}{250\hbar c\eta_\pm}$$

and N is Avogadro's number and N_a/N is the fractional population of absorbers in state a. This equation assumes that Beer's law is obeyed and does not allow for non-linear effects that would occur at high light intensities. The electronic excitations producing a band are localized, and the concentration of the species is sufficiently low that interaction is negligible.

The dichroism of a system is the difference in absorbance between LCP and RCP light

$$\Delta A = A_- - A_+ \ . \quad (13)$$

Substituting for A_- and A_+ from Equation 12 yields

$$\frac{\Delta A}{E} = \gamma\{\textstyle\sum_{a,j}\left(\frac{N_a}{N}\right)[|\langle a|m_-|j\rangle|^2 - |\langle a|m_+|j\rangle|^2]\delta(E_{ja}-E)\}cz \quad (14)$$

where $\gamma=\gamma_+=\gamma_-$ and $\eta_+=\eta_-$. This equation is general and applies to natural circular dichroism as observed in optically active molecules. Magnetic optical activity and MCD are not perturbations of natural optical activity but arise from different polarizabilities which are zero when an external magnetic field is absent. Natural and magnetic optical rotations and dichroism are additive.

If a system has no natural circular dichroism and no magnetic field is present, then $\Delta A = 0$ and $|\langle a|m_+|j|^2 = |\langle a|m_-|j\rangle|^2$. In this case we can define the zero field absorbance (ZFA) as

$$A^o = A^o_+ = A^o_- = \tfrac{1}{2}(A^o_+ + A^o_-) \tag{15}$$

At this point it is convenient to apply the Born-Oppenheimer approximation (BO) and the Franck-Condon approximation (FC) to a description of the ZFA. The Born-Oppenheimer approximation assumes that the zero-field eigenstates can be written as a product of wavefunctions

$$\begin{aligned} |A_\alpha a\rangle &= \Psi_{A_\alpha}(r,R)\chi_a(R) \qquad && \alpha = 1 \text{ to } d_A \\ |J_\lambda j\rangle &= \Psi_{J_\lambda}(r,R)\chi_j(R) \qquad && \lambda = 1 \text{ to } d_J \end{aligned} \tag{16}$$

where Ψ indicates an electronic wave function with a parametric dependence upon the instantaneous nuclear configuration; $\chi_a(R)$ and $\chi_j(R)$ are vibrational wavefunctions and dependent upon the nuclear coordinates R and the particular electornic configuration; r is the electron coordinate; and the degeneracies of states a and j are given by d_A and d_J, respectively. The eigenfunction equations are

$$H_o^o|A_\alpha a> = E_a|A_\alpha a>$$

$$H_o^o|J_\lambda j> = E_j|J_\lambda j> \quad . \tag{17}$$

The Franck-Condon approximation is now employed to simplify the transition matrix elements

$$<A_\alpha a|m_\pm|J_\lambda j> = <a|j><A_\alpha|m_\pm{}^e|J_\lambda>^o . \tag{18}$$

The lower case letters refer to the vibrational wavefunctions, and the superscript zero indicates that the electronic matrix element is evaluated at $R = R_o$, the equilibrium configuration (the ground state vibrational functions χ_a have significant amplitude only for $R = R_o$ if nuclear motion is small). The Zeeman splittings of the ground and excited states will be independent of the vibrational level and equal to the pure electronic splittings at R_o. If the transition is only weakly allowed, the FC approximation is inadequate, and more account must be taken of the R dependence of the electronic wavefunction. Equation 14 now becomes:

$$\frac{A_\pm^o}{E} = \gamma\{\frac{1}{d_A}\sum_{\alpha,\lambda} |<A_\alpha|m_\pm{}^e|J_\lambda>|^2\}$$

$$\{\sum_{a,j}\frac{N_a}{N}|<a|j>|^2\delta(E_{ja}-E)\}cz. \tag{19}$$

Integrating over all the vibrational bands and assuming that γ is a constant for all vibronic transitions yields

$$\int\frac{A_\pm^o}{E}\,dE = \gamma\sum_{\alpha\lambda}\frac{1}{d_a}|<A_\alpha|m_\pm{}^e|J_\lambda>^o|^2 cz. \tag{20}$$

If we then let

$$\mathcal{D}_o = \frac{1}{d_a} \sum_{\alpha,\lambda} |\langle A_\alpha | m_\pm{}^e | J_\lambda{}^o \rangle|^2 \tag{21}$$

and

$$f(E) = \sum_{a,j} \left(\frac{N_a}{N}\right) |\langle a|j\rangle|^2 \delta(E_{ja} - E) \tag{22}$$

where

$$\int_o^\infty f(E)\,dE = 1$$

then the zero field absorbance is given by

$$\frac{A_\pm^o}{E} = \gamma \mathcal{D}_o f(E) cz \ . \tag{23}$$

Note that from this equation we conclude that the zero field absorbance dispersion depends only on the ground and excited state vibrational functions, and the total integrated intensity is dependent on the electronic wavefunctions at the equilibrium position, R_o. The integrated intensity is independent of the temperature, but the shape is dependent upon the temperature from the Boltzmann term (N_a/N) in Equation 22.

In the presence of a magnetic field, the absorption coefficients, $k_\pm$, exhibit field dependence, and the eigenfunction and eigenvalues of the system's Hamiltonian must be obtained as explicit functions of the field. This is feasible in analytic form only when the field dependent terms may be treated by perturbation theory which assumes that the magnetic field energy is small compared with the separation of the zero-field states. To the Hamiltonian, $\mathcal{H}_o$, of Equation 8 is now added the perturbation Hamiltonian, $\mathcal{H}'$ due to the external magnetic field

$$\mathcal{H} = \mathcal{H}_o + \mathcal{H}' \quad . \tag{24}$$

Since nuclear magnetons are three orders of magnitude lower than electronic magnetons, we can ignore the effect of nuclear moments and consider electronic contributions to the first order magnetic field perturbation.

$$\mathcal{H}' = -\sum_i \frac{e}{2mc}(\ell_{z_i} + 2S_{z_i})H \tag{25}$$

where i sums over all electrons with mass m and charge e. H is the magnitude of the magnetic field directed along the z axis; ℓ_{z_i} is the projection on the z axis of the angular momentum of the ith electron and similarly for the projection of the spin S_{z_i}. Summing over all electrons leads to

$$\mathcal{H}' = -\mu_z H \equiv \beta(L_z + 2S_z)H \tag{26}$$

where μ_z is the electronic magnetic moment along z, and β is the electronic Bohr magneton = 4.6681×10^{-5} cm^{-1}/gauss. L_z and S_z are the corresponding total orbital and spin angular momenta along the z axis. This equation is recognized as describing the Zeeman splittings induced by the magnetic field and leads to population changes in the ground state. The Boltzmann term in Equation 22 can now be described in terms of the magnetic moments and the external magnetic field:

$$\frac{N_\alpha}{N} = \frac{d_\alpha exp\{-<A_\alpha|L_z+2S_z|A_\alpha>\beta H/kT\}}{\sum_\alpha d_\alpha exp\{-<A_\alpha|L_z+2S_z|A_\alpha>\beta H/kT\}} \qquad (27)$$

where α sums over the Zeeman states of A. For high temperatures and/or low field strengths the exponentials can be expanded via

$$e^{-x} = 1 - x + \frac{x^2}{2!} - \ldots \qquad (28)$$

whereby

$$\frac{N_\alpha}{N} = \frac{1}{d_a}\{1-<A_\alpha|L_z+2S_z|A_\alpha>\beta H/kT\} \ . \qquad (29)$$

If one assumes that the Zeeman shift merely changes the position of the absorption band along the energy axis and does not change the shape of the band, the shifted lineshape function can be expressed in terms of the unshifted function by a Taylor's series expansion. This approach is called the rigid shift approximation and is especially valid for broad bands where the Zeeman shift is small compared with the band width. The assumption that the band moves rigidly will usually be a good zero-order approximation, but may require modification since little is known about the variation of line shapes in magnetic fields and we are implicitly ignoring any magnetic field perturbations to the transition moment operators.

Finally, the manner in which the circularly polarized absorption is modified by the magnetic field using Equations 13, 19, 27 and the above considerations leads to an expression for the MCD:

$$\Delta A = +\gamma\{\mathcal{A}_1\left(-\frac{\delta f}{\delta E}\right) + \left(\mathcal{B}_0 + \frac{\mathcal{C}_0}{kT}\right) f\}(\beta H)cz \qquad (30)$$

where

$$\mathcal{A}_1 = +\frac{1}{d_a}\sum_{\alpha,\lambda}\left[\,|\langle A_\alpha|m_-|J_\lambda\rangle^{o}|^2 - |\langle A_\alpha|m_+|J_\lambda\rangle^{o}|^2\right]$$

$$\times\ \left[\langle J_\lambda|L_z+2S_z|J_\lambda\rangle^{o} - \langle A_\alpha|L_z+2S_z|A_\alpha\rangle^{o}\right]$$

$$\mathcal{B}_0 = -\frac{2}{d_a}\sum_{\alpha,\lambda}\mathrm{Re}\{\sum_{K_k\neq J}[\,\langle A_\alpha|m_-|J_\lambda\rangle^{o}\langle K_k|m_+|A_\alpha\rangle^{o}$$

$$-\ \langle A_\alpha|m_+|J_\lambda\rangle^{o}\langle K_k|m_-|A_\alpha\rangle]\frac{\langle J_\lambda|L_z+2S_z|K_k\rangle^{o}}{W_K^{o} - W_J^{o}}$$

$$+\sum_{K_k\neq A}[\langle A_\alpha|m_-|J_\lambda\rangle^{o}\langle J_\lambda|m_+|K_k\rangle^{o} - \langle A_\alpha|m_+|J_\lambda\rangle^{o}$$

$$\times\ \langle J_\lambda|m_-|K_k\rangle^{o}]\frac{\langle K_k|L_z+2S_z|A_\alpha\rangle^{o}}{W_K^{o} - W_A^{o}}\ \}$$

$$\mathcal{C}_0 = -\frac{1}{d_a}\sum_{\alpha,\lambda}\left[\,|\langle A_\alpha|m_-|J_\lambda\rangle^{o}|^2 - |\langle A_\alpha|m_+|J_\lambda\rangle^{o}|^2\right]$$

$$\langle A_\alpha|L_z+2S_z|A_\alpha\rangle^{o}\ .$$

The three terms in this equation are referred to as the $\mathcal{A}_1$, $\mathcal{B}_0$ and $\mathcal{C}_0$ terms and the shape of the MCD can be deconvolved into these component parts. Conversely, calculation of these terms can be used to predict the sign and shape of the MCD dispersion. The maximum contributions to the MCD of the three terms are related as

$$\mathcal{A}_1 : \mathcal{B}_0 : \mathcal{C}_0 \sim \frac{Z}{\Gamma} : \frac{Z}{\Delta W} : \frac{Z}{kT} \qquad (31)$$

where Γ is the bandwidth of an electronic transition; ΔW is the order of magnitude of an electronic energy gap; k is the Boltzmann constant; and T is the absolute temperature. Z is the Zeeman energy.

In examining Equation 30 one notes that the existence of a $\mathcal{C}_o$ term indicates that the ground state is degenerate, and the $\mathcal{C}_o$ term depends upon the magnetic moment of the ground state and the circularly polarized transition moments. Since the $\mathcal{C}_o$ term is divided by kT, for $\mathcal{C}_o \neq 0$ the temperature dependence of the MCD depends upon the magnitude of the $\mathcal{C}_o$ term. Note also that the $\mathcal{C}_o$ term is multiplied by the lineshape function, f.

The presence of an $\mathcal{A}_1$ term indicates that the ground state and/or the excited state is degenerate and, since it is multiplied by the derivative of the lineshape function, depends strongly on the bandwidth of the transition. Thus the MCD experiment provides information on the magnetic moments, symmetries, and electronic wavefunctions of the ground and excited states.

The $\mathcal{B}_o$ term contribution to the MCD depends upon mixing of the electronic wavefunctions via the magnetic field perturbation and is the chief cause of the Faraday effect being present in all substances, since there will always be some mixing, however slight, with other states k.

The subscripts on the three MCD terms in Equation 30 and $\mathcal{D}_o$ in Equation 21 refer to the moments of the MCD and ZFA curves that yield these values. In 1965 Henry, Schnatterly and Slichter introduced the moments method of analyzing MCD of color centers.[41] The moments of a spectrum are averaged properties where the nth moment of the ZFA and MCD are defined as

$$\langle A^{o}_{\pm}\rangle^{E^{o}}_{n} = \int \frac{A^{o}_{\pm}}{E}(E-E^{o})^{n}dE \tag{32}$$

and

$$\langle \Delta A\rangle^{E^{o}}_{n} = \int \frac{\Delta A}{E}(E-E^{o})^{n}dE \tag{33}$$

where E^{o} is the energy of the center of the band about which the moment is taken. The terms are related to the moments by

$$\langle A^{o}\rangle_{o} = \langle \varepsilon^{o}\rangle cz = 326.6\mathcal{D}_{o}cz \tag{34}$$

$$\langle \Delta A\rangle_{o} = \langle \Delta\varepsilon^{o}\rangle cz = 326.6[\mathcal{B}_{o} + \frac{\mathcal{C}_{o}}{kT}](\beta H)cz \tag{35}$$

$$\langle \Delta A\rangle_{1} = \langle \Delta\varepsilon\rangle^{\bar{E}}_{1} cz = 326.6\mathcal{A}_{1}(\beta H)cz \tag{36}$$

Thus one can obtain the values for the terms from the experimental curves and compare these with the calculated terms from Equation 30. In order to define the moments properly, the band must be completely resolved from neighboring bands at all fields. The moments must be taken over the entire set of vibronic transitions allowed in conjunction with the electronic excitation.

For overlapping systems the MCD remains an additive function of the individual contributions and allows one to separate bands that overlap in absorption spectra but have different signs or magnitude of the component MCD terms. The effect is observed for TaO in these studies where oppositely signed $\mathcal{C}_{o}$ terms allow separation of previously unresolved band systems. If the two overlapping bands are very close in energy and the magnitude of the $\mathcal{C}_0$ terms are comparable, then the MCD will have a "pseudo-A" term with the appearance of a derivative when in actuality it is merely an overlap phenomenon (see Figure 1). A similar "pseudo-A" term can sometimes be observed when strongly interacting states lead to oppositely signed $\mathcal{B}_0$ terms.

Selection Rules for MCD and Angular Momentum of Diatomic Molecules

Photons possess well-defined values of angular momentum and are emitted and absorbed by systems which are characterized by well-defined values of their angular momenta.[42] Since angular momentum is conserved, the selection rules characterizing transitions involving photons with angular momenta must take this into account.

Let us begin by considering the transitions occurring in an isolated atom with total angular momentum J. When no magnetic field is present the state is degenerate to the extent of 2J+1 corresponding to the number of distinct eigenvalues m_J. The field about the atom is spherically symmetric, and there is no preferential direction for the angular momentum. When an external magnetic field is introduced, this degeneracy is lifted via the space quantization imposed by the field direction. Figure 2 shows the Zeeman splitting of the eigenstates of atoms with total angular momentum J=0 and J=1 in a magnetic field and the three possible transitions allowed.

The probability for the absorption of a photon of electric dipole radiation for a transition from states a to j

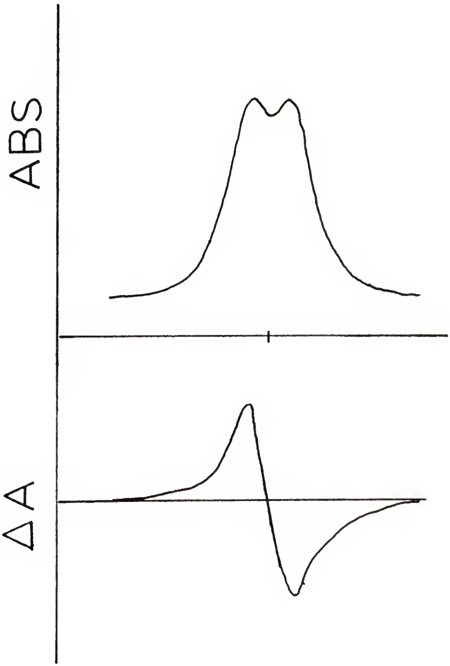

Figure 1. Pseudo-A_1 terms generated by oppositely signed C_o or B_o terms for overlapping transitions.

Figure 2. Magnetic field splittings and polarized transitions to an atomic P-state.

Transition a is RCP.

Transition b is polarized parallel to the magnetic field.

Transition c is LCP.

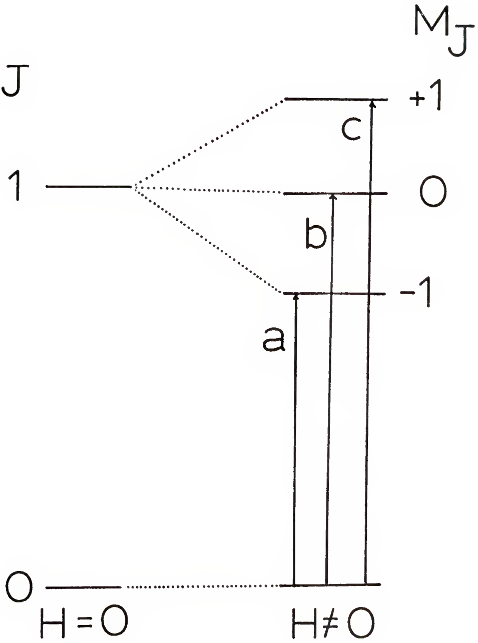

M_J
J
+1
c
1
0
b
-1
a
0
H = 0
H ≠ 0

is proportional to the square of the transition dipole moment matrix element along the direction of the photon polarization.

$$(\vec{u}\cdot\vec{m}_{ja}) \equiv (\vec{u}\cdot\langle a|m|j\rangle) \tag{37}$$

where $\vec{u}$ is a unit vector determining the polarization of the light, and $\vec{m}_{ja}$ is the transition electric dipole moment. We can now derive the selection rules for the three transitions of Figure 2 by considering the three possible polarizations of light (x,y,z) on Equation 37 and the properties of the wavefunctions as described by the spherical harmonics.[42]

First considering the polarization parallel to the field, the z direction, Equation 37 vanishes for all cases except where $\Delta J = \pm 1$ and $\Delta m_J = 0$. This situation is of no interest in MCD since the z polarization is the light propagation direction in MCD and is unavailable.

When considering the two possible polarizations of the light, $\vec{u}_x$ and $\vec{u}_y$, when the light is propagating along z, it is more convenient to examine the two linear combinations $\vec{u}_x \pm i\vec{u}_y$ corresponding to the two possible circular polarizations. The + combination is right circular polarized, and the - is left circular polarized. For RCP, Equation 37 vanishes except for $\Delta m_J = m_{J'} - m_{J''} = -1$ and conversely, the selection rule for LCP is $\Delta m_J = +1$, and $\Delta J = \pm 1$ for both cases. From these considerations we can conclude that transition b in Figure 2 will not be observed, whereas transition a will correspond to RCP and transition c to LCP. Thus in this case circularly polarized light corresponds to electric dipole photons having J=1 and $m_J = +1$ for LCP and $m_J = -1$ for RCP. Although these selection rules were derived for the case of atoms, the law of conservation of angular momentum makes the absorption by any system subject to similar selection rules.

We shall now turn to the special considerations that apply to the angular momenta of diatomic molecules. In atoms the electronic orbital angular momentum, $\vec{L}$, is a constant of the motion of the electrons due to the spherical symmetry of the force field. In a quantum system which does not have spherical symmetry, the orbital angular momentum is not an integral of the motion. In diatomic molecules the force field is axially symmetric about the internuclear axis, and the component of the orbital angular along this axis is a constant of the motion. $\vec{L}$ precesses in a classical sense about the axial electric field of the nuclei with constant component $m_L = L, L-1, \ldots -L$. Unlike motion in a magnetic field, reversing the motion of the electrons about the electric field does not change the energy, and m_L and $-m_L$ are equivalent. Therefore, it is more appropriate to classify the electronic states of diatomic molecules according to the absolute value of m_L, and the quantum number of interest in diatomics is designated

$$\Lambda = |m_L| . \tag{38}$$

The value of Λ is represented in the term symbol by Σ, Π, Δ, and Φ according to $\Lambda = 0,1,2,3$, respectively.

Except for Σ states all diatomic states are doubly degenerate. External space quantization can occur via the introduction of an external magnetic field to lift this degeneracy, whereby a $^1\Pi$ state would split into two different m_Λ states rather than the three states corresponding to the three values of m_L as observed in ^1P atomic states. This is illustrated in Figure 3.

Just as in atoms, the spin of the electrons can add vectorially to yield a total resultant spin, $\vec{S}$. In the case where $\Lambda \neq 0$, there is an internal magnetic field due to the orbital motion of the electrons which causes space quantization along the internuclear axis. The classical precession of $\vec{S}$ about the internuclear axis has a constant projection designated Σ which can have the values

$$\Sigma = S, S-1, \ldots, -S \ . \tag{39}$$

In contrast to Λ, Σ can have positive or negative values.

To carry the comparison between atoms and diatomic molecules further, the total angular momentum in atoms is designated $\vec{J}$ and is the vector sum of $\vec{L}$ and $\vec{S}$. The corresponding quantum number in diatomic molecules is simply the algebraic sum of Λ and Σ, since they both lie on the internuclear axis, and is

$$\Omega = |\Lambda + \Sigma| \ . \tag{40}$$

The symbol for a diatomic term is

$$^{2S+1}\Lambda_\Omega$$

Figure 3. Magnetic field splittings in atoms and diatomics with L or $\Lambda = 1$.

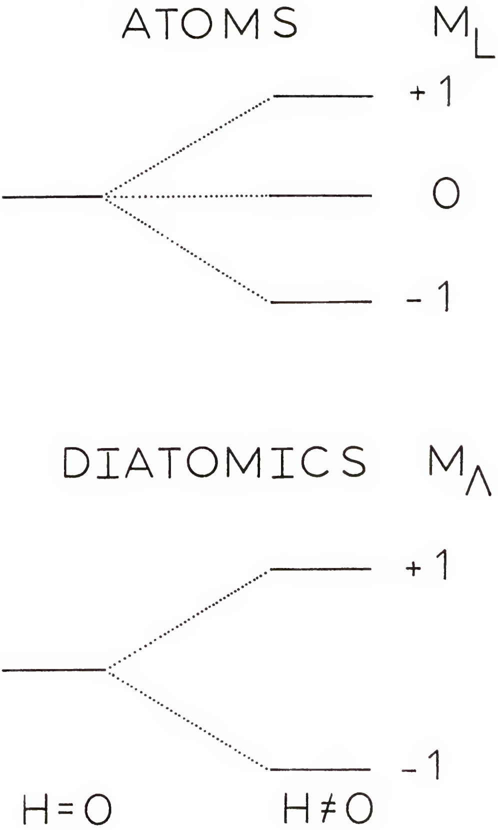
ATOMS
M_L
+1
0
-1
DIATOMICS
M_Λ
+1
-1
H=0
H≠0

where 2S+1 is the multiplicity, and $\Lambda = \Sigma,\Pi,\Delta,\Phi$ for values of $\Lambda = 0,1,2,3$.

An electronic term with a given $\Lambda \neq 0$, splits into a 2S+1 multiplet of components of different energies due to the interaction of Σ and Λ, spin-orbit coupling. The electronic energy of a multiplet term is given to a first approximation by

$$T_e = T_o + A(\Lambda\Sigma) \tag{41}$$

where T_o is the term value when spin is neglected. A is a constant for a given multiplet, increases rapidly with the number of electrons as in atoms, and may be either positive or negative. Figure 4 shows the multiplet splittings and vectors for the ground state of TiO. As long as $\Lambda \neq 0$, each of the multiplet components is doubly degenerate, even those with $\Omega = 0$ and will split in a magnetic field as in Figure 3 except in those situations where the values of the orbital angular momentum and the spin angular momentum cancel each other to give no net magnetic moment. An example of this cancellation occurs in the $^3\Delta_1$ state of TiO, *vide infra*.

When the interaction of the spin and orbital angular momenta are so strong that Λ and Σ are no longer valid quantum numbers, the selection rules presented above must be modified. This strong coupling often occurs in species containing nuclei with high atomic numbers, and Ω is the only valid quantum number in these species. The MCD selection rule then becomes $\Delta m_\Omega = \pm 1$ and is known as

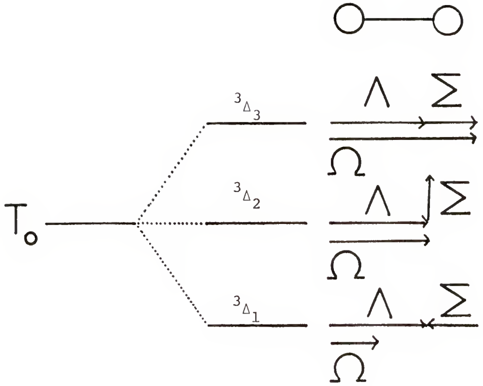

Figure 4. Spin-orbit coupling in diatomic molecules. Relative orientations of Λ, Σ and Ω are shown.

Hund's case c. When the coupling is weak, as in species containing light nuclei, the MCD selection rules are $\Delta m_\Lambda = \pm 1$ and $\Delta m_\Sigma = 0$. This later situation is called Hund's case a. These two cases are the extreme situations, and often molecules will display properties intermediate between case a and case c.

To illustrate how the various magnetic field splittings give rise to the MCD A_1 and C_o terms, Figure 5 shows the MCD transitions for the cases where either the ground state or excited state is split. The A_1 term arises when the excited state or ground state is split by the magnetic field. A positive A_1 term is shown where the positive-going lobe is to the higher energy corresponding to the absorption of LCP light being more energetic than RCP light. Two cases are illustrated for the case where the ground state is split. When the temperature is high the populations of all the ground substates will be equal and the MCD dispersion will be as illustrated in the middle spectrum. As the temperature is lowered, the population in the lowest magnetic sublevels begins to increase according to Boltzmann distribution statistics. The lobe for the higher sublevels decreases while the lobe for the lower levels increases, the resulting dispersion is illustrated by the dashed curve in the spectrum on the right.

Figure 5. Magnetic field splittings of ground and excited states illustrating the origin of A_o and C_o terms.

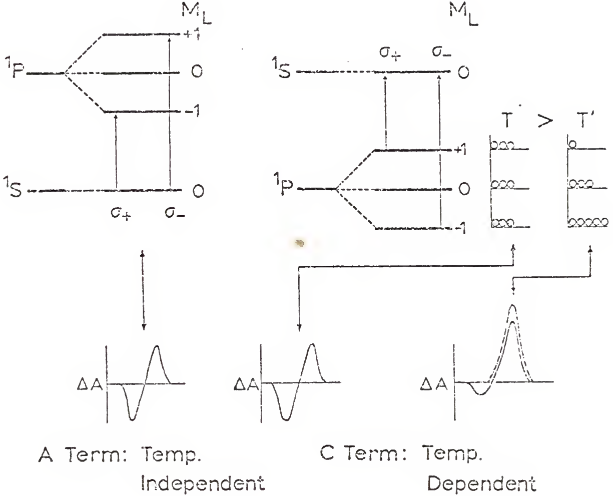
M_L
^1P
+1
0
-1
^1S
0
σ_+
σ_-
ΔA
A Term: Temp. Independent
M_L
^1S
σ_+
σ_-
0
^1P
+1
0
-1
T > T'
ΔA
ΔA
C Term: Temp. Dependent

CHAPTER III

MATRIX ISOLATION APPARATUS

This section contains a detailed description of the apparatus constructed for matrix isolation including the electronics and optical systems used in the absorption and MCD experiments. Figure 6 shows a schematic representation of the furnace and matrix isolation device. A rather compact furnace was required, because it had to fit within the confines of a small Alpha Model 4600 4-inch adjustable gap electromagnet. The distance between the Knudsen cell and the cold window was 3.5 inches, which caused some problems due to the radiation flux from the Knudsen cell, *vide infra*.

Originally, a large furnace design was used which had the bulk of the furnace outside of the magnet, and the distance between the Knudsen cell and the cold window was approximately 10 inches. This design proved unsatisfactory, because this longer distance allowed a greater dispersion of the molecular beam effusing from the Knudsen cell with concommitantly weaker absorbing matrices.

The molecular beam was generated in a resistively heated Knudsen cell made of either tungsten or tantalum. These materials were suitable for high temperature studies because of their refractory nature; however, some difficulties did exist. The tantalum cells were made from lengths

Figure 6. Matrix Isolation Apparatus

A. Viewport for high temperature measurements
B. Magnetic shutter
C. Exit to vacuum pumps
D. Water-cooled copper electrodes
E. Knudsen cell
F. Water-cooled heat shield
G. Isolant gas inlet
H. Vacuum shroud
I. Heat shield cooled to 77°K
J. Closed-cycle helium refrigerator
K. Calcium fluoride window

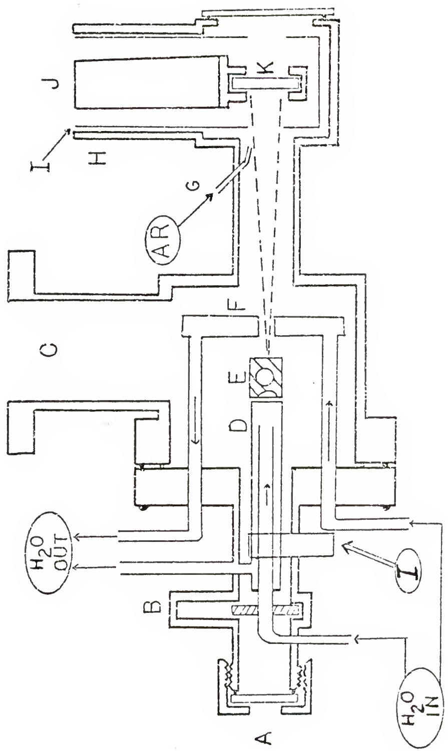
A
B
C
D
E
F
G
H
I
J
K
AR
H_2O OUT
H_2O IN
I

of 0.25 inch outer diameter tubing with a wall thickness of 0.035 inch. At the high temperatures required for formation of the diatomic oxides studied, Ta rapidly reacted with the oxides, and often the cell failed via cracking before the required temperatures could be maintained. Tantalum cells were used only in the TaO experiments.

The more expensive and fragile tungsten cells were used with the other experiments because of the inertness of tungsten. These cells were expensive--$30 per cell from Chemetal. Tungsten was also very brittle and care had to be taken when putting the effusion hole in the cell. This hole (~0.05 inch) had to be ground, not drilled; and even with care to avoid thermally shocking the cell, they seldom lasted more than three runs. The only end cap material available for the Knudsen cells was tantalum, which proved to be convenient since a small amount of TaO observed in the matrix was often used as an internal standard for the sign of the MCD.

The Knudsen cell was mounted by tantalum straps to two water cooled copper electrodes. One of these electrodes was electrically isolated from the furnace flange, and the other was electrically connected to the entire outside of the furnace; therefore, one needed to be cautious when using the magnetic shutter that the magnet did not cause arcing across the electrodes. Up to 300 amp, 60 Hz, alternating current was passed through the small area of the cell wall enabling operation at 2500° C. This high current was obtained by means of a Variac^{R} variable transformer and a step-down transformer.

Cooling of the furnace was achieved by water flowing through 0.25 inch copper tubing soldered to the outer shell of the furnace. During depositions at temperatures above 2000° C, it was necessary to wrap the furnace with wet cotton strips and pour liquid nitrogen on the furnace in order to maintain the integrity of the furnace "O" ring seals. The temperature of the cell surface was measured using a Leeds-and-Northrup optical pyrometer with subsequent surface emissivity correction for the type of cell material. The magnetic shutter was closed except during temperature measurements to prevent the formation of mirror-like films on the viewport which affected the temperature readings.

A large proportion of the heating of the outside of the furnace was due to radiation from the Knudsen cell. Very little heat transfer was from conduction through the furnace since the pressure was maintained below 4×10^{-5} torr. In order to prevent this radiant flux from overloading the cooling capacity of the cold window (4 watts at 14°K), it was necessary to place a water cooled heat shield between the Knudsen cell and the cold window. This heat shield was made by sandwiching a spiral of 0.25 inch copper tubing between two 0.125 inch copper plates. A 0.125 inch hole was drilled through both plates which also served to improve the collimation of the molecular beam, thus reducing the thermal load of molecules hitting parts of the cold window assembly other than the actual sample window. Careful alignment of the heat shield hole and the Knudsen cell hole was necessary to ensure that the molecular beam impinged correctly on the cold window.

The molecular beam was cocondensed with an inert gas on the surface of the cold window. The temperature of the window was kept at ~14° K using an Air Product Displex^R Model CS 202 closed cycle helium refrigerator. The temperature of the cold window was monitored using a Kp/Au-0.07 at % Fe thermocouple mounted near the bottom of the cell window assembly. This assembly was made from a high purity, oxygen-free copper block with a ¼"-28 threaded stud for mounting to the second stage of the refrigerator. Indium gaskets were used to give good thermal conduction between the window holder and the refrigerator. These gaskets were also used between the cold window and its holder and between the heat shield and the first stage of the refrigerator.

The cold window was a disk of CaF_2 1 inch in diameter and 0.25 inch thick. A Suprasil II quartz window was originally used; however, this material was unsatisfactory for MCD since it exhibited a strongly temperature-dependent birefringence, probably induced during cooling by strain due to differences in the coefficients of thermal expansion of copper and quartz. Although CaF_2 could exhibit strain birefringence--it was used as a material for photoelastic modulators--perhaps the strain of cooling was more easily relieved since CaF_2 was somewhat softer than quartz. The windows on the outside of the vacuum shroud were 2-inch diameter Suprasil I quartz, and no birefringence could be detected due to their presence in the light beam. The temperature of the cold window was controlled by a 10 watt variable duty cycle heater in a feedback loop with the thermocouple signal. There was a 2° K temperature gradient between the top and the bottom of the window holder. The minimum temperature obtainable was 10° K.

The inlet nozzle for the isolant gas was made from a 16 gauge Yale stainless steel needle which was silver-soldered to a 0.25 inch diameter stainless steel tube. This tubing was silver-soldered through a hole in the wall of a short length of brass tubing which joined the furnace and the vacuum shroud of the cryostat. A 0.25 inch vacuum quick connect joined the inlet nozzle assembly to a 0.25 inch stainless steel tube leading to a glass inert gas manifold. The inert gas was fed into the vacuum system via a Nupro Extra Fine Metering Valve. The gas was passed through a liquid nitrogen cooled, stainless steel trap as an extra precaution to remove any contaminants. The entire gas manifold was diffusion pumped to 1×10^{-6} torr and baked at 60° C under vacuum for several days before the high purity gas was introduced into the three liter reservoirs via a Hoke 0.25 inch stainless steel needle valve.

A diagram of the rare gas manifold is shown in Figure 7. Note that there are two reservoir bulbs enabling rapid change between different isolant gases. The diffusion pump was a 3 inch Varian M2 loaded with 100 ml of Dow Corning 704 silicone oil. Ace Glass Company Teflon^{R} valves were

Figure 7. Inert Gas Manifold

1. Outlet to vacuum pumps
2. Glass, liquid nitrogen cooled trap
3. Three-liter gas storage bulbs
4. Ionization gauge
5. Mercury manometer
6. Isolant gas cylinder
7. Liquid nitrogen Dewar
8. Outlet to isolation apparatus
9. Extra-fine metering valve

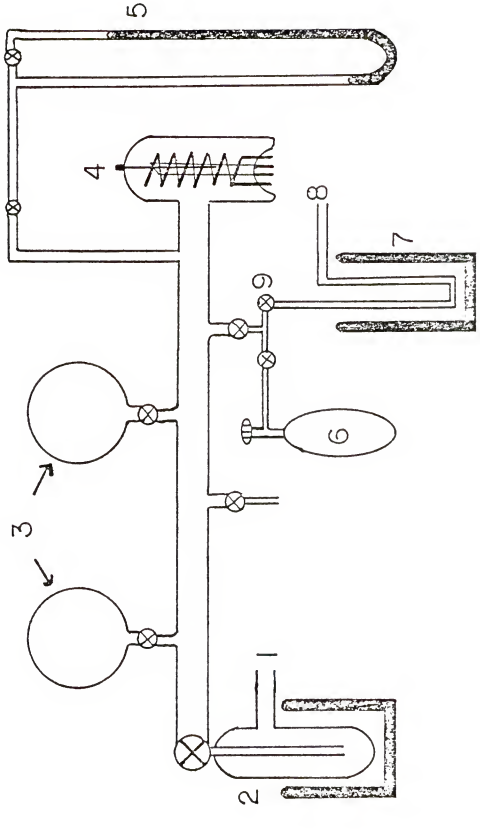

used for all other connections. The flow rate of the inert gas was measured using a standard mercury side-arm manometer.

During deposition of a matrix, the pressure in the system had to be low enough that the mean free path of the effusing molecules was longer than the distance from the furnace to the cold window. The pressure was maintained below 4×10^{-5} torr by a diffusion pumping system shown in Figure 8. The lowest pressure obtained with this system was 4×10^{-7} torr when the furnace was not in operation. The pressure was monitored by an ionization gauge and thermocouple gauge connected to a Granville-Phillips Series 270 Gauge Controller. The ionization gauge was mounted as close as possible to the Knudsen cell. The thermocouple gauge was mounted on the 0.25 inch line used for rough pumping of the system before the diffusion pump was opened to the system via a 2-inch diameter Consolidated Vacuum Company gate valve. A stainless steel liquid nitrogen trap was between the gate valve and the 2 inch Consolidated Vacuum Company diffusion pump, charged with 80 ml of Dow Corning 704 silicone oil. The system was rough pumped to a pressure below 200 microns before the gate valve was opened. Both of the roughing pumps were Welsh Scientific Company Duo Seal Model 1400.

Spectroscopic Apparatus

The cryostat was rotated so that the cold window faced the furnace and nozzle during deposition. When spectroscopic

Figure 8. Vacuum Pumping System

1. Inlet to furnace
2. Ionization gauge
3. Gate valve
4. Liquid nitrogen cooled trap
5. Baffle
6. Diffusion pump
7. Bypass valve
8. Thermocouple gauge
9. Bypass valve
10. To rough pump

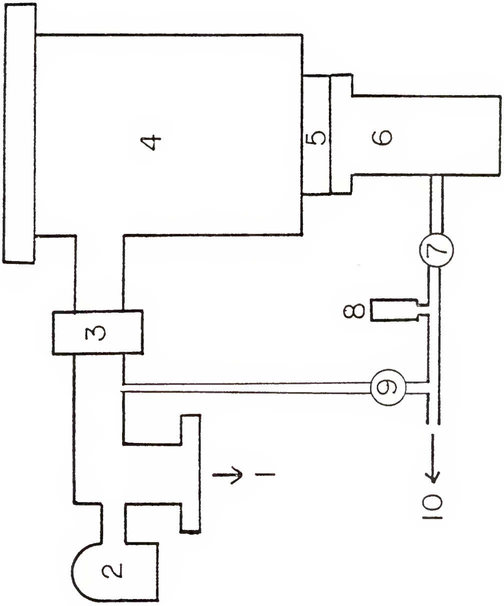

experiments were performed, the window was rotated 90° to intercept the light beam. Both MCD and absorption experiments were performed with approximately 15 minutes required for interchange between the two modes of operation.

This section deals with the optics and electronics for the absorption and MCD experiments. Finally, a description of the computer system and interface is presented.

A diagram of the absorption optics is given in Figure 9. The apparatus was designed to operate as a "pseudo-double beam" spectrometer. The reference beam was not passed through a matched cell, but since the various optical components and the matrix gases were transparent over the spectral regions studied, this presented little problem. Scattering from the matrices did cause some background drift at the shorter wavelengths, but the lamp emission spectrum was effectively nulled over most of the spectral range.

Spectra were obtainable over the range of 2500 to 8500 Å. There was a strong emission peak in the spectrum of the high pressure xenon lamp around 8400 Å which exceeded the dynamic range of the lock-in amplifiers used. This region gave poor nulling of the background during absorption experiments. The lamp was a 300 watt Eimac^R made by Varian Associates. This lamp operated at a pressure of 115 atmospheres of xenon and had a built-in parabolic reflector and a sapphire window yielding a well-collimated intense beam. The lamp was housed in a small hood for removal of

1. High pressure Xenon lamp
2. Monochromator
3. Collimation lens
4. Dual chopping wheel
5. Sample

5! Reference mirrors

6. Photomultiplier tube

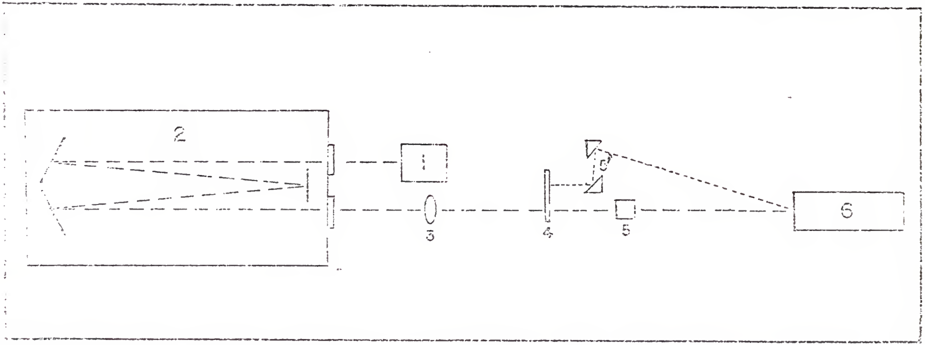

Figure 9. Absorption experiment optics.

the ozone generated during operation. This hood was attached to a Spex 0.75 meter Czerny-Turner Spectrometer with a 1200 line/mm grating blazed at 3000 Å with an f-number of 6.8. The slits were set for a spectral band pass of 1.5 to 3 Å which is about the limit of resolvable structure in Ar and Kr matrices.

The beam emerging from the monochromator was passed through a 3 inch quartz lens (f/3). This lens spread the beam so that it could pass through two sets of slots on a spinning wheel. The wheel was driven by a hysteresis-synchronous motor at 1800 rpm. The wheel contained 5 outer slots and 9 inner slots giving chopping frequencies of 150 Hz and 270 Hz. These frequencies were selected to minimize ac powerline pick-up since they were not integral multiples of the ac line frequency.

The light beam chopped at 270 Hz was passed through the matrix and onto the photocathode of an EMI 9683 QB photomultiplier tube in a Fact-50^R Peltier effect cooler. The spectral response of the tube was extended S-20, and the temperature of the tube could be maintained at -30° C for minimization of dark current. The light beam chopped at 150 Hz was reflected around the matrix by two Edmund Scientific aluminized front-surface mirrors and onto the same photomultiplier tube.

The chopping wheel assembly was equipped with two small 1.5 volt light bulbs and two phototransistors located on opposite sides of the chopping wheel from the lights such that the signal from the phototransistors were used as reference signals for the respective chopping frequencies. These signals were amplified by two RCA 3140 operational amplifiers. Both the light bulbs and the amplifiers were powered by batteries. A diagram of the absorption electronics is given in Figure 10.

The current output from the photomultiplier tube ($\sim 10^{-7}$ amp) was converted to a voltage by a 15 kΩ resistor connected to the ground. Part of the signal was amplified by a factor of 100 using an Analog Devices 52 k low-drift operational amplifier and sent to an oscilloscope for monitoring the wave shape during the experiment. The rest of the signal was presented in parallel to the inputs of two lock-in amplifiers: an Ithaco Model 353 Phase-lock Amplifier and an Ithaco Dynatrac 391A Lock-in Amplifier. The Model 353 amplifier was locked to the 150 Hz reference frequency from the chopping wheel, and its output was proportional to the lamp emission spectrum, monochromator dispersion characteristics, and the photomultiplier spectral response. The Model 391A was locked to the 270 Hz reference signal, and its output was proportional to the factors mentioned above plus the absorption spectrum of the matrix. Both outputs were connected to a Semiconductor Circuits, Inc., Log Amplifier which took the logarithm of both signals and performed an analog subtraction to give an absorbance output. This output was connected in parallel to the computer interface, *vide infra*, and the input of a Texas Intruments, Inc., Servo/Riter^{R} II Potentiometric Recorder.

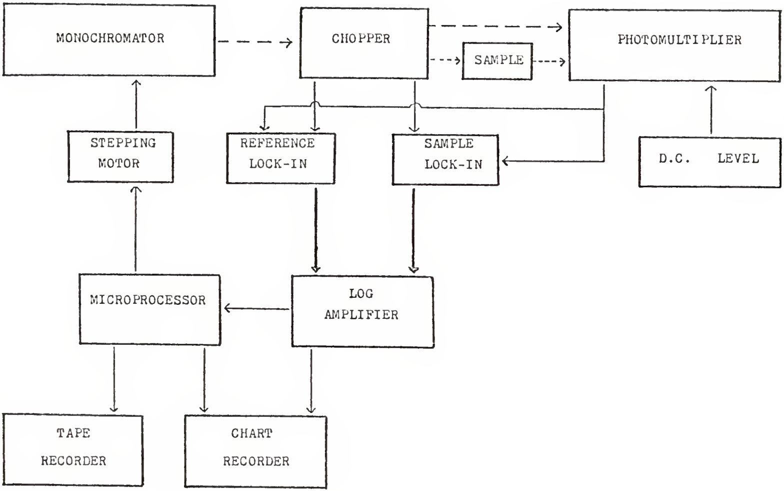

Figure 10. Electronics for absorption experiment.

The MCD experiments were performed with the same light source and monochromator. The mirror, lens, and chopping wheel for the absorption experiments were replaced by a cylindrical quartz lens (f/7) to collimate the beam which was passed through a Glan-Thomson prism oriented at an angle of 45° to the modulation axis of a Morvue Electronic Systems PEM-3^R photoelastic modulator. All current high sensitivity MCD instrumentation was based upon phase modulation using either electro-optic modulators (EOM) or photoelastic modulators (PEM). All EOM employed ADP/KDP crystals and required high voltages applied longitudinally. The angular aperture was small, and the transparent range was somewhat limited. A PEM was chosen because of the larger angular aperture and lower voltages. See Figure 11 for a diagram of the MCD optics.

An Alpha Model 4600 electromagnet with a 4 inch adjustable pole face gap was used in the MCD experiments. This magnet had a 0.75 inch hole collinear with the magnetic field, as required for MCD, and was mounted on tracks of case-hardened steel via open ball-bushings. This mobile mounting allowed the magnet to be freely moved in and out of position as required.

Figure 12 shows the MCD electronics. The signal from the photomultiplier tube was connected to an Ithaco Model 193 Lock-in Amplifier which was locked to the 50 kHz reference signal from the PEM. The bipolar output of this lock-in amplifier was level shifted to yield only positive voltages

OPTICAL TRAIN FOR MCD EXPERIMENTS

1. SOURCE
2. MONOCHROMATOR
3. COLLIMATION LENS
4. POLARIZER
5. MODULATOR
6. MAGNET
7. SAMPLE
8. DETECTOR

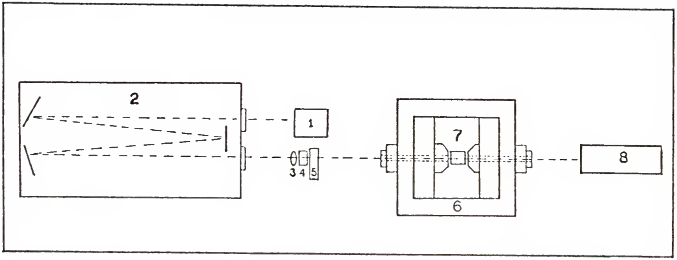

Figure 11. Optics for MCD experiments.

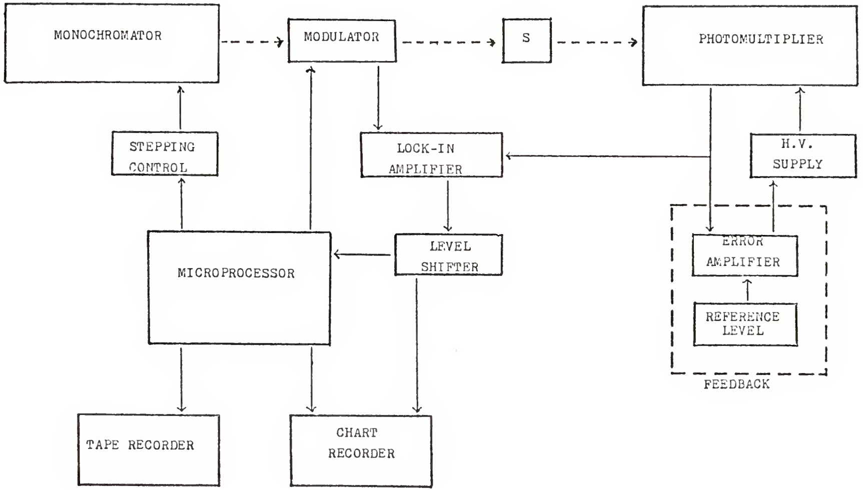

Figure 12. Electronics for MCD experiments.

suitable as chart recorder input and input to the computer interface. The output from the Analog Devices 52 k operational amplifier was sent to an error amplifier-feedback circuit.

This feedback circuit (see Figure 13) was similar to that of Krausz and Cohen,[43] but employs a Bertan PMT-20 (Option 3) programmable high voltage power supply. The reader should be cautioned that there are errors in the schematic in the Krausz and Cohen article and the circuit presented there will not function as drawn. The feedback circuit controlled the gain of the photomultiplier tube in an inverse relation to the dc output of the photomultiplier tube. The signal from the PM tube consists of a relatively small 50 kHz ac component riding on a larger dc component which is proportional to the lamp emission spectrum and the sample absorbance. Maintaining a constant dc level by the feedback circuit automatically corrects for these background effects in the MCD spectrum.

Both the absorption and MCD experiments were computer controlled. The original design employed a KIM I system from MOS Technology, Inc., but this system was later replaced by the more powerful Commodore PET 2001 microprocessor. The scanning of the wavelength was accomplished by pulses sent from the computer to a SLO-SYN^R Model MOGI-FD-301 stepping motor attached to the hand-scan control on the monochromator. This motor stepped 200 times per revolution allowing 0.25 Å/step.

Figure 13. Feedback Circuit for MCD

A. Input from Analog Devices 52K (DC level)
B. 15 v reference level
C. RCA 3140 operational amplifier
D. Voltmeter
E. Bertan programable high voltage power supply
F. 6.8 v Zener diode
G. Switch for manual or feedback control
H. 100 kΩ, 10 turn potentiometer
I. 5 kΩ, 10 turn potentiometer
J. 53.2 kΩ, 1% resistor
K. 1 kΩ, 1% resistor

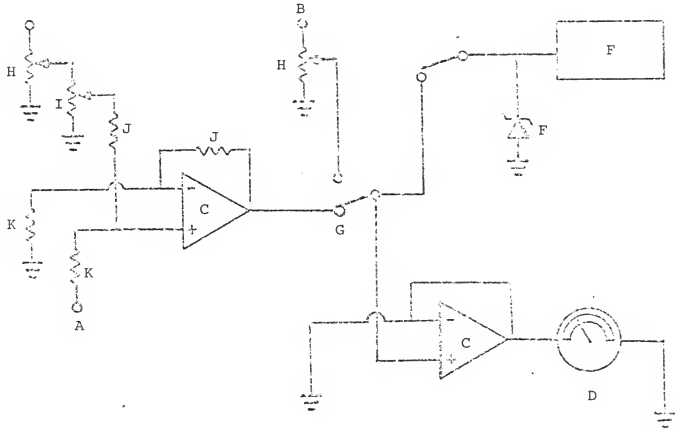
B
H
H
I
J
J
F
F
C
G
K
K
A
C
D

The data were digitized every angstrom using a Datel Systems, Inc. ADC-Ek8B analog-to-digital converter with 8 bit resolution. Because the PET computer had a rather modest memory capacity (8000 bytes), the maximum number of data points that could be taken and stored by the computer was 2000. The microprocessor was based on 6502 architecture which required data storage in blocks containing no more than 256 data points; therefore, the data were stored in 250 point blocks which were labeled alphabetically from A to H. After collecting a spectral scan, the data were stored on magnetic cassette tapes. A complete listing of the program for data collection and storage is found in the appendix.

The computer also controlled the photoelastic modulator synchronized with the wavelength drive. The wavelength of quarter-wave retardation by the modulator depended upon the amplitude of the stress applied to the quartz crystal which was linearly dependent upon an input voltage to the modulator. The program calculated the required voltage after each 0.25 Å step, and this output was sent to the modulator via a Datel Systems, Inc., DAC-IC8BC digital-to-analog converter. This same device was also used when a second program read data from the magnetic cassette tapes for output to the chart recorder or to the Nicolet 1180 computer. This program is also listed in the appendix.

A program was written in 1180 BASIC for the input of data fields up to 2000 Å wide into the Nicolet 1180 computer, storage on the Diablo disk system, and scaled plotting on the digital plotter for hard copy files. The program displayed the spectrum on the digital oscilloscope and plotted it using scale lengths determined by the operator. This program is also listed in the appendix along with a second program in 1180 BASIC used to assemble a full 8500 to 2500 Å scan from data blocks stored on the disk and for calibration of the final spectra. The assembled spectrum was then stored on the disk for later plotting using another program which is also listed in the appendix.

CHAPTER IV

EXPERIMENTAL TECHNIQUES

This chapter is concerned with the experimental procedure employed in obtaining a matrix isolated sample of the high temperature oxide of interest. The general techniques were very similar for all the oxides studied; the only real difference being the furnace temperatures employed. The various calibration procedures are also presented.

As mentioned in Chapter III, the material employed for the Knudsen cells was either tungsten or tantalum. These materials were made by a reductive extrusion process in the presence of an atmosphere of hydrogen, which became trapped in the metal interstices. Therefore, the cells were outgassed by heating to 2200°C under vacuum conditions for approximately 30 minutes. The release of hydrogen was readily monitored by observing the pressure in the furnace.

The cell was then loaded through the effusion hole with the required metal oxide. The cell was loaded as fully as possible since some of the oxide invariably blew out into the vacuum chamber during pump down and warm-up of the furnace. Any dust remaining from previous experiments was removed from the vacuum system by washing with Kimwipes soaked with acetone. The furnace flange and Displex^{R}

shroud O-rings were thoroughly cleaned and greased with Apiezon-N^R.

The Knudsen cell was then mounted via tantalum straps to the water-cooled copper electrodes making certain the effusion hole was aligned with the holes in the water-cooled heat shield and the CaF_2 window. This alignment was visually checked by sighting the Knudsen cell from the CaF_2 window while heating the cell to a dull red glow. Then by turning off the current to the furnace, the effusion hole in the cell could be observed as a spot glowing more brightly than the surrounding cell wall for several seconds. This effect was due to the fact that the interior of the Knudsen cell cooled more slowly than the exterior, and this technique helped insure proper alignment. This method was only employed after the system was under vacuum conditions.

The furnace was first rough pumped for 5 to 10 minutes using the bypass line to isolate the diffusion pump and liquid nitrogen trap. Rough pumping was continued until the system pressure was below 200 microns as monitored by the thermocouple gauge. The gate valve to the diffusion pump was then gradually opened; the bypass line was closed; and the system was diffusion pumped below 2×10^{-5} torr. Standard acetone spraying techniques were employed to check for leaks.

The furnace cell was then gradually heated to the deposition temperature while maintaining the pressure below 2×10^{-5} torr. Too rapid warm-up caused blow-out of material from the cell and led to weakly absorbing matrices; this preheating usually took several hours to accomplish. During this time the Displex^R was rotated so that the heat shield protected the clean CaF_2 window from material effusing from the furnace. This material could be observed as a film on the heat shield.

The CaF_2 window had to be cleaned with acetone between subsequent experiments in order to insure good matrices. Merely warming the window to remove a matrix without also washing with acetone was not sufficient cleaning since the next matrix deposited was invariably cloudy.

After preheating, the cell was often cooled to 800°C and left overnight at this temperature. The cell was then heated to 200°C below the deposition temperature; the Displex^R compressor was turned on to cool the window to 14°K. The rare gas cold trap was then filled with liquid nitrogen, and the leak valve opened so that 1 to 3 mmol/hr flowed into the system. The CaF_2 window was rotated so that the rare gas could impinge on the cold surface for 10 minutes before the furnace temperature was increased to the deposition temperature.

The flow rate for the rare gas was kept low to insure clear matrices and avoid polarization scrambling in the MCD experiments. The ratio of oxide to rare gas was estimated to be 1000:1. Deposition continued 45 to 60 minutes, and many of the matrices showed pronounced color. The furnace temperature was then reduced to 800°C, and the rare gas was allowed to flow for 5 minutes longer. The CaF_2 window was then rotated 90° so that its absorbance could be measured. If the absorbance of the strongest bands was below 0.5, further deposition was carried out until the absorbance was in the range of 0.5 to 0.95. The maximum signal-to-noise ratio in MCD experiments occurred when the absorbance was 0.87.[44] If the absorbance was deemed sufficient, the furnace was allowed to cool to room temperature.

Both MCD and absorption experiments were performed before and after annealing at 30 to 33° K for 30 minutes. Spectra were taken at 14 and 24° K. If the spectra exhibited any temperature dependence, they were recorded at 2 to 3° K intervals between 14 and 24° K.

The monochromator was calibrated to within 0.5 Å using the lines from a Spectra Physics 4W argon ion laser. Wavelength scanning was always from low to high energy insuring maximum phototube sensitivity and avoiding a 1 Å backlash error in the stepping motor assembly.

The MCD spectra were recorded at 5.5 kilogauss as determined by an F. W. Bell Model 640 Gaussmeter. Zero field dichroism spectra were recorded to determine the zero line in the MCD. With the magnet power supply turned off there was a residual field of 62 gauss.

The MCD apparatus was calibrated for each matrix spectra obtained using aqueous solution of the dichroic complex $[Co(en)_3]Cl\cdot$(d-tartrate) with an absorbance of 1.00 at 4690 Å as measured on a Cary 14 spectrometer. The procedure was similar to that of Tacon,[45] and the circular dichroism

(CD) of this solution was measured at 4930 Å using the same conditions under which each MCD was obtained. McCaffery and Mason[46] measured the CD and absorption spectra of this compound. The absorption band at 4690 Å has a CD maximum at 4930 Å with $\Delta A_{max}/A_{max}$ equal to 0.0225.* The compound was synthesized using the method of Broomhead[47] and had the same specific rotation, $[\alpha]_D$, of +103° as reported. This same solution was used to calibrate the absorbance experiment. Equation 42 below was used in the calibration of the digitized MCD data.

$$\Delta A = 0.0202\left(\frac{f(sam)}{f(std)}\right)\left(\frac{I_\lambda(sam)-I_\lambda(O)}{I_\lambda(std)-I_\lambda(O)}\right) \tag{42}$$

where

$f(sam)$ = lock-in amplifier sensitivity for MCD of the sample

$f(std)$ = lock-in amplifier sensitivity for CD of the standard

$I_\lambda(sam)$ = digitized value for sample MCD at wavelength λ

$I_\lambda(O)$ = digitized value for the zero field value at wavelength λ.

---

* Value reported in McCaffery and Mason's article.[46] Value used in Tacon's Thesis 0.0202.

CHAPTER V

RESULTS OF TiO EXPERIMENTS

This chapter and the next are concerned with the experimental results obtained for the group IVb diatomic oxides. The results for ZrO and HfO will be discussed together. The spectra of ZrO and HfO are similar since their ground state configurations are the same but differ from that of TiO. This reversal of configuration also occurs in group Vb in which VO differs from NbO and TaO. Table 1 lists the ground state configurations of groups IVb and Vb.

Although titanium is relatively abundant in the earth's crust (0.6 %)[48] and TiO is one of the most stable compounds known--its dissociation energy is 159.8±3 kcal/mole[49]--the diatomic oxide of titanium is seldom encountered on earth. The preferred form is TiO_2 which occurs in the minerals rutile, anatase and brookite.

Even though relatively rare terrestrially, TiO is one of the most widely spectroscopically studied transition metal oxides. With the exception of ScO, TiO is the simplest transition metal oxide with d electrons involved in chemical bonds. Any adequate theory of chemical bonding must be able to account for the role that d electrons play. The spectra of relatively cool class M and S stars are dominated by

TABLE 1

Ground State Configurations of the Diatomic Oxides of Groups IVb and Vb

Oxide	Spectroscopic Term	Configuration
TiO	$^3\Delta_R$	$(\delta\sigma)$
ZrO	$^1\Sigma^+$	(σ^2)
HfO	$^1\Sigma^+$	(σ^2)
VO	$^4\Sigma^-$	$(\delta^2\sigma)$
NbO	$^2\Delta_R$	$(\delta\sigma^2)$
TaO	$^2\Delta_R$	$(\delta\sigma^2)$

absorption lines attributable to TiO; therefore any theories of the thermodynamics of stellar atmospheres must include consideration of the role of TiO. It is possible to use the rotational profile of TiO to determine the temperature of stellar atmospheres. The visible spectrum of TiO has been studied extensively since the early work of Lowater[50] on the γ system published in 1927 and Christy's work[51] on the α system in 1929. Since that time, well over 60 articles have appeared in the literature concerning the spectrum of the molecule. Tracing the changes in state assignments through the literature from 1927 to the present demonstrates the complexity involved in the analysis of the spectrum of this simple oxide. For example, the α and γ systems' assignments have been revised several times. In the late 1920's, the α system was considered to be a $^3\Pi$-$^3\Pi$ transition, and the γ was $^3\Sigma$-$^3\Pi$. In the early 1950's, Phillips[52] revised the assignment of the γ system to $^3\Delta$-$^3\Pi$ by analysis of spectra taken using a grating spectrometer 21 ft long. In 1954, Uhler[53] suggested that the ground state of TiO was $^3\Delta_R$ on the basis of comparison with the spectra of ZrO. The assignments had to be revised again, and the presently accepted assignment for the α system is $C^3\Delta$-$X^3\Delta$. The MCD results presented here confirm these assignments.

Carlson and Moser[54] and Carlson and Nesbet[55] carried out the first *ab initio* calculations on a heteronuclear molecule containing a transition metal. The TiO molecule was chosen for study since it was the best characterized diatomic of this type with the fewest number of electrons. At that time the cost of calculation of Hartree-Fock wavefunctions for even the simplest compounds containing third row elements was prohibitively expensive; therefore, they employed a very limited basis set representing the normally occupied atomic orbitals and those orbitals of higher angular momentum which substantially contributed to the representation of polarization and distortion of atomic valence orbitals. Nineteen basis functions were used that had been previously optimized as a minimal self-consistent field basis for the atoms.[56] These calculations confirmed Uhler's prediction that the ground state of TiO was $^3\Delta_R(\delta\sigma)$. This assignment was in contrast to a predicted $^3\Sigma^-(\delta^2)$ ground state proposed by Berg and Sinanoglu[57] based on the ligand field splitting of the d-orbital degeneracies for the metal ion, $Ti^{2+}(3d^2)$, in the field of the oxide ion. The $^3\Sigma^-$ term was actually predicted by Carlson's calculations to be very high in energy due to large electron repulsion effects and has not been observed experimentally. A simple molecular orbital diagram for the ground state of TiO is presented in Figure 14. Later calculations by Carlson and Moser[58] indicated that in the ground state configuration of TiO, $^3\Delta_R(\delta\sigma)$, the δ electron density is located primarily on the Ti atom, and the σ density is located primarily on the O atom.

The two lowest-lying singlet states, $^1\Delta$ and $^1\Sigma^+$, were attributed to the configurations $(\delta\sigma)$ and (σ^2), respectively. The $^1\Sigma^+$ state was observed earlier by Peterson[59] and Peterson and Lindgren[60] and the $^1\Delta$ state by Phillips.[61]

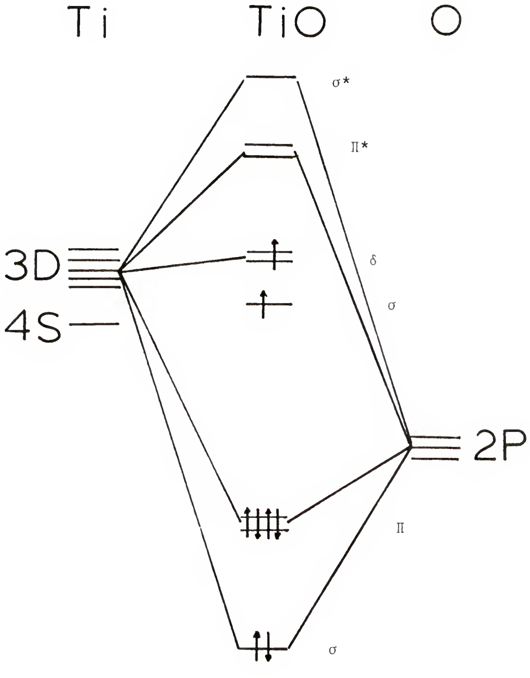

Figure 14. TiO MO diagram.

The prediction of a $^3\Delta_R$ ground state was confirmed by Weltner and McLeod[62] in the first matrix isolation study of TiO in 1965. By employing ^{18}O-substitution and comparison with gas phase results, they were able to establish (0-0) band positions and vibrational progressions for the α, γ and γ' systems in neon and argon matrices.

The TiO matrices reported in this dissertation were prepared in argon under similar conditions using TiO_2 powder (Alfa, 99+% optical grade). Knudsen cell temperatures were in the range of 2150 to 2250°K with argon flow rates 2.5 mmol/hr. The α, γ and γ' systems were observed in addition to the weak ε system later reported by McIntyre, Thompson and Weltner.[63] The ZFA band positions in argon are listed in Table 2, and a representative ZFA spectrum for the α, γ and γ' systems is presented in Figure 15.

The α bands compose the shortest wavelength grouping and clearly demonstrate the potential utility of MCD in assignment of symmetry. Since the multiplet splitting of the $^3\Delta_R$ ground state is regular, the ground multiplet is $^3\Delta_1$. The next higher energy state is the $^3\Delta_2$, which is 96.4 cm^{-1} above the $^3\Delta_1$ state. The $^3\Delta_3$ state is 101.1 cm^{-1} above the $^3\Delta_1$ state.[64] Assuming a Boltzmann distribution at 24°K, only 3 molecules in 1000 would be in the $^3\Delta_2$ state and 7 molecules in a million would be in the $^3\Delta_3$ state. Therefore, the only absorptive transitions observed under these conditions will originate from the $^3\Delta_1$ state. For case a coupling, $^3\Delta_1$ is a rather special state since its magnetic moment will be zero due to the opposition of the

Figure 15. ZFA of TiO.

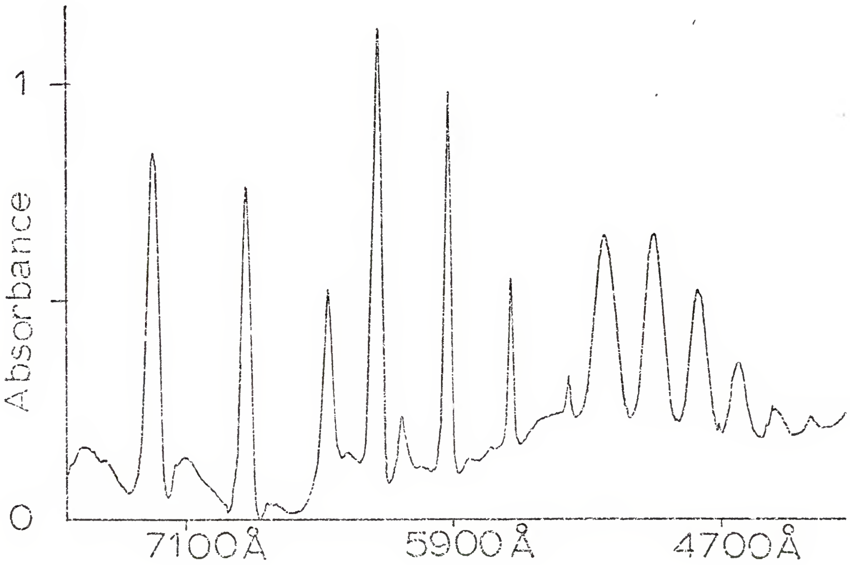
1
Absorbance
0
7100 Å
5900 Å
4700 Å

TABLE 2

Absorption Bands of TiO in an Argon Matrix

Band	v'	λ, Å*	λ, Å†	ν, cm^{-1}	$\Delta G'_{v'+\frac{1}{2}}$, cm^{-1}
γ	0	7253	7254	13785	841
	1	6839	6837	14626	832
	2	6470	6469	15458	842
	3	6142.5	6135	16300	
γ'	0	6254.5	6254	15990	845
	1	5941	5940	16835	848
	2	5657	5655	17683	836
	3	5400.5	5400	18519	
α	0	5241.5	5241	19080	824
	1	5023.5	5024	19904	817
	2	4825	4826	20721	817
	3	4645	4634	21580	741
	4	4478	4480	22321	
ε	0	8394	8390	11919	910
	1	7798	7795	12829	
	?	8166	8160	12255	

---

* See References 61 and 62.

† Experimental data.

spin and orbital angular momenta, i.e., $<{}^3\Delta_1|L_z+2S_z|{}^3\Delta_1> = 0$. A similar situation arises in ${}^2\Pi_0$ states which also have zero magnetic moment. Since TiO contains comparatively light nuclei with an atomic number of 22 for Ti and 8 for O, one would expect case a coupling which would cause all transitions ${}^3\Delta$-${}^3\Delta$ to be forbidden in MCD. In case c coupling only one transition would be allowed, i.e., ${}^3\Delta_2 \leftarrow {}^3\Delta_1$ where $\Delta m_\Omega = \pm 1$. Figure 16 shows the magnetic field splitting for these states and the only allowed MCD transition in case a or case c. Figure 17 shows the ZFA spectrum recorded in this region. The lack of an MCD signal is good evidence for case a coupling in TiO. Phillips[65] also notes that in the gas phase spectra all of the triplet systems in TiO correspond to Hund's case a. The small positive MCD peak at 4835 Å is due to the presence of Ti atoms which are present in the matrix, *vide infra*. This Ti atomic absorption is responsible for the distortion observed in the (2-0) band of the α system. This transition was observed in a matrix isolation study of Ti atoms by Gruen and Carstens[66] and was assigned by them to the $z^3D_1^0 \leftarrow a^3F_2$ transition. This peak exhibited the temperature dependent behavior expected for the C-term characteristic of a ${}^3F_2$ ground state.

Laser excitation into the α system of TiO was used by Brom and Broida[67] in 1975 to measure the relative energy spacing between the singlet and triplet manifolds. The value obtained was 3500 cm^{-1} between the isoconfigurational $a^1\Delta$ and $X^3\Delta$ states which was in good agreement with theoretical predictions but was in conflict with the 1952 results of

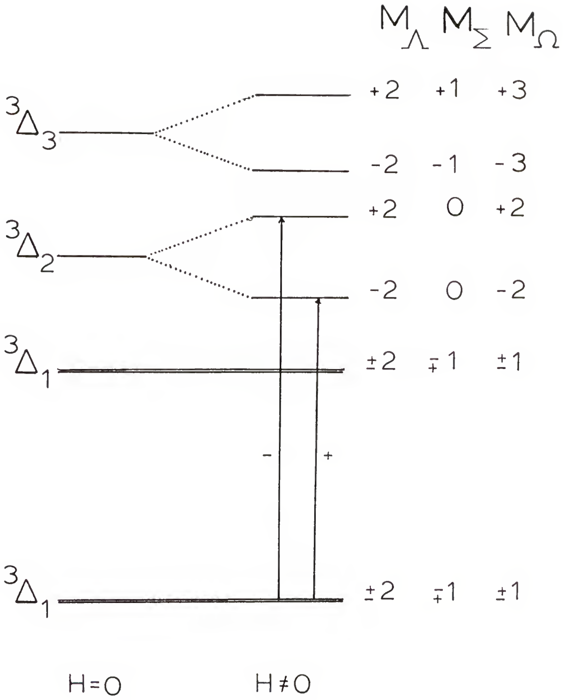

Figure 16. Magnetic field splittings and MCD allowed transitions in the α bands of TiO.

Figure 17. ZFA and MCD spectra for the α bands of TiO.

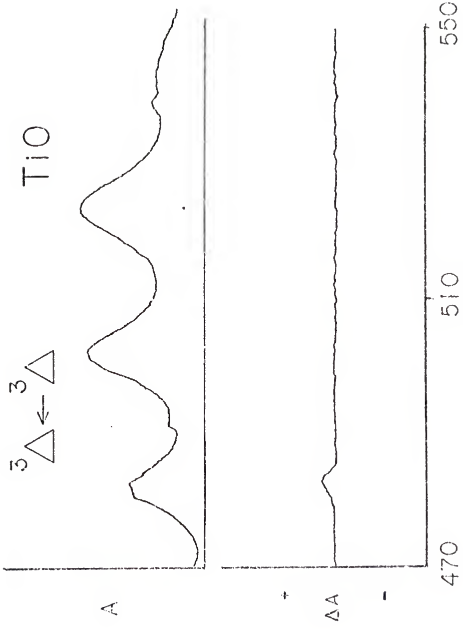
TiO
$^3\Delta \leftarrow {}^3\Delta$
A
+
ΔA
-
470
510
550
NM

Phillips.[68] The earlier work was based on population analyses of gas phase spectra and stated that an energy difference ranging from 274 to 804 cm^{-1} with an average difference of 581 cm^{-1} existed between the low-lying $a^1\Delta$ level and the ground state which was considered to be $^3\Pi$ at that time.

Several unsuccessful attempts were made to use excitation with a Spectra Physics 4W Argon ion laser to observe magnetic circularly polarized emission. The small bore of the magnet and the long distance required between the sample and the photomultiplier tube resulted in the unsuccessful completion of these experiments. The photomultiplier tube had to be at least 20 in from the matrix because of the large effect of the magnetic field on the gain of the tube. Other attempts to observe magnetic circularly polarized emission using a more compact superconducting magnet were also unsuccessful.[69]

After the α system the next lower energy band system observed in an argon matrix was the γ' system. This system was first discovered by Coheur[70] in 1943 in gas phase spectra taken using an exploding titanium wire. The γ' bands are often much stronger on astronomical plates of M-type stars than on laboratory plates[65] and are the most intense bands observed in the matrix spectra. The γ' system lies in an extremely crowded region in the gas phase spectra, and the analysis therefore has been a difficult task. Many of the rotational lines are still unassigned.

The ZFA spectrum of the γ' system is illustrated in Figure 15, and the MCD spectrum is presented in Figure 18. The assigned transition for the γ' system is $B^3\Pi \leftarrow X^3\Delta_R$. Since spin-orbit coupling occurs in the $B^3\Pi$ state, the multiplet structure of the state must be considered in the calculation of the MCD terms. Phillips[64] gives a multiplet spacing of 21.6 cm^{-1} between the lowest energy $^3\Pi_0$ and $^3\Pi_1$ multiplets and 16.2 cm^{-1} between the $^3\Pi_1$ and the highest energy $^3\Pi_2$ multiplets. The only transition allowed in case a coupling is the $B^3\Pi_0 \leftarrow X^3\Delta_1$ and is illustrated in Figure 19. The forbidden transition $B^3\Pi_1 \leftarrow X^3\Delta_1$ has been observed in gas phase spectra.[64] In MCD spectra involving case a coupling this transition is forbidden since $\Delta m_\Sigma \neq 0$, and in case c coupling the $\Delta m_\Omega = \pm 1$ selection rule is also broken. The $B^3\Pi_1 \leftarrow X^3\Delta_1$ transition is also forbidden in MCD for case a coupling since $\Delta m_\Sigma \neq 0$. The calculation of the value for the MCD term $\mathcal{A}_1/\mathcal{D}_0$ from equations 21 and 30 yields a value of +1β for the $B^3\Pi_0 \leftarrow X^3\Delta_1$ transition which agrees with the experimentally observed sign of the MCD observed for this system. Table 3 lists the positions of the positive and negative going peaks in the MCD for the v' = 0,1,2,3 of the γ' system of TiO in an argon matrix.

The broad and sharp structure present in the γ' system is illustrated in an expanded spectrum of the (0,0) band in Figure 20. This band can be considered as composed of two sharp positive $\mathcal{A}_1$ terms and one broad positive $\mathcal{A}_1$ term originating from different sites in the matrix. The other possible interpretation is that the structures might be due

Figure 18. MCD Spectrum of the γ and γ' bands of TiO.

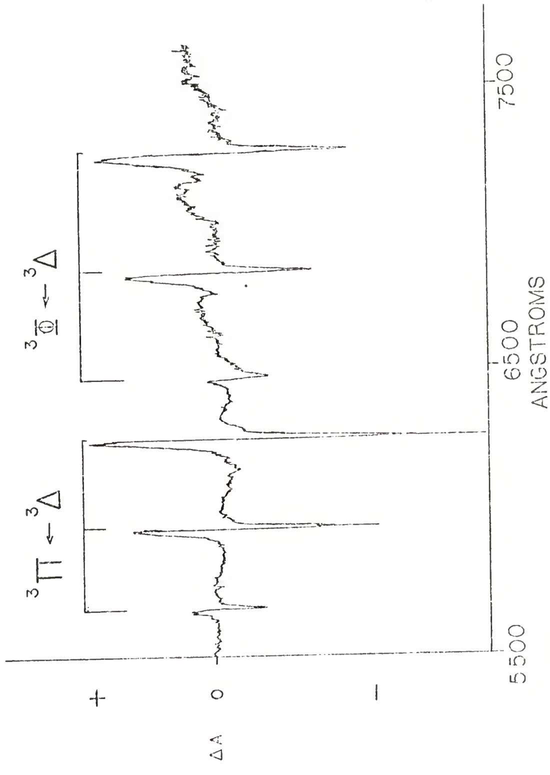
$^3\Pi \leftarrow {}^3\Delta$
$^3\Phi \leftarrow {}^3\Delta$
ΔA
+
0
−
5500
6500
7500
ANGSTROMS

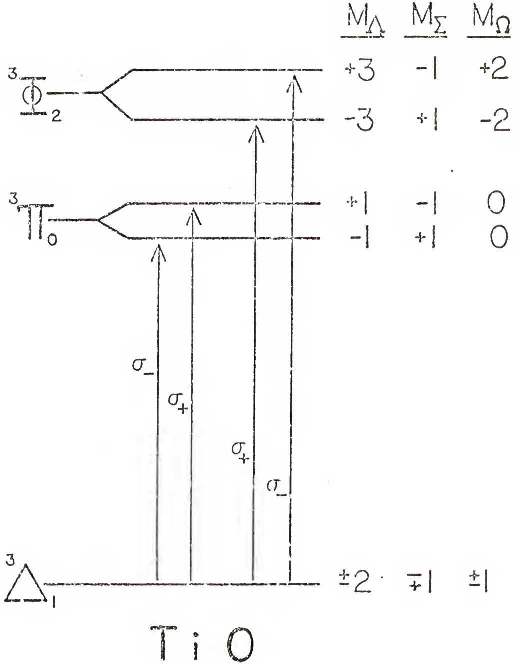

Figure 19. Magnetic field splittings and MCD allowed transitions for the γ and γ' bands of TiO.

TABLE 3

MCD Peak Positions of Positive and Negative Lobes of the γ' System of TiO in an Argon Matrix

v'	λ (Å)	$\bar{\nu}$ (cm^{-1})	Sign	Shape
0	6290	15898	−	Broad
	6264	15964	−	Sharp
	6258	15980	+	Sharp
	6256	15985	−	Sharp
	6253	15992	+	Sharp
	6248	16005	+	Broad
1	5969	16753	−	Broad
	5948	16812	−	Sharp
	5944	16824	+	Sharp
	5941	16832	−	Sharp
	5937	16844	+	Sharp
	5930	16863	+	Broad
2	5684	17593	−	Broad
	5663	17658	−	Sharp
	5654	17687	−	Sharp
	5644	17718	+	Broad
3	5404	18505	−	Broad
	5442	18376	+	Broad

Figure 20. Expanded scale MCD spectrum of the (0,0) band of the γ' system of TiO.

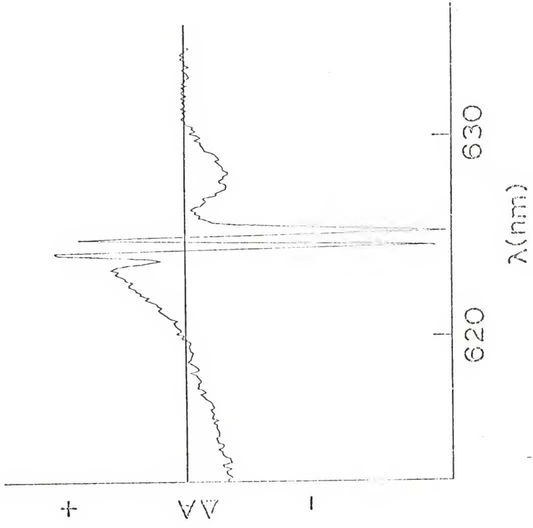
+
ΔA
−
620
630
λ(nm)

to the splittings of the multiplets $^3\Pi_0$, $^3\Pi_1$ and $^3\Pi_2$. Although the $^3\Pi_1$ state has been observed in gas phase spectra and the splitting of the sharp peaks is close to the multiplet spacing, the MCD transitions to the $^3\Pi_1$ and $^3\Pi_2$ are forbidden and a calculation of the MCD $\mathcal{A}_1/\mathcal{D}_0$ terms from equations 21 and 30 yields -1β and -3β, respectively. The interpretation of these structures as due to site effects on a single transition is also supported by the fact that the sharp structures were not observed in all matrices, and the relative intensities changed on annealing the matrix.

Different site effects are often noted in matrix isolation experiments. The site splittings noted here are among the sharpest yet observed for MCD spectra. These unique energy sites in the Ar matrix are probably due to the discontinuous and highly structured nature of the Ar film. When Ar is deposited from the vapor state at low temperatures the crystals formed are of poor crystalline quality with very small grains, which contain many twins, stacking faults, and dislocations.[71] The films are defective because the number of individually nucleated crystals rises dramatically as the temperature is lowered at constant pressure. Kovalenko and Bagrov[72] studied the diffraction of electrons from Ar films deposited at different temperatures. The electron diffraction may be interpreted in terms of small coherently diffracting blocks where the block size is roughly the distance between dislocations in the crystal. For Ar deposited at 16-23°K the block size was estimated to be 70-80 Å and 20-30 Å for deposition at 5-15°K.

Assuming a block size of 30 Å for deposition at 14°K, the isolation temperature used for TiO, it is possible to calculate the relative number of substitutional sites on the surface and in the interior of these blocks. The total number of atoms in a face-centered cubic lattice of Ar 30 Å on an edge is approximately 1000. There are 370 substitutional sites on the outer surface layer and 468 sites within one layer of the surface. Therefore, approximately half of the sites are on the surface of these small Ar crystals. Annealing at 30-35°K allows the diffusion of TiO to different sites, but the temperature must be raised to 48°K for the size of these Ar crystals to change.

Very broad peaks are observed to lower energies of the γ' and γ bands. These peaks are most likely due to the presence of other species present in the matrix. These peaks were also present in the spectra taken by Weltner.[73] Some of the pertinent observations are listed below:

1. The intensity of the broad peaks relative of the γ and γ' bands in the ZFA and MCD spectra varies between matrices. The spectrum of Ti atoms dominate below 4000 Å, and the matrices which have strong bands for Ti atoms also have strong bands for these broad features.

2. The MCD bands of the broad peaks display the characteristic inverse temperature dependence of C_o terms, implying that the ground state is magnetically degenerate. Figure 21 shows the MCD temperature dependency of the broad peak at 3574 Å.

3. The relative intensity of the broad peaks to the γ and γ' bands varies greatly between the ZFA and MCD spectra. In the MCD spectra the broad peaks are much more intense than in the ZFA spectra which would further support the C_o observation since the magnitude of a C_o term contribution is much greater than an A_1 term.

Figure 21. Temperature dependent MCD spectra of the broad 7600 Å band observed in Ar matrices of TiO.

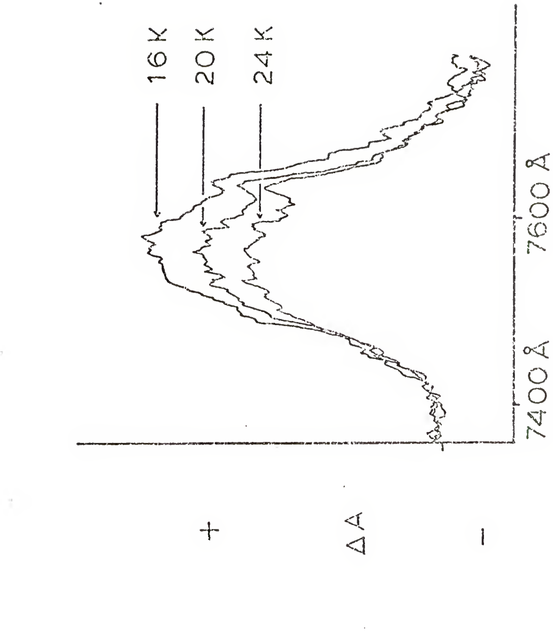
16 K
20 K
24 K
7400 Å
7600 Å
+
ΔA
−

4. The sign of the C_0 term for the broad peaks associated with the γ' system is negative and positive for the γ system.

5. As the temperature of the Knudsen cell during deposition was increased from 2140 to 2260°K, the proportion of these broad peaks also increased.

Table 4 lists the ZFA and MCD peaks for these broad bands associated with the γ and γ' systems. The vibrational spacings are close to the values obtained for the γ and γ' transitions. Due to the breadth of the transitions the peak maxima are uncertain by about 20 cm^{-1} and there is a shift to lower energies in the MCD spectra.

Recently, Hildenbrand[74] has measured the equilibrium constant for the gaseous reaction $Ti + TiO_2 \rightleftarrows 2TiO$ between 1975 and 2222°K. The equilibrium constant was found to vary between 5.05×10^{-2} @ 1975°K to 2.72×10^{-2} @ 2222°K. The mole percent of TiO and Ti in a vapor at 1975°K is 45% each with 10% TiO_2. The percentage of TiO_2 decreases slightly to 8% upon increasing the temperature to 2222°K. Although Weltner[63] did observe infrared bands at 940 cm^{-1} attributable to TiO_2 in Ne matrices, the effect of temperature on the equilibrium and the opposite effect noted in observation 5 above would disfavor TiO_2. By illumination with a mercury lamp, he also observed emission from TiO_2 in Ne, but the (0,0,0)-(0,0,0) band of the transition occurred at 5295 Å, a much shorter wavelength than the present broad bands. The fact that bulk TiO_2 is white would also tend to eliminate it from consideration. Electric deflection studies[75] of TiO_2 also indicate that it has a permanent dipole moment indicative of a bent structure. Therefore, the orbital

TABLE 4

ZFA and MCD Peak Positions for Broad Bands Associated with the γ and γ' Systems of TiO Isolated in Argon Matrices

	ZFA λ (Å)	MCD λ (Å)	MCD ν (cm^{-1})	$\Delta G'_{v+\frac{1}{2}}$ (cm^{-1})
	7537	7574	13203	795
γ Band	7112	7144	13998	863
	6711	6729	14861	
	6469	6484	15423	840
γ' Band	6134	6149	16263	819
	5834	5854	17082	

contribution to the ground state magnetic moment will be zero since it will be orbitally non-degenerate; however, this does not exclude a spin contribution which could yield a $\mathcal{C}_o$ term.

The close association of the broad peaks with the γ and γ' systems indicates a similarity between the unknown species and TiO. The likely possibilities include aggregates of TiO molecules in a geometry suitable for a ground state magnetic moment to be generated or for a weak complex of Ti and TiO. With the available data it is impossible at this time to make a conclusive assignment.

The γ bands correspond to the transitions $A^3\Phi \leftarrow X^3\Delta_R$. From the Boltzman population considerations above only transitions from the $^3\Delta_1$ level are observed in these studies. Figure 15 shows the ZFA absorbance spectrum of the γ band system. The only MCD allowed transition is the $A^3\Phi_2 \leftarrow X^3\Delta_1$. The magnetic field splitting is illustrated in Figure 19, and evaluation of the $\mathcal{A}_1$ term which is observed in the MCD spectrum is illustrated in Figure 18. The site splittings observed in the γ' system is much less pronounced in the γ system. Several matrix MCD spectra at 14°K show splitting of the negative-going lobes of several wavenumbers, but these features disappear on warming the matrix to 24°K due to the general broadening of the transitions at higher temperatures. Table 5 lists the wavelengths for the positive- and negative-going lobes of the MCD of the γ system. The zero crossing positions in Table 5 and the ZFA

TABLE 5

MCD Peak Positions for γ System of TiO Isolated in an Ar Matrix

v'	γ (Å)	$\bar{\nu}$ (cm^{-1})	MCD Sign	Zero (Å) Crossing
0	7270	13755	−	7253
0	7235	13822	+	
1	6853	14592	−	6840
1	6826	14650	+	
2	6481	15430	−	6469
2	6457	15487	+	
3	6150	16260	−	6142
3	6133	16305	+	

maxima in Table 2 agree within one Ångstrom as would be predicted for an MCD $\mathcal{A}_1$ term.

The very weak ε system was first observed in matrices by Weltner et al.[63] and assigned to the transition $E^3\Pi \leftarrow {}^3\Delta_R$. The only MCD allowed transition is illustrated in Figure 19 as in the $B^3\Pi$ state. These weak bands occur in the near IR region where instrumental sensitivity is poor due to low photomultiplier tube response and decreasing light levels. Often, the most sensitive lock-in amplifier range was required to detect the MCD signal. A strong lamp emission band occurs near the (0,0) transition and causes considerable difficulty in ZFA spectra of that region.

The MCD spectrum of the (0,0) band of the ε system is shown in Figure 22, and the predicted positive $\mathcal{A}_o$ term is present. Strong site splitting is observed as in the $B^3\Pi$ state. Three distinct sites are noted in this matrix spectrum, but in other matrices the intermediate energy site is much more dominant.

The ultraviolet region of the spectrum is somewhat congested due to the presence of many electronic transitions of both TiO and Ti. Pathak and Palmer[76] observed a triplet-triplet emission system designated $D\text{-}X^3\Delta$ in the flame spectrum of TiO. They were not able to assign vibrational progressions because the spacing was irregular. Shortly after this work was published, Weltner[63] was able to observe this system in absorption of TiO isolated in Ne matrices at 4°K. The same type of features were observed in the matrix spectra which indicated that the bands arose from at least

Figure 22. MCD spectrum of the ε band of TiO.

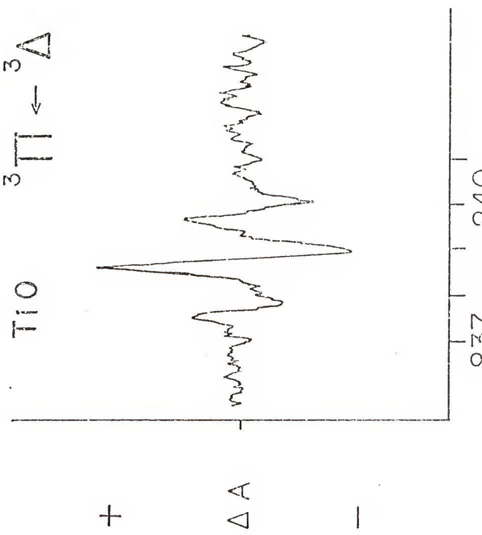
TiO
$^3\Pi \leftarrow {}^3\Delta$
837
840
NM
+
ΔA
−

two perturbing electronic states designated as systems I and II. Both systems appeared to be perturbed at several vibrational levels since the vibrational progressions do not exhibit any regular behavior.

An absorption spectrum of an argon matrix containing TiO and Ti is presented in Figure 23. The bands for Ti atoms are more intense than TiO in this spectrum and correlate well with Ar matrix spectra of Ti analyzed by Gruen and Carstens.[77] Since the ground state of Ti is $^3F_2$ and magnetically degenerate, strong C_0 terms are observed in the MCD spectrum illustrated in Figure 24. These C_0 terms dominate the weaker A_1 terms for TiO, but the temperature independent, derivative character of the A_1 terms facilitates the assignment of the TiO peaks. Table 6 presents the correlation between the Ne matrix spectra of TiO obtained by Weltner[63] and the Ar matrix spectra obtained in this work. The presence of positive A_1 terms indicate that the D state of TiO cannot be a $^3\Delta$ state, but does not distinguish between $^3\Pi$ and $^3\Phi$ states, suggested by Wentink and Spindler[78] for the D state of TiO.

The sign of the C_0 terms observed for the Ti atomic transitions can be used to check the tentative assignments of Gruen and Carstens.[77] Table 7 lists the Ti atomic transitions observed in Ar matrices along with the observed MCD signs and calculated MCD C_0 terms based upon the proposed assignments. Two of the MCD signs are in conflict with the assignments of Gruen and Carstens. The band at 2874 Å has a negative MCD C_0 term, but the value predicted from their

Figure 23. ZFA spectrum of the ultraviolet region of an Ar matrix of TiO and Ti.

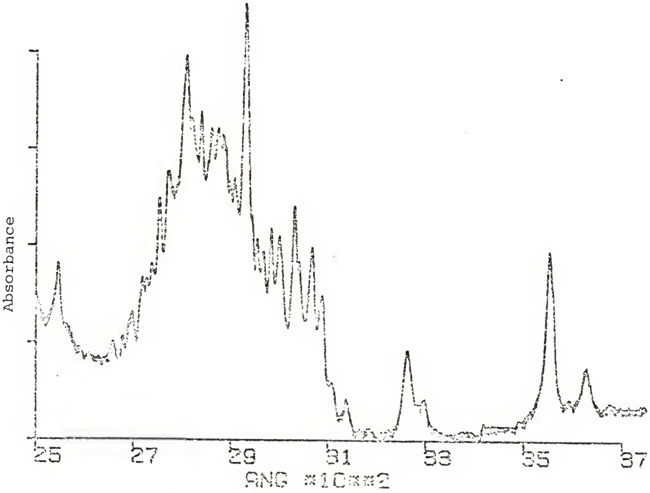
Absorbance
25
27
29
31
33
35
37
RNG *10**2

Figure 24. MCD spectrum of the ultraviolet region of an Ar matrix of TiO and Ti.

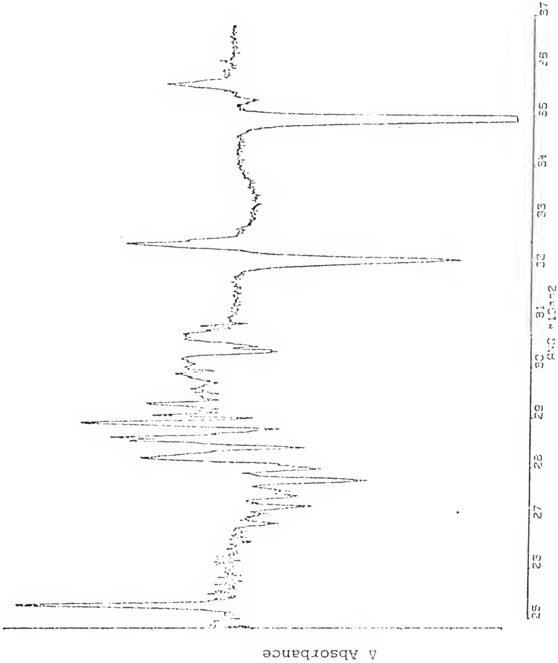
25
26
27
28
29
30
31
32
33
34
35
36
37
ENG *10**2
Δ Absorbance

TABLE 6

Ultraviolet Transitions Observed for TiO in Argon and Neon Matrices

Ne Matrix* λ (Å)	Ar Matrix† λ (Å)	MCD Shape	System
3117	3137	$+A_1$ term	I
3061	3087	$+A_1$ term	II
3013	3032	$+A_1$ term	I
2969	2998	$+A_1$ term	II
2932	2956	$+A_1$ term	I
2879	2907	$+A_1$ term	II
2805	2831	$+A_1$ term	II

---

* Reference 63.

† This study.

TABLE 7

Ti Atomic Transitions Observed in an Argon Matrix at 14°K

Results of Gruen and Carstens[77] λ (Å)	Tentative Assignment by Gruen and Carstens[77]	Results of This Study λ (Å)	Observed MCD Sign of C_o Term	Predicted MCD Sign of C_o Term
5025	$^3F_2$	5012	+	+
4850	$^3D_1$	4840	+	+
4484	$^3G_3$	4480	−	−
3893	$^3F_2$	3890	+	+
3842	$^3D_1$	3840	+	+
3638	$^3F_2$	3632	+	+
3563	$^3G_3$	3555	−	−
3306	Not Assigned	3296	+	
3272	$^3G_3$	3266	−	−
3086	$^3G_3$	3070	−	−
2928	Not Assigned	2931	+	
2871	$^3F_2$	2874	−	+
2821	Not Assigned	2808	−	
2784	Not Assigned	2754	−	
2552	$^3F_4$	2550	+	None

$^3F_2$ assignment is positive. The negative MCD C_o term indicates that this transition is to the $^3F_3$ state observed in gas phase spectra at 2934 Å. The strong peak at 2550 Å displays a strongly positive C_o term which would be forbidden if the $^3F_4$ assignment were correct. The MCD indicates that the state is probably the $^3D_2$ state located at 2633 Å in the gas phase spectra.

Three other medium intensity bands are observed at 2985 Å, 2842 Å and 2808 Å. The two longer wavelength bands have positive C_o terms, and the other band has a negative C_o term. These transitions were not observed by Gruen and Carstens but are probably due to Ti atoms.

CHAPTER VI

RESULTS OF ZrO AND HfO EXPERIMENTS

Introduction

Due to the effects of the lanthanide contraction, both the atomic radii of Zr (1.45 Å) and Hf (1.44 Å) and the radii of the ions Zr^{+4} (0.74 Å) and Hf^{+4} (0.75 Å) are nearly identical. The chemical properties of the compounds formed from these elements are more similar than any other pair of cogeneric elements. In all geological deposits of Zr, Hf is found in the range of fractions of a percent, and their separation is very difficult.[48] As mentioned previously, the ground states of ZrO and HfO are the same, $^1\Sigma^+$, and different from the ground state of the other group IVb oxide TiO, $^3\Delta_R$. The reversal of ground state configuration of $(\sigma\delta)$ for TiO, as shown in Figure 14, to $(\sigma)^2$ for ZrO and HfO is presumably due to a combination of heavy atom properties and electron correlation effects.[37] This chapter involves a discussion of the experimental results obtained for ZrO and HfO isolated in Ar matrices.

Results for Zirconium Monoxide

Like TiO, ZrO has been studied for years because of its astrophysical importance in Class S stars, e.g., R And and

R Cyg.[79] One of the characteristic differences between the low surface temperature R and S stars is that in S stars the bands for ZrO are more prominent than TiO bands. Two ZrO singlet bands, designated A and B, were first identified in gas phase spectra taken in 1950,[80,81] and six triplet emission systems have also been observed. In 1957, Åkerlind[82] showed that the A and B transitions do not involve a common upper or lower state. The first matrix isolation study was carried out by Weltner and McLeod[62] in 1965. Until their work, the ground state of ZrO was considered to be $^3\Delta$ like TiO, but since they only observed transitions originating in the $^1\Sigma^+$ state at very low temperatures, the ground state designation was changed to $^1\Sigma^+$.

The ZrO matrix deposition conditions used in this study were those used by Weltner and McLeod. The Knudsen cell was loaded with ZrO_2 (99.9% Alfa), and deposition carried out at 2630°K.

Table 8 lists the wavelength absorption bands of the ZFA observed for ZrO in Ar matrices, by Weltner and McLeod[62] along with the MCD and ZFA peak positions found in this study. Several ZrO bands were observed by Bates and Gruen[83] in a recent study of Zr atoms isolated in rare gas matrices, and these are also listed in Table 8. It should be noted that the wavelength of the peak observed by Bates and Gruen at 5681 Å and attributed by them to the (3,0) band of ZrO is shifted by 22 Å from the peak at 5659 Å. A state diagram for the known transitions and states of ZrO is presented in Figure 25.

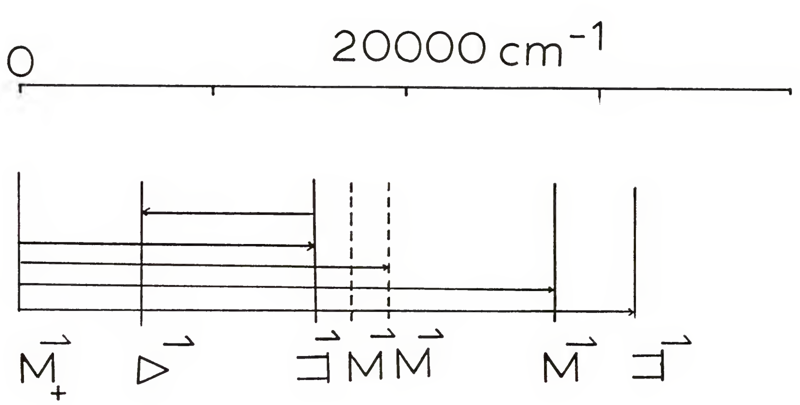

Figure 25. Singlet electronic states and observed transitions of ZrO.

TABLE 8

ZFA and MCD Bands for ZrO

Gas Band System	v'	ZFA* λ (Å)	ZFA†	ZFA√	MCD√	Sign
C	0	6633	6634	6635	6674 6598	− +
	1	6270	6276	6275	6301 6244	− +
	2	5947	5951	5950	5971 5930	− +
	3	5659	5681	5659	5675 5647	− +
	4	5406		5400	Too Weak	
D	0	6024	6021	6024	6020	+
	1	5729		5728	5728	+
	2	5461	5471	5460	Too Weak	
Forbidden Transition	0	5302		5304	5320 5292	− +
	1	5084		5080	5098 5064	− +
A	0	3678		3678		
	1	3572		3570	No MCD	
	2	3470		3469		
				3371		
				3260		

---

* Results of Weltner and McLeod.[62]

† Results of Bates and Gruen.[83]

√ Results of this study.

The band system with its (0,0) transition at 6635 Å in Ar is designated as the C system and corresponds to the gas phase singlet system at 6495 Å. Weltner's assignment of the transition to $e^1\Pi \leftarrow X^1\Sigma^+$ was confirmed by Balfour and Tatum[84] in an analysis of the arc emission spectrum of ZrO. This region of the emission spectrum is dominated by the γ system, $A^3\Phi - X^3\Delta$. The red-degraded head of the C system occurs between the (0,0) and (1,1) band heads of the γ system and is completely overlapped by the γ system which makes the interpretation of this region very difficult.

The predicted magnetic field splittings and circularly polarized transitions for the C system of ZrO are illustrated in Figure 26. Since the ground state, $^1\Sigma^+$, is magnetically non-degenerate, the ground state will not be split, and the only possible MCD terms for ZrO are $\mathcal{A}_1$ and $\mathcal{B}_0$ terms. The predicted MCD $\mathcal{A}_1$ term for the C system is $+1\beta$ and is readily confirmed by the positive temperature independent $\mathcal{A}_1$ term observed for this band in Figure 27. The ZFA spectrum for this wavelength region is also shown in Figure 27.

Weltner[62] noted weak matrix site effects in the wings of the ZrO bands in Ar. Small amounts of blue shading occurs in the ZFA bands of the C system. Weak site effects are also noted to the blue of the (0,0) and (1,0) and as a broadening of the (2,0) and (3,0) bands in the MCD. The intensity of these sites changed on annealing the matrix. The spacing between the sites on the (0,0) and (1,0) MCD bands is 851 cm^{-1} which is very close to the spacing of

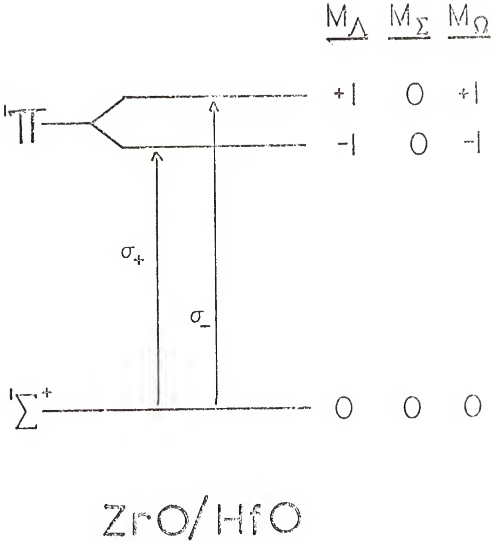

Figure 26. Magnetic field splitting and MCD allowed transitions of ZrO and HfO.

Figure 27. MCD and ZFA spectra of the C and D systems of ZrO in an Ar matrix.

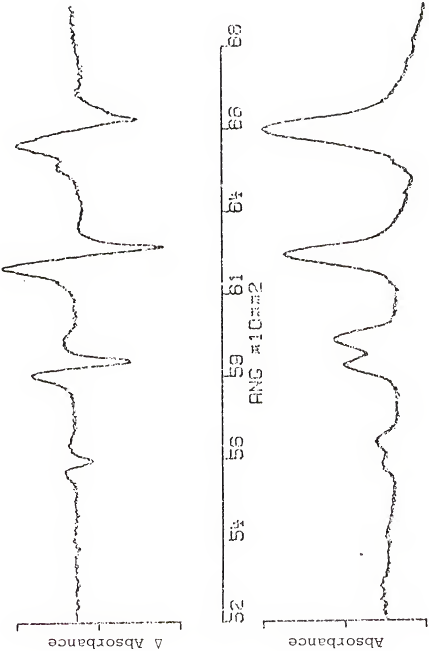
Δ Absorbance
Absorbance
ANG *10**2
52
54
55
59
61
64
66
69

859 cm^{-1} between the nearby positive lobes of the (0,0) and (1,0) MCD bands.

The (2,0) band of the C system overlaps with the (0,0) band of the D system. In the ZFA spectrum shown in Figure 27 the intensity of the bands for the D system is greater than the overlapping bands belonging to the C system at shorter wavelengths, but in the MCD spectrum of Figure 27 this situation is reversed and the C system bands are relatively more intense. Both MCD band systems show no variation with temperature, and the bands for the D system do not show the characteristic derivative shape for an A_1 term but follow the lineshape function. The maximum of the D system bands in the ZFA and MCD spectra correspond.

The assignment of the D system to the $^1\Pi(\pi^3\delta) \leftarrow X^1\Sigma^+(\pi^4\sigma^2)$ transition was deemed very uncertain by Weltner[62] and could have also been assigned to the $^1\Sigma^+(\sigma\sigma^*) \leftarrow X^1\Sigma^+(\pi^4\sigma^2)$ transition. Both of these transitions would be allowed in ZFA spectra. The transition to the $^1\Pi$ state should yield a positive A_1 term in MCD spectra; whereas the transition to the $^1\Sigma^+$ state would be forbidden in MCD unless there was a B_0 term induced by magnetic field mixing with a nearby state. The most likely candidate for this mixed in state is the C system in which the $e^1\Pi$ state does possess a magnetic moment. The assignment of the D system to the $^1\Sigma^+(\sigma\sigma^*) \leftarrow X^1\Sigma^+(\pi^4\sigma^2)$ transition seems more logical in light of the MCD sign, shape, intensity, temperature independence, and the presence of the nearby $e^1\Pi$ state for mixing to form a B_0 term. Recently Phillips and Davis[85] have examined this wavelength region closely in the arc emission spectrum of ZrO and discovered a $^1\Sigma^+ \rightarrow X^1\Sigma^+$ transition with the (0,0) band at 5860 Å, which is close to the 6024 Å band in Ar matrices. The spacing between the vibrational levels is 870, 867 and 855 cm^{-1} for ^{99}ZrO, ^{97}ZrO and ^{96}ZrO, respectively, which is also close to the 858 cm^{-1} spacing for the vibrational levels of the D system in Ar matrices.

An example of a $^1\Sigma^+ \leftarrow {}^1\Sigma^+$ transition where there is no nearby state available to form a $\mathcal{B}_0$ term in MCD is demonstrated in the A system of ZrO. This system shows a prominent progression in ZFA spectra in the range between 3700 Å and 3200 Å as illustrated in Figure 28. Weltner noted three members of the progression, and two more have been added in this study. The spacings between the vibrational bands are not quite regularly anharmonic, but this may be due to overlap with Zr atomic bands which overlap the 3371 Å and 3678 Å bands. The Zr atomic transitions are discussed below.

The original assignment of the A system by Uhler and Akerlind[81] was doubtful because a $^1\Sigma$-$^1\Sigma$ transition could not be distinguished from a $^1\Delta \rightarrow {}^1\Delta$ transition. Weltner favored the former assignment on the basis of the correspondence between the infrared vibrational frequency of ZrO in a Ne matrix (975 cm^{-1}) and that in the lower state of the A gas emission system (969.7 cm^{-1}), rather than in the lowest $^1\Delta$ state (931 cm^{-1}). The results of this MCD study further confirm this assignment. The MCD spectrum

Figure 28. ZFA spectrum of the A system of ZrO in an Ar matrix.

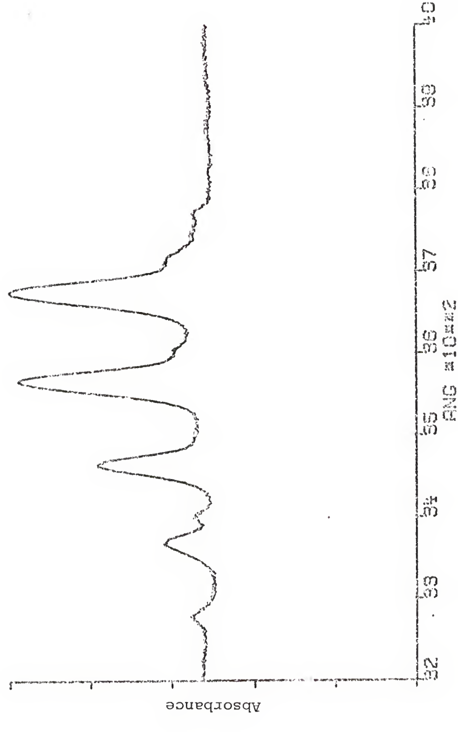
Absorbance
ANG *10**2
32
33
34
35
36
37
38
39
40

of the wavelength region of the A system (see Figure 29) shows only those transitions attributable to Zr atomic $\mathcal{C}_o$ terms and none for the MCD forbidden $^1\Sigma^+ - {}^1\Sigma^+$ transition of the A system.

Two very weak transitions are observed at 5304 Å and 5080 Å which were also observed by Weltner[62] and assigned by him to the forbidden transition $B^3\Pi \leftarrow X^1\Sigma^+$, based on an upper state vibrational frequency of 836 cm^{-1} in Ne matrices as compared with the known gas phase $\nu' = 838.8\ cm^{-1}$ for the $B^3\Pi$ state. Although the $\Delta S=0$ selection rule is violated in transitions to all three of the $^3\Pi$ multiplet states, only the transition to the $B^3\Pi_1$ state does not also violate the $\Delta\Sigma=0$ selection rule as illustrated in Figure 30. Note also that the MCD transition to the $\Omega=1$ multiplet is the only one that does not violate the $\Delta M_\Sigma=0$ selection rule for MCD. Lauchlan, Brom and Broida[86] excited this state using the 5145 Å line of an Ar^+ ion laser on a Ne matrix containing ZrO where the transition occurred at 5154 Å. They observed strong $B^3\Pi_0 \rightarrow X'^3\Delta_1$ emission with this excitation which strongly supports the assignment. Weak MCD transitions are observed for this system (see Figure 31) with positive $\mathcal{A}_1$ terms which further supports the assignment since the predicted $\mathcal{A}_1$ term for the $B^1\Pi_1 \leftarrow X^3\Sigma^+$ is also positive.

Five other weak bands were noted by Weltner[62] for ZrO matrices in Ar, and four of these bands can now be assigned. Two of these weak bands at 4855 Å and 4632 Å show positive $\mathcal{A}_1$ terms in the MCD (see Figure 31). Their vibrational

Figure 29. MCD spectrum of the A system region of ZrO in an Ar matrix. (Spectral peaks are due to Zr atoms)

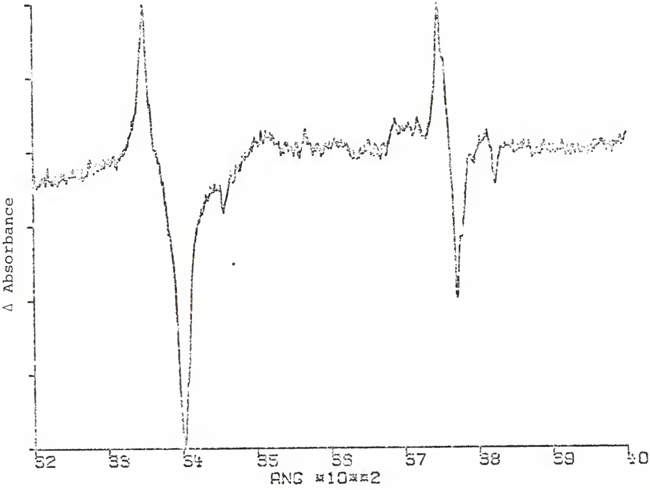
Δ Absorbance
52
53
54
55
56
57
58
59
60
ANG *10**2

Figure 30. Magnetic field splittings and A_1 terms for the $^3\Pi \leftarrow {}^1\Sigma^+$ transition of ZrO.

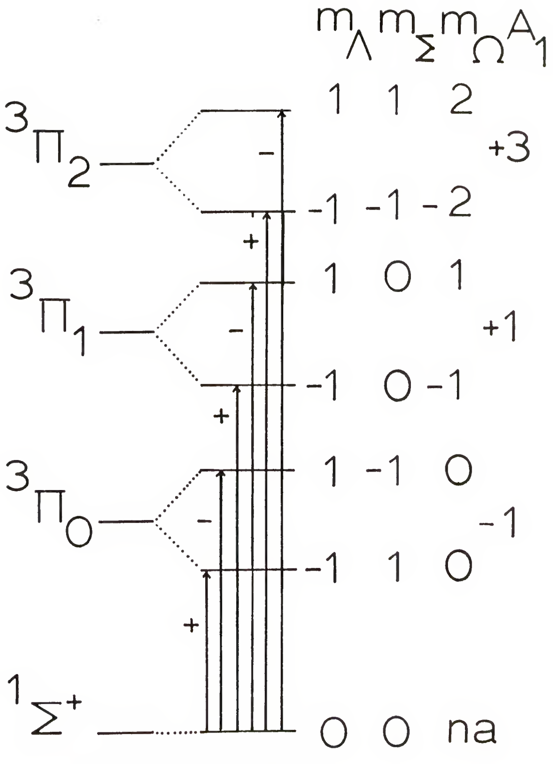
mΛ mΣ mΩ A1
1 1 2
+3
-1 -1 -2
1 0 1
+1
-1 0 -1
1 -1 0
-1
-1 1 0
0 0 na
3Π2
3Π1
3Π0
1Σ+
-
+
-
+
-
+
H=0 H≠0

Figure 31. MCD spectrum of the weak visible bands of ZrO in an Ar matrix (Arrow indicates 2689 Å Zr transition)

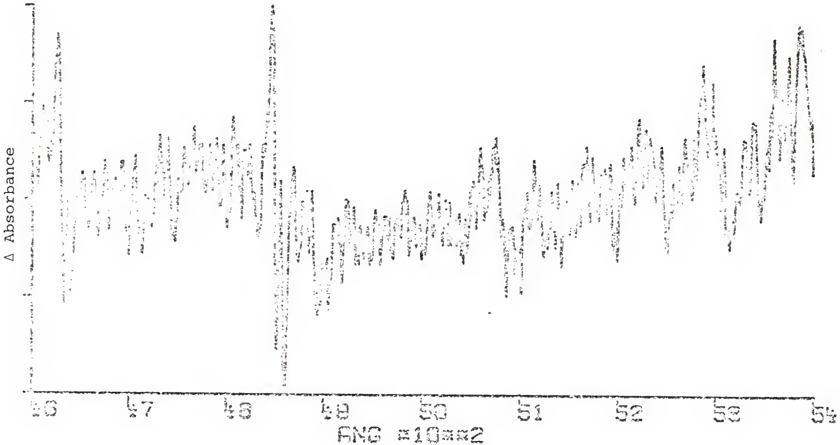
Δ Absorbance
46
47
48
49
50
51
52
53
54
ANG *10**2

spacing is 992 cm^{-1}, with some site splitting in the MCD shown in Figure 31. Unfortunately, only spectra of $Zr^{16}O$ were obtained in Ar matrices, and therefore, any shifts that might help assign the (0,0) transition for these bands are not known. $Zr^{18}O$ spectra were obtained by Weltner for Ne matrices; however, these transitions were not noted in the Ne matrix spectra. This transition may be the $^1\Pi(\pi^3\delta) \leftarrow X^1\Sigma^+(\pi^4\sigma^2)$ transition previously tentatively assigned to the D system which was revised to the $^1\Sigma^+(\sigma\sigma^*) \leftarrow X^1\Sigma^+(\pi^4\sigma^2)$, *vide supra*.

Two of the other weak transitions observed in ZFA spectra in Ar matrices at 3770 Å and 3721 Å are readily attributable to Zr atomic transitions which were observed recently by Bates and Gruen.[83] These transitions are readily observed in the MCD spectra since their overlap with the A bands of ZrO is removed by the forbidden character of the MCD of the A bands (see Figure 29). The ground state of Zr is $^3F_2$ and therefore shows strong $\mathcal{C}_o$ term behavior in MCD spectra. Although the experiments in this study were directed toward ZrO, enough Zr atoms are present under these experimental conditions to observe all of the moderately intense Zr atomic transitions observed by Bates and Gruen. These transitions are listed in Table 9. Although Bates and Gruen did not make any correlations between the gas phase spectra and the observed matrix transitions, the sign of the MCD $\mathcal{C}_o$ terms for the Zr atomic transitions allows prediction of the Ω values for the upper states which are

TABLE 9

Zr Atomic Transitions Observed in Ar Matrices

λ (Å)[†]	Strength	λ (Å)[✓] This Work	MCD Sign	Final Ω
*		4494	−	3
4367	m	4368	−	3
4300	vw	4322	+	1 or 2
4005	vw	4028	+	1 or 2
3819	m	3825	−	3
3771	vs	3770	−	3
3719	s	3721	+	1 or 2
3459	w	3457	−	3
3401	vs	3400	−	3
3349	s	3350	+	1 or 2
3050	m	3037	+	1 or 2
2906	m	2901	+	1 or 2
2865	s	2848	+	1 or 2
2812	vw	2796	−	3
2729	w	2733	+	1 or 2
2691	ms	2689	+	1 or 2
2594	w	2600	−	3

---

* Not reported.

[†] Results of Bates and Gruen.[83]

[✓] Results of this study.

also presented in Table 9. All of the peaks listed show the expected temperature variations for an MCD C_o term.

The ZFA spectrum from 2500 Å to 3250 Å is shown in Figure 32. A large number of strongly absorbing bands are noted in this region, some of which are attributable to the Zr atomic transitions listed in Table 9. The majority of the bands in this region are not due to Zr atoms, but are probably due to previously unidentified bands of ZrO. The shortest wavelength bands noted by Weltner[62] comprise the A system between 3700 Å and 3200 Å. Although no mention is made for the shortest wavelength examined in the ZrO spectra, he does note that the region below 3100 Å was not examined in the HfO spectra. In the arc emission studies of Afaf[80] in 1950, the shortest wavelength bands observed was the ϕ triplet system between 3121 Å and 2940 Å with the (0,0) transition located at 2941 Å. This system was very weak, and only transitions from the v'=0 level were observed. The low intensity of emission is not surprising since this state is over 34000 cm^{-1} above the ground state and the fractional population in the excited state is very low.

The MCD spectrum of this region is shown in Figure 33. The Zr atomic bands are much enhanced in the MCD spectra since they are due to C_o terms which are much more intense than A_1 terms. An example of this enhancement can be seen by comparing the small shoulder Zr transitions at 2689 Å in the ZFA spectrum of Figure 32 with the much stronger peak in the MCD spectrum of Figure 33.

Figure 32. ZFA spectrum of the ultraviolet region of a matrix containing Zr and ZrO.
(Arrow indicates 2689 Å Zr transition)

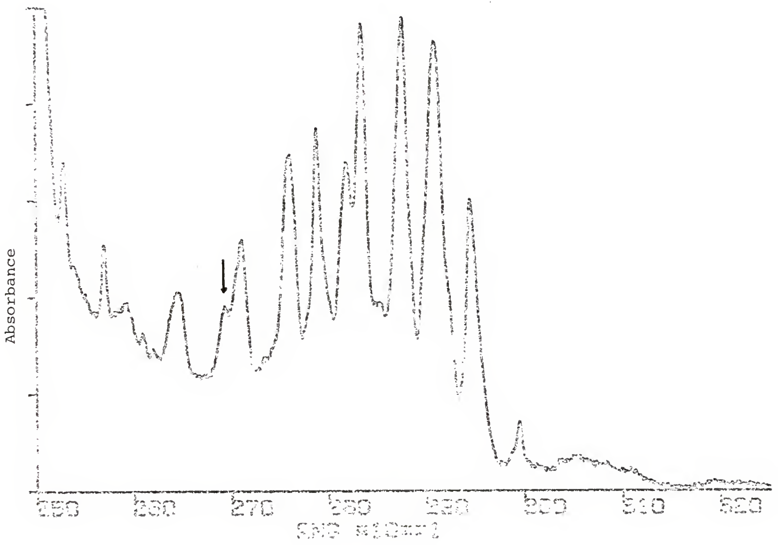
Absorbance
250
260
270
280
290
300
310
320

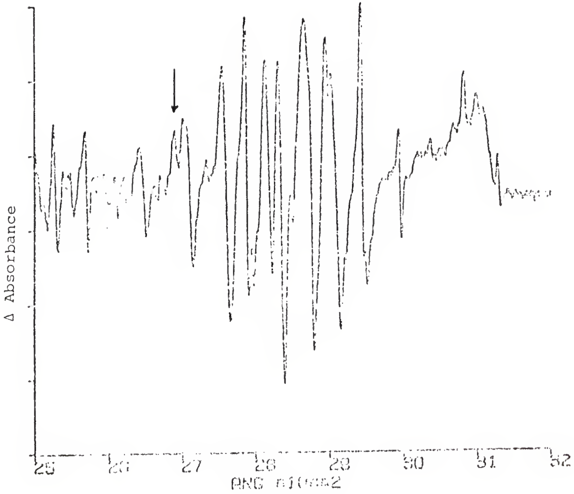

Figure 33. MCD spectrum of the ultraviolet region of an Ar matrix containing Zr and ZrO.

Table 10 lists the peak positions for the ultraviolet ZrO bands in the ZFA and MCD spectra. In all cases the middle of the ZFA band is located in the middle of the two MCD lobes. This agreement is readily seen in Figure 34 where both spectra are plotted with the same abcissa. Each MCD band appears as a temperature independent, positive A_1 term which indicates that the transitions are most likely $^1\Pi \leftarrow {}^1\Sigma^+$. More than one transition is indicated by the Deslandres table illustrated in Figure 35. States that have overlapping energy levels often perturb each other so that the vibrational progressions do not show a regular anharmonic behavior as seen in the TiO ultraviolet bands of System I and II. A possible grouping of vibrational bands is indicated in Table 10; however, due to the strong overlap, these assignments are very tentative.

The possibility that these bands are due to ZrO_2 is not completely eliminated. Weltner observed one strong band at 965 cm^{-1} for $Zr^{16}O$ in Ar matrices and other bands at 887, 880, 822, 816 and 794 cm^{-1}. Linevsky[87] observed bands at 819 and 884 cm^{-1} in the infrared spectra of ZrO in Ar matrices which he attributed to ZrO_2 absorption. The observed frequencies differ by about 5 cm^{-1} between Weltner's work and Linevsky's data. In mass spectrometer studies of the vaporization of ZrO_2, Chupka, Berkowitz and Inghram[88] observed ZrO_2 as a component in the vapor state, although ZrO was the dominant species with the $(ZrO)^+/(ZrO_2)^+$ ratio of about 6. Conlon and Doyle[89] have examined the optical absorption of thin films of ZrO_2 in the region between

TABLE 10

Ultraviolet Bands Observed for ZrO in Ar

	Abs	MCD	Sign	Temperature Dependence		Possible $\Delta G_{v'+\frac{1}{2}}$
33389	2995	2997 2993	– +	None		
33956	2945	2951 2943	– +	None	975 cm^{-1}	
34364	2910	2916 2895	– +	None		815 cm^{-1}
34771	2876	2880 2867	– +	None	909 cm^{-1}	
35273	2835	2840 2830	– +	None		715 cm^{-1}
35486	2818	2822 2812	– +	None	959 cm^{-1}	
35881	2787	2790 2784	– +	None		746 cm^{-1}
36232	2760	2765 2754	– +	None	1019 cm^{-1}	
36900	2710	2715 2705	– +	None	893 cm^{-1}	
37793	2646	2650 2641	– +	None	521 cm^{-1}	
38314	2610	2612 2608	– +	None	596 cm^{-1}	
38910	2570	2573 2569	– +	None		
39557	2528	2532 2528	– +	?		

Figure 34. ZFA and MCD spectra of the ultraviolet region of a matrix containing Zr and ZrO.

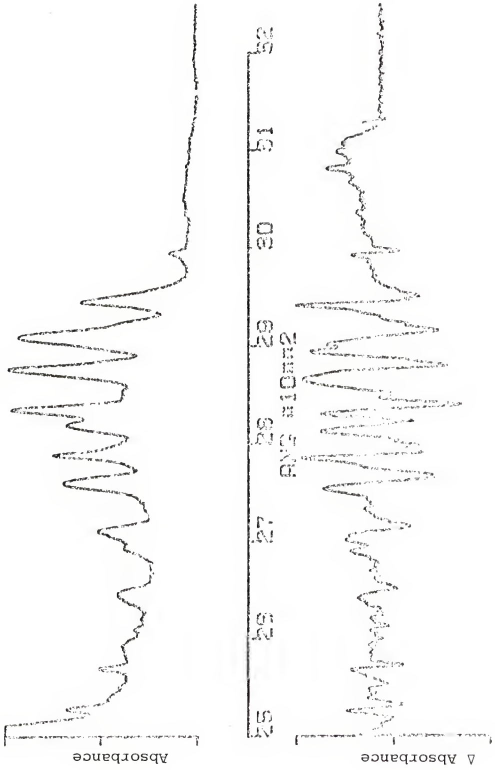
Absorbance
Δ Absorbance
25
26
27
28
29
30
31
32
WVN ×10E2

Figure 35. Deslandres Table for the ultraviolet transitions of ZrO.

λ (Å)	2995	2945	2910	2876	2835	2818	2787	2760	2710	2646	2610	2570	2528
(cm^{-1})	33389	33956	34364	34771	35273	35486	35881	36232	36900	37793	38314	38910	39557
2995 (33389)	0	567	975	1382									
2945 (33956)		0	408	815	1316								
2910 (34364)			0	407	909	1122							
2876 (34771)				0	502	715	1110						
2835 (35273)					0	213	608	959					
2818 (35486)						0	395	746	1414				
2787 (35881)							0	351	1019				
2760 (36232)								0	668	1561			
2710 (36900)									0	893	1414		
2646 (37793)										0	521	1117	
2610 (38314)											0	596	1243
2570 (38910)												0	647
2528 (39557)													0

2050 and 10000 Å. These films were generated by oxidation of thin films of Zr deposited on fused quartz disks. Therefore their spectra are properties of solid state ZrO_2. The absorption threshold of ZrO_2 is about 2300 Å and rises sharply to their limit of measurement at 2050 Å. These authors attribute the absorption to exciton formation or band-to-band transitions which would probably not be observed in Ar matrices.

If the transitions were due to ZrO_2, the only way the MCD would be seen is if ZrO_2 were linear so that orbital degeneracy could occur or if the transitions were forbidden assuming ZrO_2 has a singlet ground state. These possibilities do not seem likely since TiO_2 has been shown to be bent, and the intensity of the transitions seems to rule out intermultiplicity transitions.

The group of bands in the region 3025 Å to 3140 Å is observed in spectra of ZrO and HfO (see Figure 36). These bands are much less intense in the ZFA spectra (see Figure 32) and are readily attributable to the R system of TaO as observed in the gas phase at 3088 Å by Cheetham and Barrow.[90] These bands were also observed in our studies of TaO isolated in Ar matrices.[38] The other bands observed in matrices of ZrO and less intensely in HfO matrices are listed below:

K(0,0) at 4500 Å
K(1,0) at 4365 Å
L(0,0) at 4325 Å
$\left.\begin{array}{l}\mathrm{K(2,0)}\\ \mathrm{M(0,0)}\end{array}\right\}$ at 4180 Å

L(1,0) at 4160 Å
$\left.\begin{array}{l}\mathrm{K(3,0)}\\ \mathrm{M(1,0)}\end{array}\right\}$ at 4035 Å
L(2,0) at 4015 Å

Figure 36. MCD of ZrO and HfO matrices illustrating the presence of TaO in the matrices.

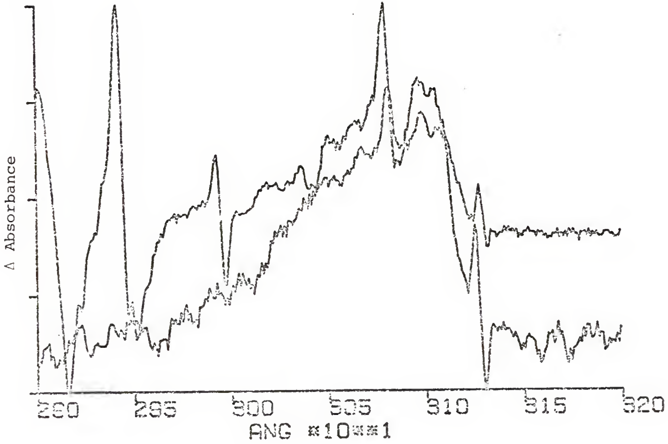
Δ Absorbance
290
295
300
305
310
315
320
ANG *10**1

The presence of TaO in the matrices is due to oxidation of the Ta end-caps in the Knudsen cell at the high temperatures required for formation of HfO and ZrO.

Results of Hafnium Monoxide

A scant five years after the discovery of the element hafnium, Meggers[91] published the first study of HfO in 1928. This report was followed by the work of King[92] in 1929 and Shaw and Ketcham[93] in 1934; however, no detailed level assignments could be made at that time. In 1951, Krishnamurti[94] published a preliminary report on HfO but never followed up with a detailed analysis. The Vatican Atlas,[95] published in 1957, gave spectra and preliminary assignments for 9 sequences in HfO.

The first matrix isolation study of HfO was published in 1965 by Weltner and McLeod.[62] By using ^{18}O labeling techniques, they were able to determine the (0,0) transitions for six band systems in Ar and Ne matrices at 4 and 20°K. The wavelengths obtained for the bands of these systems are presented in Table 11 along with ZFA and MCD spectral wavelengths obtained in the present study under the same matrix deposition conditions.

As noted above, the properties of Zr and Hf are very close, and this similarity extends to the oxides. The ground state constants for ZrO and HfO are listed on the next page:

	Term	Reduced Mass	r_e (Å)	ω_e (cm^{-1})
ZrO	($X^1\Sigma$)	13.55	1.711	969.8
	($X'^1\Delta$)		1.728	936.5
HfO	($X^1\Sigma$)	14.69	1.723	974.1

The correlation of ω_e values in the ground state carries over into the excited states where the ZrO bands shift very little in going to HfO bands. This correspondence holds very well in Ne matrices but less well in Ar matrices, as shown in Table 11, and was used by Weltner and McLeod to assign the D, E and F states as $^1\Pi\leftarrow{}^1\Sigma$, $^1\Pi\leftarrow{}^1\Sigma$, and $^1\Sigma\leftarrow{}^1\Sigma$, respectively. These assignments agree with the designations by Gatterer et al.[95] based on the appearance of the gas phase bands. The A, F and G systems have the appearance of $^1\Sigma\leftarrow{}^1\Sigma$ transitions, while the B, D and E systems are typical of $^1\Pi-{}^1\Sigma$ transitions. This gas phase analysis was further refined by Edvinsson and Nylen[96] in 1971 in an examination of 13200 spectral lines of the A, B, D, E, F and G systems. Later, Edvinsson[97] revised the assignment of the A and B systems from $A^1\Sigma$ to the $^3\Pi_0$ and $B^1\Pi$ to the $^3\Pi_1$ levels of a triplet state. The high resolution data fit either assignment.

The ZFA and MCD spectra of the two $^1\Sigma-{}^1\Sigma$ ultraviolet bands F and G are presented in Figure 37. The ZFA shows a distinct 3 member progression for both systems, but the MCD shows no signal as expected for transitions between non-degenerate states.

The spectral region between 3700 Å and 4400 Å contains the overlapping D and E systems. The ZFA spectrum of the

TABLE 11

Correlation between ZrO and HfO Bands in Ne and Ar Matrices

Compound	Band System	Ne Matrix λ (Å)	$\Delta G_{v'+\frac{1}{2}}$ (cm^{-1})	Ar Matrix λ (Å)	$\Delta G_{v'+\frac{1}{2}}$ (cm^{-1})
ZrO	A	3660	838	3678	807
HfO	F	3642.5	838	3689	833
ZrO	D	5872	872	6024	854
HfO	E	3912.5	874	3920	830
ZrO	C	6446	854	6633	873
HfO	D	4195.5	862	4240	838

Figure 37. ZFA and MCD spectra of the ($^1\Sigma-^1\Sigma$) F and G bands of HfO in an Ar matrix.

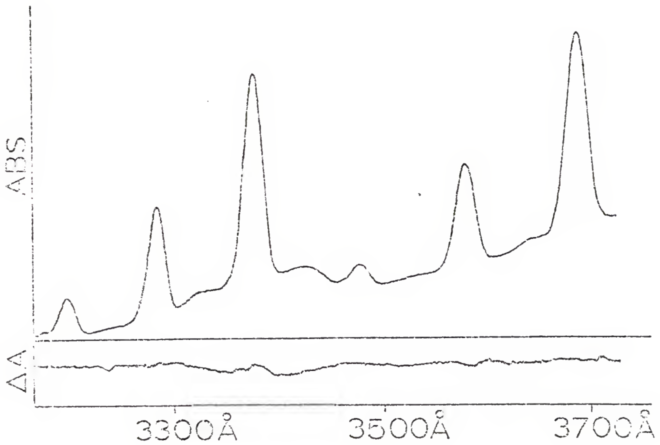
ABS
ΔA
3300Å
3500Å
3700Å

region is shown in Figure 38, and the MCD spectrum is in Figure 39. The gas phase analysis of Edvinsson and Nylen[96] shows that there are perturbations between the D(v'=2) and E(v'=0) levels, the D(v'=3) and E(v'=1) levels, etc. These perturbations occur in the regions where the stronger D system overlaps the E system. The perturbations are manifest by irregular isotopic effects in the 0-0 sequence of the E system and by the non-proportionality between J(J+1) and the Λ-type doubling in perturbed levels. For the $E^1\Pi(v'=1)$ level, the Λ-type doubling changes sign at J=106.

Both D and E systems are assigned to $^1\Pi$ states which show magnetic field splittings as illustrated in Figure 26. The predicted positive $\mathcal{A}_1$ term is readily evident in the D system bands. The less intense bands for the E system are broad and overlap with the D bands, which makes the $\mathcal{A}_1$ terms less evident. The middle of the derivative shape for the E bands in MCD correspond to the band maxima observed in the ZFA spectra, which indicates that the assignment for the E state of $^1\Pi$ is correct.

The A and B band systems of HfO do not have any counterparts in the ZrO spectra; therefore, Weltner and McLeod[62] were unable to assign these states. They presumed that they are forbidden transitions to lower triplet states which are made more "allowed" by the internal heavy atom effect in the heavier HfO molecule. The analysis of Gatterer et al.[95] assigned the A system to a $^1\Sigma$ state and the B system to a $^1\Pi$ state. Edvinsson and Nylen[96] concurred

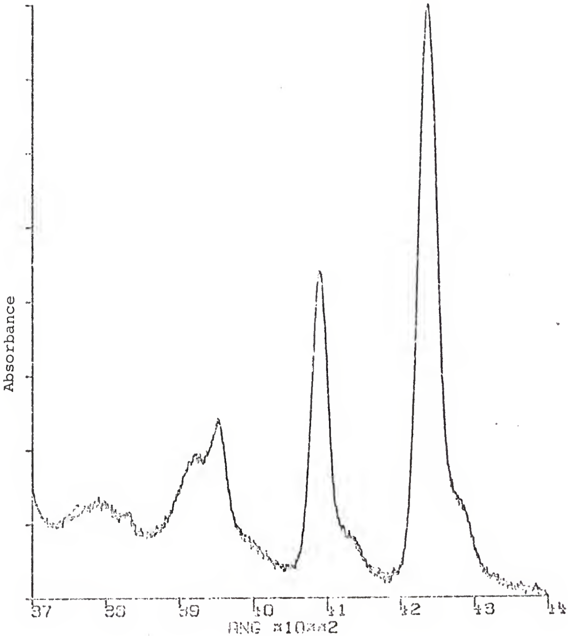

Figure 38. ZFA spectrum of the ($^1\Pi$-$^1\Sigma$) D and E bands of HfO in an Ar matrix.

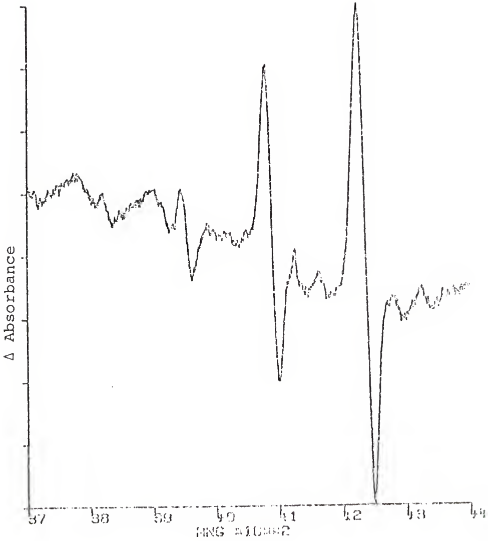

Figure 39. MCD spectrum of the $(^1\Pi-^1\Sigma)$ D and E bands of HfO in an Ar matrix.

with this assignment based on analysis of very high resolution spectra obtained using a Jarrel Ash 4.5 m Fastie spectrograph with a dispersion between 3.5 and 6.5 Å/mm and a microwave discharge source. These level assignments were later changed by Edvinsson.[97] The high resolution data fit either assignment, but Edvinsson attributes the A and B systems to $^3\Pi_0$ and $^3\Pi_1$ levels of a triplet state, respectively.

Intermultiplicity transitions are favored in heavier molecules such as HfO, but the spin-orbit coupling constant for Hf is 1300 cm^{-1} whereas the spacing between the band heads for the A and B systems is 935 cm^{-1}. This lower energy separation would tend to disfavor the assignment as multiplets of a $^3\Pi$ state.

The MCD transitions from the $^1\Sigma$ ground state to the $^3\Pi_1$ and $^3\Pi_0$ states have predicted positive and negative A_1 terms, respectively. The transition to the $^3\Pi_1$ state is allowed in Hund's case a coupling or in case c coupling which would be expected to be favored by the high molecular weight of the molecule. The transition to the $^3\Pi_0$ state would not be allowed in either case a or case c (see Figure 40).

The ZFA and MCD spectra of the A and B bands are presented in Figure 41. The intensity of these bands is very weak, and they are also rather broad. The MCD spectrum was obtained on the most sensitive scale of the lock-in amplifier, and the signal-to-noise ratio is not as high as on other spectra obtained in this study. The observation that the A and B bands have different shapes in both ZFA and MCD spectra would disfavor the intermultiplicity assignment.

Figure 40. Predicted magnetic field splitting and A_1 terms for the forbidden transitions ($^3\Pi_1-^1\Sigma$ and $^3\Pi_0-^1\Sigma$) of HfO.

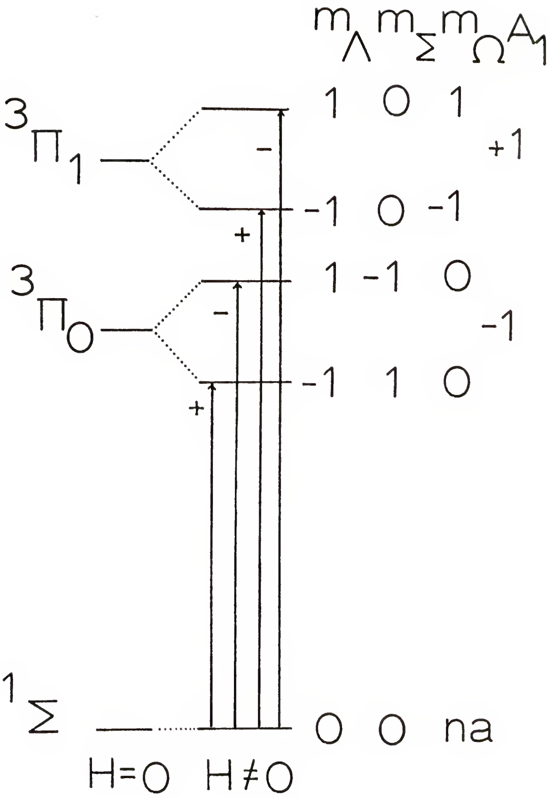
m_Λ m_Σ m_Ω A_1
$^3\Pi_1$
$^3\Pi_0$
$^1\Sigma$
1 0 1
+1
-1 0 -1
1 -1 0
-1
-1 1 0
0 0 na
−
+
−
+
H=0
H≠0

Figure 41. ZFA and MCD spectra of the A and B bands of HfO in an Ar matrix.

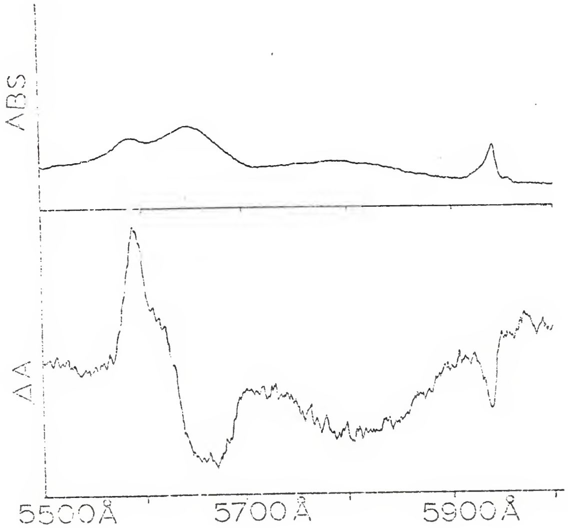
ABS
ΔA
5500Å
5700Å
5900Å

It is interesting to note that the A bands at 5957 Å and 5944 Å are reversed in intensity from Weltner and McLeod's[62] study. In their work they observed a reversible increase in intensity of the 5944 Å band on cooling the matrix from 20°K to 4.2°K and argued that this was due to site effects. The site effect hypothesis is supported by the reversal of intensity observed in this study which is obstensibly due to different matrix deposition conditions. Weltner and McLeod's matrices were deposited at 4.2°K, whereas 14°K was the deposition temperature in this study.

The shape of the MCD of the A band lends support to the earlier assignment as $^1\Sigma$, since no derivative shape is observed, which would be expected for a $^3\Pi_0$. The presence of the negative-going MCD band is attributable to a $\mathcal{B}_0$ term due to mixing with the nearby Π state of the B system.

By use of ^{18}O labeling, Weltner[62] observed two (0,0) bands (5589 and 5649 Å) in the B system which overlap each other. The shape of the MCD bands do not conclusively indicate the presence of a singlet or triplet Π state.

Several bands are observed in the ZFA spectra of the ultraviolet region between 2500 Å and 2900 Å. These bands are listed in Table 12 and the spectra are presented in Figure 42. The four bands observed between 2650 Å and 2900 Å are due to TaO present in the matrix. The intensity ratio of these peaks to the HfO bands is not constant for different matrices, and the wavelengths match those found for TaO matrices.

TABLE 12

ZFA Peak Positions in the Ultraviolet Spectra of HfO in Ar Matrices

ZFA λ (Å)	Comment
2850	TaO
2807	TaO
2746	TaO
2683	TaO
2627	+ A_1 term in MCD
2613	+ A_1 term in MCD
2603	+ A_1 term in MCD
2559	No MCD
2553	No MCD
2505	No MCD

Figure 42. ZFA and MCD spectra of the ultraviolet region of an Ar matrix containing HfO.

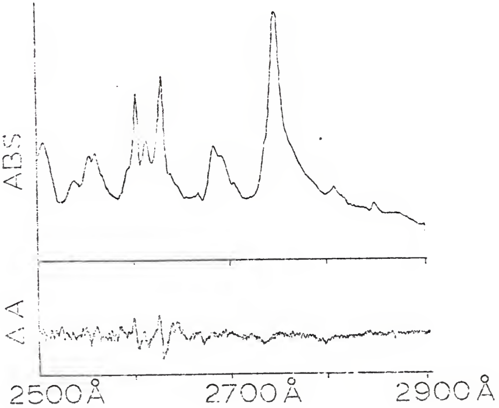
ABS
ΔA
2500 Å
2700 Å
2900 Å

The group of three peaks near 2600 Å all display $+A_1$ term behavior in the MCD and are probably due to a band previously observed by Edvinsson and Nylen[96] in gas emission studies at 2735.5 Å. This correlation implies a matrix shift to the blue of about 1700 cm^{-1}. The presence of the positive A_1 term implies that this state is $^1\Pi$.

Unfortunately, in the experiments of Edvinsson and Nylen, the region between 2300 and 2700 Å was completely obscurred by SiO bands, and no correlation can be made between the matrix bands observed below 2600 Å and gas phase spectra.

CHAPTER VII

CONCLUDING REMARKS

The combination of magnetic circular dichroism and matrix isolation techniques has been shown by this study to be a powerful tool for the molecular spectroscopist. By employing an asymmetric probe such as circularly polarized light and the unique selection rules for MCD, it is possible to determine more readily the electronic symmetry of molecular species than in ZFA spectra. The use of the various lineshape and temperature dependent parameters of MCD gives the spectroscopist more criteria to use in the assignment of molecular and atomic states.

The future of this technique is bright and should be rather productive since so few species have been studied thus far. As illustrated in the spectra of TiO, MCD will be very helpful in studies of matrix site effects since MCD is able to resolve much finer details than have been observed previously in ZFA spectra. The use of MCD to determine magnetic moments is also a field which should prove very fruitful.

Several possibilities exist for improvement of the apparatus built for this experiment. The results have shown that a relatively modest magnetic field (5500 gauss) is sufficient to obtain excellent MCD data; however, the small diameter and long axial holes in the pole pieces of standard electromagnets precludes circularly polarized emission studies. A more compact design split coil, superconducting magnet or a high field, rare earth permanent magnet should improve the chances for observation of circularly polarized luminescence.

The size of the PET microcomputer memory should be expanded to 32K in order to be able to store a full 8000 to 2500 Å scan in memory. This would eliminate the necessity of storage of partial spectra on magnetic tapes for subsequent output to the Nicolet 1180 computer.

It would be very interesting to excite TiO or ZrO bands with the Spectra Physics Ar^+ laser and dye laser available in our laboratory and observe changes in the infrared spectrum due to depopulation of the ground state. This experiment should be particularly helpful in assignment of bands in matrices containing more than one species. The Nicolet FT-IR in our laboratory is an excellent IR detector for these experiments, and a mobile matrix isolation device is currently under construction for this purpose.

Since the lowest temperature obtainable in this study was 14°K, it was impossible to obtain Ne matrices. The construction of a liquid He cryostat for deposition at 4.2°K would be an excellent addition. TiO spectra in Ne matrices would help resolve the problems of differentiation between site effects and the presence of other species in the matrix.

Currently, an effort is being made in this laboratory to observe the MCD of Group IVb atoms in Ar matrices. The ZFA spectra of a large number of atomic species in matrices have been examined for a number of years, and the matrix deposition conditions for many atomic species are well established. It would also be interesting to look at the vaporization products of solid TiO, ZrO and HfO, which were made in this study by vaporization of the corresponding dioxide. The monoxides can be made in bulk quantities with a purity exceeding 90% by sintering a mixture of the dioxide with the element and heating for several hours. The vaporization products of the monoxide obtained in this way have not been examined.

APPENDIX

The various computer programs used in this research are presented below along with brief comments on each program. The programs for the PET were written in the PET BASIC language. There were some major drawbacks to this language due to the microprocessor design. Data sets cannot be longer than 256 points, and the process of outputing data to the tape cassette must take into account the operation of the tape buffer. The programs for the Nicolet computer were written in the Nicolet 1180 BASIC language.

The first program, called MCD11, controlled both absorption and MCD experiments, as well as data collection and storage. The command RUN30 was used to start the program, which is listed below.

MCD11

```
10 J=O
11 J=J11
12 IF J<A GOTO 11
13 RETURN
20 SAVE"MCD11"
30 POKE 4.0E4,0
31 POKE 3. 3E4,127
32 POKE 4.0E4,4
33 POKE 3.9E4,0
34 POKE 4.9E4,0
35 POKE 4.8E4,255
36 POKE 4.9E4,4
37 POKE 3.8E4,0
38 POKE 3.7E4,0
39 POKE 3.8E4,4
```

```
 40 GOTO 350
 50 M=N/4
 60 DIM A%(250)
 61 DIM B%(250)
 62 DIM C%(250)
 63 DIM D%(250)
 64 DIM E%(250)
 65 DIM F%(250)
 66 DIM G%(250)
 67 DIM H%(250)
 70 FOR L=2 TO M
 80 NP=INT((L-1)/250)
 90 I=L NP*250
 95 AP=NP+1
100 ON AP GOTO 110,120,130,140,1420144,146,148
110 A%(I)=PEEK(3.7E4)
115 GOTO 150
120 B%(I)=PEEK(3.7E4)
125 GOTO 150
130 C%(I)=PEEK(3.7E4)
135 GOTO 150
140 D%(I)=PEEK(3.7E4)
141 GOTO 150
142 E%(I)=PEEK(3.7E4)
143 GOTO 150
144 F%(I)=PEEK(3.7E4)
145 GOTO 150
146 G%(I)=PEEK(3.7E4)
147 GOTO 150
148 H%(I)=PEEK(3.7E4)
149 GOTO 150
150 POKE 3.9E4,8
160 WL=WL-.25
170 GOSUB 320
180 POKE 3.9E4,9
190 GOSUB 10
200 FOR S=1 TO 3
210 T=0
220 T=T+1
230 IF T<2 GOTO 220
240 POKE 3.9E4,8
250 WL=WL-.25
260 GOSUB 320
270 POKE 3.9E4,9
280 GOSUB 10
290 NEXT S
300 NEXT L
310 RETURN
320 V=.0010497*(WL/2)*(255/7.94)+.5
325 D=INT(V)
330 POKE 4.8E4,D
335 RETURN
350 PRINT"DELAY FACTOR=";
360 INPUT A
```

```
 370 PRINT"INITIAL ANGSTROMS=";
 380 INPUT X
 390 WL=X
 400 GOSUB 320
 410 PRINT"FINAL ANGSTROMS=";
 420 INPUT Y
 430 N=(X-Y)*4
 440 PRINT"DATA? YES=1, NO=0"
 450 INPUT DC
 460 IF DC=1 THEN GOSUB 50
 470 IF DC=1 GOTO 550
 480 POKE 3.9E4,8
 490 WL=WL-.25
 500 GOSUB 320
 510 POKE 3.9E4,9
 520 N=N-1
 530 GOSUB
 540 IF N>0 GOTO 480
 550 PRINT"END OF SCAN"
 560 PRINT"SAVE DATA? YES=1 NO=0"
 600 INPUT DS
 700 IF DS=1 THEN GOSUB 800
 750 END
 800 PRINT"LOAD DATA TAPE"
 900 PRINT"INPUT FILE NAME"
 950 INPUT A6$
1000 PRINT"INPUT # DATABLOCKS"
1100 INPUT N
1150 OPEN 1,1,1,A6$
1200 FOR L=1 TO N
1300 ON L GOTO 1400,2000,2700,3400,3910,3920,3930,
     3940
1400 FOR I-1TO 250
1500 X%=A%(I)
1600 T6=T1
1700 PRINT#1,X%
1800 IF T1-T6>120 THEN GOSUB 61900
1900 NEXT I
1950 GOTO 4000
2000 FOR J=1 TO 250
2100 XX=B%(J)
2200 T6=T1
2300 PRINT#1,X%
2400 IF T1-T6>120 THEN GOSUB 61900
2500 NEXT J
2600 GOTO 4000
2700 FOR K=1 TO 250
2800 X%=C%(K)
2900 T6=T1
3000 PRINT#1,X%
3100 IF T1-T6>120 THEN GOSUB 61300
3200 NEXT K
3300 GOTO 4000
3400 FOR I=1 TO 250
3500 X%=D%(I)
```

```
 3600 T6=T1
 3700 PRINT#1,X%
 3800 IF T1-T6>120 THEN GOSUB 61900
 3900 NEXT I
 3905 GOTO 4000
 3910 FOR I=1 TO 250
 3911 X%=E%(I)
 3912 T6=TI
 3913 PRINT#1,X%
 3914 IF T1-T6>120 THEN GOSUB 61900
 3915 NEXT I
 3916 GOTO 4000
 3920 FOR I=1 to 250
 3921 X%=F%(I)
 3922 T6=T1
 3923 PRINT#1,X%
 3924 IF T1-T6>120 THEN GOSUB 61900
 3925 NEXT I
 3926 GOTO 4000
 3930 FOR I=1 to 250
 3941 X%=G%(I)
 3932 T6=T1
 3933 PRINT#1,X%
 3934 IF T1-T6>120 THEN GOSUB 61900
 3935 NEXT I
 3936 GO TO 4000
 3940 FOR I=1 TO 250
 3940 X%=H%(I)
 3942 T6=T1
 3943 PRINT#1,X%
 3944 IF T1-T6>120 THEN GOSUB 61900
 3945 NEXT I
 4000 NEXT L
 4100 CLOSE 1
 4200 PRINT"RIGHT COMPLETE"
 4300 RETURN
61900 POKE 59411,53:T6=T1
61910 IF T1-T6<6 THEN 61910
61920 POKE 59411,61:RETURN
62990 PRINT"TYPE ANY KEY WHEN READY"
63010 GET B6$:IF B6$=""THEN 63010
63020 RETURN
```

The second program was called READ6 and was used to retrieve both absorption and MCD data from tape and to output this data to the Nicolet 1180 computer. READ6 is listed below and is executed by the command RUN5000.

READ 6

```
  10 J=0
  11 J=J+1                          Delay Subroutine
  12 IF J<A GOTO 11
  13 RETURN
5000 DIM A%(250)
5001 DIM B%(250)
5002 DIM C%(250)
5003 DIM D%(250)
5004 DIM E%(250)
5005 DIM F%(250)
5006 DIM G%(250)
5007 DIM H%(250)
5100 PRINT"LOAD DATA TAPE"
5200 PRINT"INPUT FILE NAME"
5300 INPUT A6$
5400 PRINT"INPUT FILE NAME"
5500 PRINT"UP TO 8 BLOCKS TO BE READ"
5600 INPUT N
5700 OPEN 1,1,0,A6$
5800 ON L=1 TO N
5900 ON L GOTO 6000,6300,6600,7000,7210,7240,7260,
     7280
6000 FOR I=1 TO 250
6100 INPUT#1,A%(I)
6200 NEXT I
6250 GOTO 7300
6300 FOR J=1 TO 250
6400 INPUT#1,B%(J)
6500 NEXT J
6550 GOTO 7300
6600 FOR K=1 TO 250
6700 INPUT#1,C%(K)
6800 NEXT K
6900 GOTO 7300
7000 FOR I=1 TO 250
7100 INPUT#1,D%(I)
7200 NEXT I
7205 GOTO 7300
7210 FOR I=1 TO 250
7215 INPUT#1,E%(I)
7220 NEXT I
7230 GOTO 7300
7240 FOR I=1 TO 250
7245 INPUT#1,F%(I)
7250 NEXT I
7255 GO TO 7300
7260 FOR I=1 TO 250
7265 INPUT#1,G%(I)
7270 NEXT I
7275 GOTO 7300
7280 FOR I=1 TO 250
```

```
 7285 INPUT#1,H%(I)
 7290 NEXT I
 7300 NEXT L
 7400 PRINT"END OF DATA READ"
 7500 POKE 4.0E4,0
 7600 POKE 3.9E4,127
 7700 POKE 4.0E4,4
 7800 POKE 3.9E4,0
 7850 POKE 4.9E4,0
 7860 POKE 4.8E4,255
 7870 POKE 4.9E4,4
 8000 PRINT"INPUT # POINTS TO BE OUTPUT"
 8100 INPUT NUM
 8110 PRINT"INPUT DELAY FACTOR WHEN 1180"
 8111 PRINT"SAYS TO OUPUT DATA FROM PET"
 8120 INPUT A
 8150 POKE4.8E4,A%(I)
 8160 POKE3.9E4,8
 8200 FOR L=1 TO NUM
 8300 NP=INT((L-1)/250)
 8400 I=L-NP*250
 8800 GO TO 9500
 8900 POKE 4.8E4,B%(I)
 9000 GOTO 9500
 9100 POKE 4.8E4,C%(I)
 9200 GOTO 9500
 9300 POKE 4.8E4,D%(I)
 9400 GOTO 9500
 9410 POKE 4.8E4,E%(I)
 9420 GOTO 9500
 9430 POKE 4.8E4,F%(I)
 9440 GOTO 9500
 9450 POKE 4.8E4,G%(I)
 9460 GOTO 9500
 9470 POKE 4.8E4,H%(I)
 9480 GOTO 9500
 9500 POKE 3.9E4,9
 9650 POKE 3.9E4,8
 9700 NEXT L
11700 END
```

The program, PEEK, was used to input data from the PET into the Nicolet 1180 using the A/D converter in the Lab 11 acquisition mode. The program stored the data on the Diablo disk system using an appropriate disk directory filename. The incoming data was displayed on the digital oscilloscope, and the data could also be plotted. The data input program, PEEK, is listed below.

PEEK

```
  100 DIM X(2001),Y(2001)
  110 PRINT"WANT TO INPIT FROM PET NO-0"
  111 INPUTQ0
  112 IFQ0=0
  113 CALL FCLEAR(X,2001)
  114 CALL FCLEAR(Y,2001)
  150 PRINT"INPUT #POINTS TO ACQUIRE"
  160 INPUT N5
  162 LET N4=N5*2+2
  165 PRINT "OUTPUT, DATA FROM PET"
  170 CALL FAQT(Y,N5,200,200,1036,0,1)
  172 PRINT"ACQUIRE DONE"
  175 PRINT "INPUT DATA FILENAME"
  176 CALL INFILE
  177 CALL FSTORE(Y,N4)
  180 PRINT " WANT TO PLOT? NO=0"
  181 INPUT Q1
  182 IFQ1=0 THEN 110
  200 PRINT"INPUT NO POINTS, X AXIS LEN,Y AXIS LEN"
  300 INPUT N,L0,L1
  700 CALL DISPOF
  800 CALL FDISPI(Y,2000,200)
 1500 CALL PLOTS
 1501 PRINT"INPUT PLOT ORIGIN:X,Y"
 1502 INPUT X9,Y9
 1503 LET Y9=Y9+0.5
 1510 CALL FDPLOT (X9,Y9,-3)
 1520 PRINT"INPUT STARTING WVELENGTH"
 1530 INPUT W1
 1535 LET N1=-1
 1540 FOR I=0TO N1
 1550 LET X(I)=W1-I
 1561 NEXT I
 1570 GOSUB 15000
 1600 LET X1$="ANG"
 1610 LET Y1$="ABS"
 1614 PRINT "AFTER FSCALE"
 1615 PRINT "X(N),X(N+1)=";X(N),X(N+1)
 1620 CALL FAXIS(0,0,X1$,3,L0,0,X(N),X(N+1),3,3)
 1630 CALL FAXIS(0,0,Y1$,3,L1,90,Y(N),Y(N+1),3,3)
 1640 CALL FLINE(X,Y,N,1,0,0)
 1650 PRINT"PLOT DONE"
 1655 PRINT"WOULD YOU LIKE TO PLOT IT DIFFERENTLY NO=0)"
 1656 INPUT Q2
 1657 IF Q2=0 THEN 110
 1658 GO TO 200
 1700 GO TO 110
15000 LETX(N)=1E30
15001 LET Y(N)=1E30
15010 LET M1=-1E30
15020 LET M2=-1E30
```

```
15030 FOR I=0TO N-1
15040 IF X(I)>X(N) THEN 15060
15050 LET X(N)=X(I)
15060 IFX(I)<M1 THEN 15080
15070 LET M1=X(I)
15080 IFY(I)>Y(N) THEN 15100
15090 LETY(N)=Y(I)
15100 IF Y(I)<M2 THEN 15120
15110 LET M2=Y(I)
15120 NEXT I
15130 LET X(N+1)=(M1-X(N))/L0
15140 LET Y(N+1)=(M2-Y(N))/L1
15150 RETURN
20000 END
```

The program, SPECAS, was used to assemble data sets stored on the disk into full spectra. Calibration and wavelength overlap of data sets was performed as well as storage and plotting of the final spectrum. This spectrum assembler program, SPECAS is listed below.

SPECAS

```
100 DIM Y1(2002),Y2(1000),Y(6002
150 CALL FCLEAR(Y,6002)
151 CALL FCLEAR(Y1,2002)
152 CALL FCLEAR(Y2,1000)
200 PRINT"INPUT NUMBER OF POINTS IN DATA BLOCK"
300 INPUT N
301 LET N1=(N*2)+2
310 PRINT"INPUT DATA FILE NAME OF INCOMING DATA"
320 CALL INFILE
330 CALL FLOAD(Y1,N1)
331 PRINT "IS THIS AN ASSEMBLY OF ABSORPTION OR MCD
    RUNS? ABS=A MCD=M"
332 INPUT B1S
333 IF B1$="A" THEN 2050
335 FOR I=0 TO N-1
336 LET Y1(I)=Y1(I)-1535
337 NEXT I
340 CALL DISPOF
350 CALL FDISPI(Y1,N,200)
400 PRINT"INPUT ZERO FIELD"
450 INPUTZ2
455 LET Z2=Z2-1535
460 PRINT"INPUT CALIBRATION FACTOR"
470 INPUT C2
475 LET C2=C2-1535
```

```
1200 PRINT"INPUT SENSITIVITY FOR STANDARD"
1300 INPUT S1
1400 PRINT"INPUT SENSITIVITY FOR DATA"
1500 INPUT D1
1600 PRINT"INPUT DELTA ABSORBANCE FOR STANDARD"
1700 INPUT S2
1800 LET F1=(D1*S2)/(S1*C2-Z2)
1900 FOR I=0 TO N-1
1950 LET Y1(I)=(Y1(I)-Z2)*F1
2000 NEXT I
2050 CALL DISPOF
2060 CALL FDISPI(Y1,N,200)
2100 PRINT"INPUT STARTING WAVELENGTH"
2300 INPUT W1
2310 PRINT"WANT OVERLAP ADJUSTMENT NO=0
2311 INPUT Q1
2312 IF Q1=0 THEN 2395
2313 FOR I=0 TO 5999
2314 LET Y(I)=Y(I)/1E5
2315 NEXT I
2320 PRINT"INPUT SHORTEST WAVELENGTH IN OVERLAPPING
     REGION"
2330 INPUT W2
2335 LET S1=0
2339 LET W3=W1-W2
2340 FOR I=0 TO W3
2350 LET S1=S1+Y(8500-W1+I)-Y1(I)
2360 NEXT I
2370 LET A1=S1/(W3+1)
2371 PRINT"AVG DIF. IN OVERLAP=";A1
2380 FOR I=0 TO W3
2384 LET Y2(I)=Y1(I)
2385 LET Y1(I)=Y1(I)+A1
2390 NEXT I
2395 LET N1=N-1
2400 FOR I=0 TO N1
2500 LET J=8500-W1+I
2600 LET Y(J) =Y1(I)
2700 NEXT I
2701 FOR I-0 to 5999
2702 LET Y(I) =Y(I)*1E5
2303 NEXT I
2710 CALL DISPOF
2720 CALL FDISPI(Y,6002,200)
2725 PRINT" DOES OVERLAP LOOK OKAY? YES=Y"
2730 INPUT Q$
2735 IFQ$="Y" THEN 2800
2740 FOR I=0 TO W3
2750 LET Y1(I)=Y2(I)
2760 NEXT I
2770 PRINT"INPUT A DIFFERENT AVG OVERLAP DIFFERENCE"
2780 INPUT A1
2790 GO TO 2380
2800 PRINT"MORE DATA NO=N"
```

```
  700 PRINT"INPUT STARTING WAVELENGTH"
  800 INPUT W1
  805 PRINT"WOULD YOU LIKE TO PLOT A SMALL PART? YES=Y"
  806 INPUT Q1$
  807 IF Q1$="Y" THEN 810
  808 GO TO 900
  810 PRINT "INPUT LONGEST AND SHORTEST WAVELENGTHS"
  820 INPUT W3,W2
  825 FOR I=0 TO W3-W2
  830 LET Y(I)=Y(W1-W3+I)
  840 NEXT I
  850 LET N=W3-W2+1
  860 LET W1=W3
  900 FOR I=0 TO N-1
 1000 LET X(I)=W1-I
 1100 NEXT I
 1200 PRINT"LIKE SAME SCALE FACTOR AS LAST PLOT? YES=Y"
 1210 INPUT Q2$
 1220 IF Q2$="N" THEN 1300
 1230 LET X(N)=X3
 1235 LET X(N+1)=X4
 1240 LET Y(N)=Y3
 1245 LET Y(N+1)=Y4
 1250 GO TO 1700
 1300 LET X1$="CM-1"
 1400 LET Y1$="ABS"
 1450 LET X2$="ANG"
 1500 PRINT"INPUT X,Y AXIS LENGTHS"
 1600 INPUT L0,L1
 1601 PRINT"INPUT ORIGN X,Y"
 1602 INPUT 01,02
 1603 CALL FDPLOT(01,02,-3)
 1610 GOSUB 15000
 1615 LET L3=0
 1620 CALL FAXIS(0,L3,X2$,3,L0,0,X(N),X(N+1),4,4)
 1630 CALL FAXIS(0,0,Y1$,3,L1,90,Y(N),Y(N+1),4,2)
 1700 CALL FLINE(X,Y,N,1,0,0)
 1701 PRINT"WANT WAVENUMBER SCALE? NO=N"
 1702 INPUT T2$
 1703 IF T2$="N" THEN 20000
 1705 FOR I=0 TO N-1
 1706 LET X(I)=1/((W1-I)*1E-8)
 1707 NEXT I
 1710 LET R=0
 1720 GOSUB 15000
 1730 LET W1=1/(M1*1E-8)
 1746 LET W=-X(N+1)
 1750 CALL FAXIS(0,0,X1$,4,L0,0,W1,W,4,3)
 1760 CALL FDPLOT(0,L3,3)
 1770 CALL FDPLOT(0,0,2)
 1780 CALL FDPLOT(L0,0,2)
 1800 GO TO 20000
15000 LET X(N)=1E30
15001 LET Y(N)=1E30
```

```
15010 LET M1=-1E30
15020 LET M2=-1E30
15030 FOR I=0 TO N-1
15040 IF X(I)>X(N) THEN 15060
15050 LET X(N)=X(I)
15060 IF X(I)<M1 THEN 15080
15080 IF Y(I)>Y(N) THEN 15100
15090 LET Y(N)=Y(I)
15100 IF Y(I)<M2 THEN 15120
15110 LET M2=Y(I)
15120 NEXT I
15121 IF R=0 THEN 15130
15122 PRINT"INPUT TRUNCATION FACTOR"
15123 INPUT T1
15125 LET X9=X(N)/T1
15126 LET X(N)=T1*INT(X9)
15127 LET M1=INT(M1/T1)*T1+T1
15130 LET X(N+1)=(M1-X(N))/L0
15140 LET Y(N+1)=(M2-Y(N))/L1
15150 LET X3=X(N)
15160 LET X4=X(N+1)
15170 LET Y3=Y(N)
15180 LET Y4=Y(N+1)
15190 LET R=1
15200 RETURN
20000 PRINT"WANT TO PLOT MORE DATA? YES=Y"
20001 INPUT S1$
20002 IF S1$="Y" THEN 60
20005 END
```

REFERENCES

1. M. Faraday, *Faraday's Diary*, Volume 9, London: Bell, 1933.

2. S. F. Mason, Quart. Rev. 17, 20 (1963).

3. L. Rosenfeld, Z. Phys. 57, 835 (1929).

4. H. A. Kramers, Proc. Acad. Sci. Amsterdam 33, 959 (1930).

5. R. Serber, Phys. Rev. 41, 489 (1932).

6. P. J. Stephens, Ph.D. Dissertation, Oxford University, 1964.

7. J. A. Spencer, J. Chem. Phys. 54, 5139 (1971).

8. P. J. Stephens, Ann. Rev. Phys. Chem. 25, 201 (1974).

9. A. D. Buckingham and P. J. Stephens, Ann. Rev. Phys. Chem. 17, 399 (1966).

10. J. LoMenzo, B. D. Bird, G. A. Osborne and P. J. Stephens, Chem. Phys. Lett. 9, 332 (1971).

11. M. J. Harding and B. Briat, Mol. Phys. 25, 745 (1973).

12. G. W. Hodgson, E. Peterson, K. A. Kvenvolden, E. Bunnenberg, B. Halpern and C. Ponnamperuma, Science 167, 763 (1970).

13. G. Barth, R. Records, E. Bunnenberg, C. Djerassi and W. Voelter, J. Am. Chem. Soc. 25, 57 (1971).

14. G. Barth, W. Voelter, E. Bunnenberg and C. Djerassi, J. Am. Chem. Soc. 94, 1293 (1972).

15. J. Finkel, J. Mol. Spectrosc. 9, 421 (1962).

16. J. Finkel, J. Opt. Soc. Am. 53, 1115 (1963).

17. R. A. Harris, J. Chem. Phys. 46, 3398 (1967).

18. R. A. Harris, J. Chem. Phys. 47, 4481 (1967).

19. E. Whittle, D. A. Dows and G. C. Pimentel, J. Chem. Phys. 22, 1943 (1954).

20. R. L. Mowery, J. C. Miller, P. N. Schatz, E. R. Krausz, S. M. Jacobs and L. Andrews, J. Chem. Phys. 70, 3920 (1979).

21. B. Meyer, *Low Temperature Spectroscopy*, New York: Elsevier, 1971.

22. A. J. Thomson in *Electronic States of Inorganic Compounds: New Experimental Techniques*, edited by P. Day, Boston: Reidel, 1974, p. 241.

23. I. Douglas, R. Grinter and A. J. Thomson, Dalton Division Symposium, Chemical Society, Autumn Meeting, University of East Anglia, 1973.

24. I. N. Douglas, R. Grinter and A. J. Thomson, Mol. Phys. 28, 1377 (1974).

25. I. N. Douglas, R. Grinter and A. J. Thomson, Chem. Phys. Lett. 28, 192 (1974).

26. E. R. Krausz, R. L. Mowery and P. N. Schatz, Ber. Bunsenses. Phys. Chem. 82, 134 (1978).

27. M. A. Goetschlackx, R. L. Mowery, E. R. Krausz, W. C. Yeakel, P. N. Schatz, B. S. Ault and L. Andrews, Chem. Phys. Lett. (to be published).

28. T. J. Barton, I. N. Douglas, R. Grinter and A. J. Thomson, Mol Phys. 30, 1677 (1975).

29. T. J. Barton, R. Grinter and A. J. Thomson, Chem. Phys. Lett. 40, 399 (1976).

30. G. A. Osborne, J. Mol. Spec. 49, 48 (1974).

31. W. Weltner, Jr., Science 155, 155 (1967).

32. R. Dirsherl, K. W. Michel and C. B. Cosmovici, Astron. Astrophys. 68, 381 (1978).

33. A. J. Sauval, Astron. Astrophys. 62, 295 (1978).

34. L. H. Dubois and J. H. Gole, J. Chem. Phys. 66, 779 (1977).

35. J. M. Scalo and J. E. Ross, Astron. Astrophys. 48, 291 (1976).

36. R. F. Wing, Mem. Soc. Roy. Liege 3, 123 (1972).

37. W. Weltner, Jr., Ber. Bunsenges. Phys. Chem. 82, 80 (1978).

38. R. D. Brittain, Ph.D. Dissertation, University of Florida, 1979.

39. P. J. Stephens, J. Chem. Phys. 52, 3489 (1970).

40. P. J. Stephens in *Advances in Chemical Physics*, Volume 35, edited by I. Prigogine and S. A. Rice, New York: Wiley, 1976, p. 197.

41. C. H. Henry, S. E. Schnatterly and C. P. Slichter, Phys. Rev. A137, 583 (1965).

42. A. S. Davydov, *Quantum Mechanics*, Reading, Mass.: Addison-Wesley, 1961, p. 302.

43. E. R. Krausz and G. Cohen, Rev. Sci. Instrum. 48, 1506 (1977).

44. R. G. Denning in *Electronic States of Inorganic Compounds: New Experimental Techniques*, edited by P. Day, Boston: Reidel, 1975, p. 157.

45. R. J. Tacon, Ph.D. Dissertation, Oxford University, 1977.

46. A. J. McCaffery and S. F. Mason, Mol. Phys. 6, 359 (1963).

47. J. A. Broomhead, F. P. Dwyer and J. W. Hogarth, Inorg. Syn. 6, 186 (1960).

48. F. A. Cotton and G. Wilkinson, *Advanced Inorganic Chemistry*, 2nd Edition, New York: Interscience, 1966.

49. L. H. Dubois and J. L. Gole, J. Chem. Phys. 66, 779 (1977).

50. F. Lowater, Proc. Phys. Soc. London 41, 557 (1927).

51. A. Christy, Phys. Rev. 33, 701 (1929).

52. J. G. Phillips, Astrophys. J. 114, 152 (1951).

53. U. Uhler, Ph.D. Dissertation, University of Stockholm, 1954.

54. K. D. Carlson and C. Moser, J. Phys. Chem. 67, 2644 (1963).

55. K. D. Carlson and R. K. Nesbet, J. Chem. Phys. 41, 1051 (1964).

56. E. Clementi and D. L. Raimondi, J. Chem. Phys. 38, 2686 (1963).

57. R. A. Berg and O. Sinanoglu, J. Chem. Phys. 32, 1082 (1960).

58. K. D. Carlson and C. Moser, J. Chem. Phys. 46, 35 (1967).

59. A. V. Peterson, Ark. Fys. 16, 185 (1959).

60. A. V. Peterson and B. Lindgren, Ark. Fys. 22, 491 (1962).

61. J. G. Phillips, Astrophys. J. 111, 314 (1950).

62. W. Weltner, Jr. and D. McLeod, Jr., J. Phys. Chem. 69, 3488 (1965).

63. N. S. McIntyre, K. R. Thompson and W. Weltner, Jr., J. Phys. Chem. 21, 3243 (1971).

64. J. G. Phillips, Astrophys. J. 169, 185 (1971).

65. J. G. Phillips, Astrophys. J. 157, 449 (1969).

66. D. M. Gruen and D. H. W. Carstens, J. Chem. Phys. 54, 5206 (1971).

67. J. M. Brom, Jr. and H. P. Broida, J. Chem. Phys. 63, 3718 (1975).

68. J. G. Phillips, Astrophys. J. 115, 567 (1952).

69. E. R. Krausz, Private Communication.

70. F. P. Coheur, Bull. Soc. Roy. Sci. Liege, 12, 98 (1943).

71. J. A. Venables and B. L. Smith in *Rare Gas Solids*, Volume 2, edited by M. L. Klein and J. A. Venables, New York: Academic, 1977.

72. S. I. Kovalenko and N. N. Bagrov, Sov. Phys. Sol. State. 11, 2207 (1970).

73. W. Weltner, Jr., Private Communication.

74. D. L. Hildenbrand, Chem. Phys. Lett. 44, 281 (1976).

75. M. Kaufman, J. Muenter and W. Klemperer, J. Chem. Phys. 47, 3365 (1967).

76. C. M. Pathak and H. B. Palmer, J. Mol. Spectrosc. 33, 137 (1970).

77. D. M. Gruen and D. H. W. Carstens, J. Chem. Phys. 54, 5206 (1971).

78. T. Wentink, Jr. and R. J. Spindler, Jr., J. Quant. Spectrosc. Radiat. Transfer 12, 1569 (1972).

79. D. N. Davis and P. C. Keenan, Publ. Astron. Soc. Pac. 81, 230 (1969).

80. M. Afaf, Proc. Phys. Soc. (London) A63, 674 (1950).

81. U. Uhler and L. Åkerlind, Ark. Fys. 10, 431 (1956).

82. L. Åkerlind, Ark. Fys. 11, 395 (1957).

83. J. K. Bates and D. M. Gruen, High Temp. Sci. 10, 27 (1978).

84. J. B. Tatum and W. J. Balfour, J. Mol. Spectrosc. 48, 292 (1973).

85. J. G. Phillips and S. P. Davis, Astrophys. J. 207, 632 (1976).

86. L. J. Lauchlan, J. M. Brom, Jr. and H. P. Broida, J. Chem. Phys. 65, 2672 (1976).

87. M. J. Linevsky in *Proceedings of the First Meeting of the Interagency Chemical Rocket Propulsion Group on Thermochemistry*, Volume 1, Silver Spring, Maryland: Chemical Propulsion Information Agency, 1964.

88. W. A. Chupka, J. Berkowitz and M. G. Inghram, J. Chem. Phys. 26, 1207 (1957).

89. D. Conlon and W. P. Doyle, J. Chem. Phys. 42, 4315 (1965).

90. C. J. Cheetham and R. F. Barrow, Trans. Far. Soc. 63, 1835 (1967).

91. W. F. Meggers, J. Res. Natl. Bur. Std. 1, 151 (1928).

92. A. S. King, Astrophys. J. 70, 105 (1929).

93. R. W. Shaw and H. C. Ketcham, Phys. Rev. A45, 735 (1934).

94. S. G. Krishnamurti, Proc. Phys. Soc. London A64, 852 (1951)

95. A. Gatterer, J. Junkes, E. W. Salpeter and B. Rosen in *Molecular Spectra of Metallic Oxides*, Vatican City: Specola Vaticana, 1957.

96. G. Edvinsson and Ch. Nylen, Phys. Scr. 3, 261 (1971).

97. G. Edvinsson, Ph.D. Dissertation, University of Stockholm, 1971.

BIOGRAPHICAL SKETCH

David H. Powell was born in Richmond, Virginia, on February 4, 1947. After graduation from Benedictine High School in 1964, he attended the University of Richmond until 1968 when he was awarded the degree of Bachelor of Science in Chemistry. He served in the United States Army from 1968 through 1970. In 1970 he returned to the University of Richmond and received the degree of Master of Science in Chemistry in 1972. He was employed by Philip Morris, Inc., from 1972 through 1974. Since September 1974 he has pursued a course of study leading to the Doctor of Philosophy Degree in chemistry at the University of Florida. He is married to Marie Louise Fitz-William of Richmond, Virginia.

I certify that I have read this study and that in my opinion it conforms to acceptable standards of scholarly presentation and is fully adequate, in scope and quality, as a dissertation for the degree of Doctor of Philosophy.

Martin T. Vala

Martin T. Vala, Chairman
Professor of Chemistry

I certify that I have read this study and that in my opinion it conforms to acceptable standards of scholarly presentation and is fully adequate, in scope and quality, as a dissertation for the degree of Doctor of Philosophy.

John R. Eyler

John R. Eyler
Associate Professor of Chemistry

I certify that I have read this study and that in my opinion it conforms to acceptable standards of scholarly presentation and is fully adequate, in scope and quality, as a dissertation for the degree of Doctor of Philosophy.

Alex E. Greene
Graduate Research Professor of Physics

I certify that I have read this study and that in my opinion it conforms to acceptable standards of scholarly presentation and is fully adequate, in scope and quality, as a dissertation for the degree of Doctor of Philosophy.

Gus Palenik

Gus R. Palenik
Professor of Chemistry

I certify that I have read this study and that in my opinion it conforms to acceptable standards of scholarly presentation and is fully adequate, in scope and quality, as a dissertation for the degree of Doctor of Philosophy.

Willis B. Person

Willis B. Person
Professor of Chemistry

This dissertation was submitted to the Graduate Faculty of the Department of Chemistry in the College of Liberal Arts and Sciences and to the Graduate Council, and was accepted as partial fulfillment of the requirements for the degree of Doctor of Philosophy.

December 1979

Dean, Graduate School